EBF1 Regulates Sensory Development in the Mammalian Cochlea

Kathryn Gorsuch Powers

A dissertation

submitted in patrial fulfillment of the

requirements for the degree of

Doctor of Philosophy

University of Washington

2025

Reading Committee:

Olivia Bermingham-McDonogh, Chair

Tom Reh

Andrea Wills

Program Authorized to Offer Degree:

Molecular and Cellular Biology

University of Washington

Abstract

EBF1 Regulates Sensory Development in the Mammalian Cochlea

Kathryn Gorsuch Powers

Chair of the Supervisory Committee:

Olivia Bermingham-McDonogh

Department of Neurobiology and Biophysics

Hair cell damage is a leading cause of sensorineural hearing loss. Unlike non-mammalian vertebrates, which regenerate hair cells throughout their lives, mammals lose the ability to spontaneously generate cochlear hair cells within the first postnatal week. Understanding the developmental programs that drive sensory development is essential for the design of effective regenerative therapeutics to fight hearing loss. However, large gaps remain in our understanding of the signals that direct cochlear development. Recent work in the Bermingham-McDonogh lab identified enrichment of EBF (Early B cell Factor) consensus DNA-binding motifs in the open chromatin of prosensory cells collected from embryonic mouse cochleae. Although *Ebf* genes are often expressed in overlapping patterns, this appears to not be the case for the cochlea. Single cell RNA-seq analysis revealed that *Ebf1* shows strong expression in the developing cochlear epithelium, whereas *Ebf2-4* show little to no expression. To determine how loss of EBF1 affects cochlear development, I generated conditional knockout mouse models. The work presented in this dissertation characterizes the role of EBF1 in cochlear development. First, *Ebf1* conditional knockout mouse phenotypes were examined, with

particular attention to how *Ebf1* excision affects cochlear patterning, prosensory proliferation, sensory differentiation and maturation, and hearing. Second, a multiomic approach that combines single nucleus RNA-seq and single nucleus ATAC-seq into a single workflow was used to identify EBF1's roles as a transcriptional activator and repressor within a regulatory network. This work provides valuable insight into how EBF1 regulates cell fate and proliferation to restrict sensory development in the mammalian cochlea, and in turn, offers valuable insight into a novel target for future regenerative strategies.

TABLE OF CONTENTS

LIST OF FIGURES AND TABLES

GLOSSARY

ABR	Auditory brainstem response
ADAM	A disintegrin and metalloproteinase
ANOVA	Analysis of variance
APC	Adenomatosis polyposis coli (regulator of Wnt signaling)
ATAC	Assay for transposase-accessible chromatin
ATOH1	Atonal homolog 1
BAF	BRG1/BRM-associated factor (mammalian SWI/SNF complex)
BMP	Bone morphogenic protein
bp	Base pairs (also kb for kilobase pairs)
BRG1	Brahma-related gene 1
C1QA	Complement C1q A chain
CC	Claudius cell
CCNJL	Cyclin J like
CD44	Cell surface glycoprotein
ChIP-seq	Chromatin immunoprecipitation sequencing
COE	Collier, OLF, and EBF (HLH transcription factors)
Cre	Cre recombinase
CreER	Inducible Cre recombinase (made by fusing the estrogen receptor to Cre)
CUT&RUN	Cleavage under targets & release using nuclease
CUT&Tag	Cleavage under targets & tagmentation

DC	Deiters' cell
DIG	Digoxigenin
DKK3	Dickkopf Wnt signaling pathway inhibitor 3
DLL	Delta like ligand
DVL	Dishevelled segment polarity protein
E	Embryonic day
EBF	Early B cell factor
EdU	5-ethynyl-2′-deoxyuridine (thymidine analog)
EPCAM	Epithelial cell adhesion molecule
ERK	Extracellular signal-related kinase
FABP7	Fatty acid binding protein 7
FAC-sorting	Fluorescent activated cell sorting
FGF	Fibroblast growth factor
FGFR	Fibroblast growth factor receptor
FM1-43	Amphiphilic fluorescent styryl pyridinium dye
FRZB	Frizzled related protein
FST	Follistatin
FZD	Frizzled class receptor
GFI1	Growth factor independent 1 transcriptional repressor
GFP	Green fluorescent protein (also EGFP for enhanced GFP)
GLI	Glioma-associated oncogene family zinc finger

GO	Gene ontology
GREAT	Genomic regions enrichment annotations tool
GSK3-β	Glycogen synthase kinase 3 beta
GTPase	Guanine triphosphatase
HBSS	Hank's balanced salt solution
HC	Hair cell (also iHC for inner HC and oHC for outer HC)
HeC	Hensen's cell
HEPES	4-(2-hydroxyethyl)-1-piperazineethanesulfonic acid
HES	Hes family BHLH transcription factor
HEY	Hes related family BHLH transcription factor with YRPW motif
HEYL	Hes related family BHLH transcription factor with YRPW motif like
Hh	Hedgehog
HLH	Helix-loop-helix protein (also BHLH for basic helix-loop-helix)
iBC	Inner border cell
ID	Inhibitor of differentiation
iPhC	Inner phalangeal cell
JAG	Jagged ligand
JNK	c-Jun N-terminal kinase
KO	Knockout (also cKO for conditional KO)
KöO	Kölliker's organ
LFNG	Beta-1,3-N-acetylglucosaminyltransferase lunatic fringe

MAML	Mastermind like transcriptional coactivator
MAPK	Mitogen-activated protein kinase
MET	Mechanoelectrical transduction
MFNG	Beta-1,3-N-acetylglucosaminyltransferase manic fringe
MKI67	Marker of proliferation Ki-67
mm10	Full genome sequences for Mus musculus (mouse) provided by UCSC
MYO7a	Myosin 7a
n	Sample size
NBT/BCIP	Nitroblue tetrazolium/ 5-bromo-4-chloro-3-indolyl-1-phosphate
NFAT	Nuclear factor of activated T cells (tonicity-responsive enhancer-binding protein)
NF-M	Neurofilament medium chain (also known as NEFM)
NGFR	Nerve growth factor receptor
NICD	Notch intracellular domain
OC90	Otoconin 90
OCT	Optimal cutting temperature compound
OTX2	Orthodenticle homeobox 2
P	Postnatal day
P2A	Self-cleaving peptide derived from porcine teschovirus-1
p75	Neurotrophin receptor p75
PAX5	Paired box 5
PBS	Phosphate buffered saline

PC	Pillar cells (also iPC for inner PC and oPC for outer PC)
PCA	Principal component analysis
PCR	Polymerase chain reaction (also qPCR for quantitative PCR)
PD	Prosensory domain
PECAM1	Platelet and endothelial cell adhesion molecule 1
PFA	Paraformaldehyde
PMEL	Premelanosome protein
POU3F4	POU Class 3 homeobox 4
POU4F3	POU Class 4 homeobox 3
PRDM16	PR domain-containing 16
PROX1	Prospero homeobox 1
PTCH	Patched homolog
RAS	Rat sarcoma (GTPase)
RBP-Jκ	Recombination signal binding protein for immunoglobulin kappa J region
RHOA	Ras homolog family member A (GTPase)
ROCK	Rho associated coiled-coil containing protein kinase
ROI	Region of interest
S	Cleavage site
SC	Support cell
scRNA-seq	Single cell RNA sequencing
SD	Sensory domain

SDS	Sodium dodecyl sulfate
SE	Sensory epithelium
SHH	Sonic hedgehog signaling molecule
SLC26A9	Solute carrier family 26 member 9
SMAD	Sma- and Mad-related protein
SMO	Smoothened (frizzled class receptor)
snATAC-seq	Single nucleus ATAC sequencing
snRNA-seq	Single nucleus RNA sequencing
SOX2	SRY-box transcription factor 2
SPRY	Sprouty RTK signaling antagonist
SWI/SNF	Switch/sucrose nonfermentable chromatin remodeling complex
TCF/LEF	T-cell factor/lymphoid enhancer factor
TECTA	Tectorin alpha
TIG/IPT	Transcription factor immunoglobin/ immunoglobulin-like fold, plexins, transcription factors
TOP2A	DNA topoisomerase 2 alpha
TX-100	Triton X-100
UMAP	Uniform manifold approximation and projection
vGLUT3	Vesicular glutamate transporter 3 (also known as SLC17A8)
WNT	Wingless-type MMTV integration site family

ACKNOWLEDGEMENTS

I have many people to thank who supported me along my journey towards and through graduate school. Before joining the Molecular and Cellular Biology graduate program at the University of Washington, I worked as an undergraduate research assistant in the Blackburn lab at Trinity College and as a postbaccalaureate research technician in the Neuropeptide (Eipper and Mains) lab at the University of Connecticut Health Center. While working with Dr. Daniel Blackburn, I discovered my passion for scientific research. I enjoyed the iterative process of incorporating gleaned insights into subsequent research endeavors as I documented a novel mechanism employed by scaled reptiles to process egg yolk nutrients. Eager to gain more experience in cell biology after my graduation, I joined the Neuropeptide lab as a research technician. My research with Drs. Richard Mains and Elizabeth Eipper focused on the role of peptidylglycine α-amidating monooxygenase in rendering peptides biologically active for neuropeptide signaling. My research experiences in their lab were formative, fascinating, and enticing. I started graduate school knowing that I wanted to pursue a career in research.

In my search for a dissertation lab, I met Dr. Olivia Bermingham-McDonogh and was instantly drawn to her work on the inner ear. Working in her lab not only nurtured the passion for developmental research that I discovered as an undergraduate but also deepened the fascination with neuroscience that I uncovered as a research technician. She was an incredibly supportive mentor, managing her lab with compassion and always keeping her office door open for me to discuss ideas and experiments. She encouraged me to make the most of my graduate school experience by helping me refine abstracts for conferences, providing guidance during grant writing, and keeping me informed about opportunities to learn more about careers in both academia and industry. I used to turn bright red during presentations, and because of her encouragement and tireless support, I now feel much more at ease speaking in front of a crowd. I am the scientist I am today because of her mentorship, and I feel profoundly grateful as I move into the next phase of my scientific career with confidence.

I also want to thank past and present Bermingham-McDonogh lab members. A former postdoctoral fellow in the lab, Dr. Brent Wilkerson, met with me over Zoom once a month to offer insight when I was getting my project off the ground. Kylie Beach, a former research scientist, patiently trained me in in situ hybridization and cochlear duct dissections during my rotation with the lab. Another former research scientist, Sophie Seo, provided invaluable help with mouse work and troubleshooting antibodies for immunostaining. Thank you also to Connor Finkbeiner and Dr. Josh Hahn for their computational expertise and for providing guidance as I analyzed my single cell RNA-seq and multiome datasets. Huge thanks to my undergraduate trainees, Jose Rodriguez and Alyssa Chu, who assisted in maintaining our mouse colony, performing immunostaining experiments, and counting cells.

Thank you to past and present members of the Reh lab: Cat Ray, Connor Finkbeiner, and Drs. Evelyn Abraham, Bindia Chawla, Kiara Eldred, Josh Hahn, Marcus Hooper, Lew Kaplan, Brennan Mahoney, Marina Pavlou, Akshaya Sridhar, Levi Todd, and Juliette Wohlschlegel. They all offered invaluable insight during my lab meeting presentations and practice talks, and they were incredible resources when I was troubleshooting experiments. I will miss our happy hours, trivia nights, and lab hikes.

I am grateful to my supervisory committee members: Drs. Sam Golden, Tom Reh, Joe Sisneros, and Andrea Wills. They helped shape my project and were amazing assets during my graduate training.

Lastly, thank you to my friends and family who supported me through my graduate training. I especially want to thank my partner, Shawn Sweeney. He was there to hold me during the lows and celebrate with me during the highs of graduate school. I feel so fortunate he is a part of my life.

Kathryn G. Powers

Seattle, 2025

CHAPTER 1: Introduction

1.1 Cochlear Mechanics

The inner ear is a small, intricate structure housed within the temporal bone of the skull. The cochlea, the spiral-shaped component of the inner ear responsible for our sense of hearing (Fig. 1.1A), is composed of three fluid-filled spaces that run along its length: the scala vestibuli, scala tympani, and scala media (Fig. 1.1B). The scala vestibuli and scala tympani are joined at the apex of the cochlea by a small opening known as the helicotrema and are filled with sodium-rich perilymph. Wedged between these two chambers, the scala media contains potassium-rich endolymph and houses the organ of Corti, the sensory epithelium of the cochlea. When an auditory stimulus is present, sound waves travel down the auditory canal and come in contact with the tympanic membrane (also known as the eardrum), causing it to vibrate. These vibrations are then relayed by the three bones of the middle ear (i.e., malleus, incus, and stapes) to the oval window, a membrane-covered opening at the base of the cochlea that leads directly into the scala vestibuli. As the stapes taps the oval window, it generates pressure waves that travel through the perilymph in the scala vestibuli and scala tympani. The round window, another membrane-covered opening at the base of the cochlea, provides a point for these pressure waves to dissipate from the scala tympani (Fig. 1.1A; Pickles, 2012).

The organ of Corti sits on top of the basilar membrane that separates the scala tympani and the scala media (Fig. 1.1B). As pressure waves move through the perilymph-filled spaces of the scala vestibuli and scala tympani, they cause the basilar membrane to wave in a tonotopic manner. The basilar membrane is narrow and very stiff towards the base of the cochlea but wide and flexible towards the apex. Because of its graded stiffness, soundwaves of different frequencies generate waves in distinct regions of the basilar membrane. More specifically, high frequencies cause waves to form at the portion of the basilar membrane near the base of the cochlea, and low frequencies cause waves to form near the apex (Pickles, 2012).

As the basilar membrane rises and falls in response to sound of a particular frequency, so does the organ of Corti. This sensory epithelium is composed of rows of hair cells (HCs) and support cells (SCs) that are arranged along the length of the cochlear duct (Fig. 1.1C). The HCs are arranged in four rows, one medial row of inner HCs (iHCs) and three lateral rows of outer HCs (oHCs). The motion of the basilar membrane causes the stereocilia bundles on the apical surfaces of the HCs to deflect. This generates tension in the tip links that connect stereocilia from adjacent rows within the bundles, and in turn, causes the mechanoelectrical transduction (MET) channels at the tips of the stereocilia to open. As a result, potassium ions from the endolymph of the scala media flow into the HCs, causing them to depolarize, release glutamate, and ultimately stimulate the sensory neurons that innervate them. While iHCs serve as the primary signal transducers of the cochlear sensory epithelium, oHCs function as the signal amplifiers. The plasma membranes of oHCs are enriched with the motor protein prestin. Sound-induced depolarization of oHCs causes their voltage-sensitive prestin to contract. Once tension in the tip links slackens, the ion channels close, potassium influx decreases, and the oHCs hyperpolarize, causing their prestin to elongate. Because the stereocilia of oHCs are embedded in the tectorial membrane, the electromotility cycle of prestin makes it possible for oHCs to enhance basilar membrane motion and improve frequency selectivity (Pickles, 2012). Both iHCs and oHCs are surrounded by SCs, which facilitate their mechanical stimulation by providing structural support within the organ of Corti and recycle potassium ions back into the endolymph following HC depolarization (reviewed in Wan et al., 2013). Together, HCs and SCs make it possible for auditory signals to be propagated to the brain and for us to perceive sound.

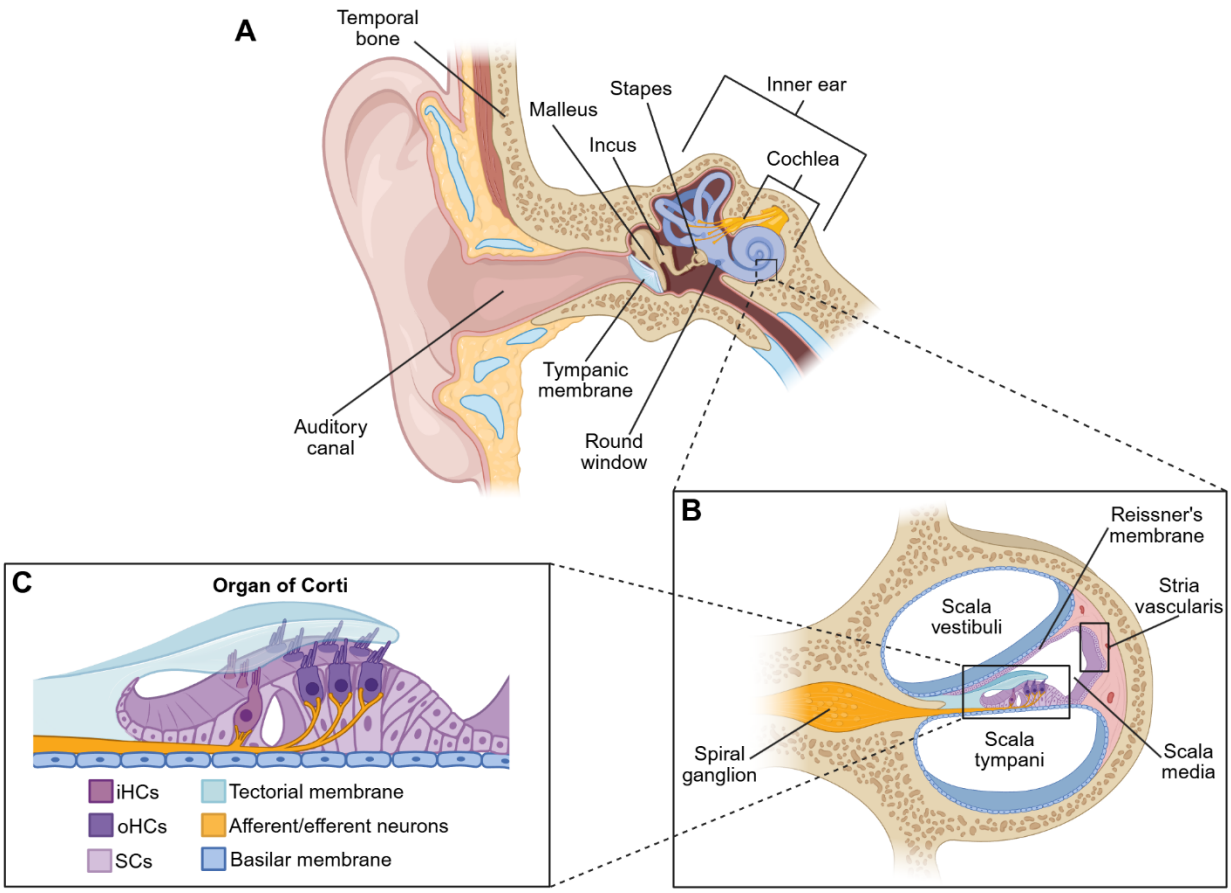

Figure 1.1. The human inner ear.

(created with BioRender.com)

(A) Diagram of the human ear, highlighting portions of the outer, middle, and inner ear. **(B)** Cross-sectional diagram one of the cochlear turns. **(C)** Cross-sectional diagram of the organ of Corti.

1.2 Hearing Loss

The Global Burden of Disease 2019 study reported that approximately 1.57 billion (one in five) people worldwide suffer from mild to profound hearing loss (Vos et al., 2020). Global population growth and improved life expectancy are anticipated to drive a 56.1% increase in the this number by 2050 (Haile et al., 2021). Auditory deficits can arise from injury to either the central or peripheral auditory systems. Peripheral hearing loss is further categorized as conductive, when the impairment is attributed to middle or outer ear damage, or sensorineural, when the impairment is due to dysfunction of the cochlea or spiral ganglion (reviewed in Cunningham and Tucci, 2017). Of the different types of hearing loss, sensorineural is the most pervasive (Wu et al., 2020). The leading causes of sensorineural hearing loss include aging, noise exposure, ototoxic drugs, and congenital conditions, all of which can lead to loss of the HCs critical for sound detection (Chen and Fechter, 2003; Jiang et al., 2006; Korver et al., 2017; Lenoir et al., 1999; Nakagawa et al., 1998; Roberston, 1980; Wu et al., 2020). Among these, aging is the strongest predictor of hearing impairment. Disabling hearing loss affects 5% of adults ages 45-54, 10% of adults ages 55-64, 22% of adults ages 65-74, and 55% of adults over 75 in the United States (NIDCD, 2023). Recreational noise is thought to pose a particular threat to the hearing of teenagers and young adults, with an estimated 12.5% of Americans in this age bracket exhibiting noise-induced threshold shifts indicative of cochlear stress or damage. Reported rates of hearing loss associated with use of aminoglycoside antibiotics, a class of ototoxic medications tightly regulated in many developed countries, range from 2% to 25% (reviewed in Sheffield and Smith, 2019). Finally, congenital hearing impairment is present in approximately two to three out of every 1000 newborns in the United States (CDC, 2010; reviewed in Morton and Nance, 2006). The multiple factors contributing to hearing loss and its high prevalence underscore the need for improved strategies to promote HC regeneration.

1.3 Understanding Sensory Regeneration Through Developmental Research

Non-mammalian vertebrates (e.g., amphibians, birds, fish, and reptiles) retain the ability to regenerate sensory HCs via direct transdifferentiation and mitotic regeneration throughout their lives. In direct transdifferentiation, SCs convert directly into HCs, leading to HC generation at the expense of the resident SC population (Shang et al., 2010; Taylor and Forge, 2005). Mitotic regeneration avoids this trade-off, as SCs divide before one or both daughter cells transdifferentiate into HCs (Baird et al., 1996; Balak et al., 1990; Corwin and Cotanche, 1988; Harris et al., 2003; Presson et al., 1996; Raphael, 1992; Raphael et al., 1994; Shang et al., 2010; Warchol and Corwin, 1996). Mammals, however, undergo a sharp regenerative decline after birth. While the adult rodent vestibular system demonstrates some limited HC regenerative potential (Burns et al., 2012; Forge et al., 1993; Forge et al., 1998; Golub et al., 2012; Kawamoto et al., 2009; Slowik and Bermingham-McDonogh, 2013a), spontaneous HC regeneration in the cochlea is restricted to the first postnatal week in mice (Cox et al., 2014). Advances in developmental research provide a foundation for identifying potential targets for regenerative therapeutics. By manipulating signaling pathways that are important in cochlear development (e.g., Notch, BMP, FGF, WNT, and Hh), researchers hope to drive HC regeneration in adult mammals affected by sensorineural hearing loss due to HC loss or damage (reviewed in Rai et al., 2022).

1.4 Signaling Pathways Involved in Cochlear Sensory Development

Coordinated signaling cascades direct cochlear development (Munnamalai and Fekete, 2020), which can be broken down into two phases: large-scale cochlear patterning and fine-scale sensory patterning (Fig. 1.2). These phases are best understood in mice, where developmental events occur in stereotyped timing defined by the Thieler stages. Between the onset of cochlear development, around E11.5, and E13.5, the floor of the cochlear duct is

patterned along the medial-lateral axis into the Kölliker's organ that remodels into the inner sulcus, the prosensory domain that gives rise to the organ of Corti, and the outer sulcus (Ohyama et al., 2010). Cells within the prosensory domain undergo cell cycle exit in a sweep that starts at the apex around E12 and reaches the base by E15 (Chen and Segil, 1999; Ruben, 1967). The second phase of cochlear development is initiated around E14 when specified sensory progenitors begin to differentiate in a base-to-apex sweep (Chen et al., 2002). As differentiation and maturation progress, the sensory cells are arranged in the highly ordered mosaic characteristic of the mature organ of Corti. More specifically, HCs are organized into four rows, one row of iHCs and three rows of oHCs, and both HC subtypes are surrounded by distinct SC populations. Inner border cells and inner phalangeal cells extend projections that wrap around the medial and lateral faces of the iHCs, respectively. Each oHC is associated with a single Deiters' cell that extends a projection around its lateral face. Inner and outer pillar cells form the tunnel of Corti between the iHC and oHC regions (Pickles, 2012). This precise organization of HCs and SCs is essential for the mechanotransduction and amplification processes that enable hearing.

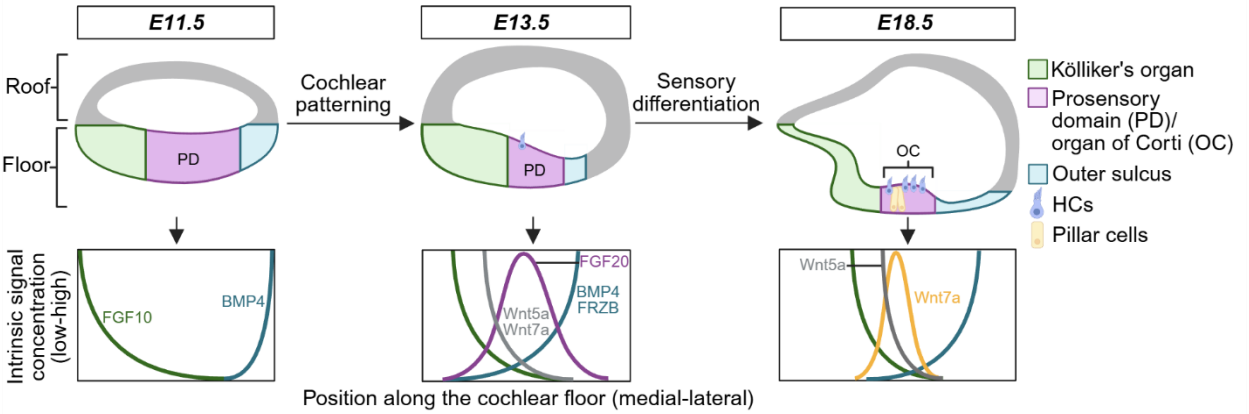

Figure 1.2. Gradients of intrinsic factors within the cochlear floor during development.

(modified version of figure from Groves and Fekete, 2012 created with Biorender.com)

(Top) Cross-sectional diagrams of cochleae at key developmental timepoints. **(Bottom)** Concentration gradients of intrinsic signals present within the cochlear floor at each timepoint.

1.4.1 Notch Signaling

Mammals express four canonical Notch receptors (Notch1-4) and five canonical ligands (JAG1/2 and DLL1/3/4). Activation of the pathway requires specific modifications to both receptors and ligands. With regards to the receptor, Notch signaling depends on the successive proteolytic cleavage of three sites (S1-S3; reviewed in Andersson et al., 2011; reviewed in D'Souza et al., 2010). Cleavage at the S1 site by furin-like convertases produces a heterodimeric receptor consisting of extracellular and transmembrane/intracellular domains (Logeat et al., 1998). This mature receptor is delivered from the Golgi apparatus to the cell membrane where it is poised to interact with Notch ligands on neighboring cells. Upon receptor-ligand binding, the ligand is ubiquitylated by E3 ubiquitin ligases Mindbomb or Neuralized. This modification promotes epsin-dependent ligand endocytosis and generates the mechanical force needed to expose the S2 cleavage site on the extracellular juxta-membrane region of the receptor (reviewed in Musse et al., 2012). The S2 site is then cut by ADAM metalloproteases (Brou et al., 2000; Mumm et al., 2000), and the remaining truncated Notch receptor undergoes a final intracellular cleavage at the intracellular juxta-membrane S3 site by γ-secretase (Struhl and Adachi, 2000), releasing the Notch intracellular domain (NICD). The NICD then translocates into the nucleus where it forms a complex with RBP-Jκ and MAML to recruit co-activators and drive transcription of effector genes (reviewed in Kopan and Ilagan, 2009).

Notch signaling plays two important roles in cochlear development (reviewed in Brown and Groves, 2020; reviewed in Kiernan, 2013; reviewed in Slowik and Bermingham-McDonogh, 2013b). First, Notch-mediated lateral induction drives establishment of the prosensory domain by E15 (Murata et al., 2006). During this window, prosensory cells express Notch1 and JAG1, the primary receptor-ligand pair associated with lateral induction in the cochlea (Basch et al., 2016b; Murata et al., 2006), and LFNG, a glycotransferase that strengthens Notch receptor affinity for DLL1 over JAG1 (Brückner et al., 2000; Hicks et al., 2000), is restricted to the

Kölliker's organ (Basch et al., 2016b; Ohyama et al., 2010). Second, Notch-mediated lateral inhibition drives differentiation of the sensory progenitors and sensory patterning starting around E14, when early HCs begin to suppress HC differentiation in neighboring SC precursors, thereby promoting the formation of the organized rows of HCs interdigitated with SCs (Murata et al., 2006). At the onset of lateral inhibition, *Jag1* expression is refined to exclude HC precursors, while *Lfng* expression is increasingly restricted to these cells. In addition to *Lfng*, the column of early HCs at the border between the prosensory domain and Kölliker's organ also express *Mfng*, another glycotransferase, as well as Notch ligands *Jag2*, *Dll2*, and *Dll3* (Basch et al., 2016b). Notch ligands and receptors expressed in the same cell attenuate each other's activity. LFNG and MFNG increase cis-inhibition between Notch1 and DLL1 but decrease cis-inhibition between Notch1 and JAG1 (LeBon et al., 2014). Like JAG1, JAG2 and DLL1 are conventional Notch ligands and signal through interactions with the Notch1 receptor (Kiernan et al., 2005a). DLL3, however, only acts through cis-inhibition (Chapman et al., 2011; Ladi et al., 2005). Because of their expression of *Lfng*, *Mfng*, and *Dll3*, early HCs undergo cis-inhibition and maintain lower levels of Notch activity compared with neighboring SC precursors, which experience minimal cis-inhibition and sustain higher levels of Notch activity. While HC Notch ligands are transiently expressed and downregulated during the first postnatal week (Hartman et al., 2007; Lanford et al., 1999; Morrison et al., 1999), expression of *Lfng*, *Mfng*, and *Jag1* persists in the mature organ of Corti. More specifically, LFNG and JAG1 are restricted to SCs (Morsli et al., 1998; Murata et al., 2006), while MFNG is restricted to HCs (Basch et al., 2016b). Though Notch ligands seem to be required for initial HC differentiation and not maintenance, increasing evidence points to Notch ligands being important in both differentiation and maintenance of SCs (Chrysostomou et al., 2020).

Downstream Notch effectors include basic helix-loop-helix transcription factors (HEY1/2, HEYL, and HES1/5) that repress the expression and activity of ATOH1 (Doetzlhofer et al., 2009; Hayashi et al., 2008a; Li et al., 2008; Tateya et al., 2011; Zheng and Gao, 2000; Zine et al.,

2001), the master transcription factor that drives HC differentiation (Bermingham et al., 1999). *Hey1/2* and *Hes1* are broadly expressed in the cochlear prosensory domain. While HEY1/2 prevent premature HC differentiation (Benito-Gonzalez and Doetzlhofer, 2014; Hayashi et al., 2008a), HES1 is thought to promote prosensory cell proliferation (Murata et al., 2009). Later, during lateral inhibition, HEY/HES transcription factors are upregulated in SC precursors where they work together to repress HC differentiation, and in turn, promote SC fates (Campbell et al., 2016; Woods et al., 2004). These transcription factors are expressed in distinct combinations that contribute to the unique identities of the SC subpopulations within the patterned organ of Corti (Doetzlhofer et al., 2009; Hartman et al., 2009; Hayashi et al., 2008a; Li et al., 2008; Zine et al., 2001). Together, these downstream Notch effectors orchestrate both the establishment of the prosensory domain and the precise arrangement of HCs and SCs along the organ of Corti.

1.4.2 BMP Signaling

In canonical BMP (Bone Morphogenic Protein) signaling, BMP ligands bind type I and type II serine/threonine kinase receptors to form a heterotetrameric complex. Type II receptors, being constitutively active, then transphosphorylate the type I receptors. Activated type I receptors proceed to phosphorylate receptor-regulated SMADs, which associate with co-mediator SMADs and translocate into the nucleus to regulate transcription (reviewed in Wang et al., 2014).

Canonical BMP4-mediated signaling plays a critical role in patterning the cochlear floor. *Bmp4* is expressed in outer sulcus of the developing cochlea starting around E11.5 (Fig. 1.2; Ohyama et al., 2010; Takemura et al., 1996). The morphogen is secreted from the this region and activates the SMAD-dependent BMP pathway, inducing SMAD-phosphorylation in a lateral-to-medial gradient within the cochlear floor (Ohyama et al., 2010). The *Id* genes are thought to be direct transcriptional targets of BMP signaling (Hollnagel et al., 1999; Nakahiro et al., 2010), and *Id1-3* are expressed in the cochlea where they suppress HC fates (Jones et al., 2006). High

BMP4 levels at the outer sulcus promote *Id2* expression and inhibit prosensory formation, intermediate levels promote prosensory cell specification, and little to no BMP4 leads to the formation of the Kölliker's organ (Ohyama et al., 2010). BMP4 suppresses Kölliker's organ development and a low level is necessary for the formation of the prosensory domain and outer sulcus.

1.4.3 FGF Signaling

FGFs (Fibroblast Growth Factors) are a group of secreted signaling molecules that bind receptor tyrosine kinases, FGFRs, and whose signaling is mediated by the ERK1/2 subfamily of MAPKs. Ligands and receptors associated with the FGF pathway are expressed in unique patterns within the developing cochlear epithelium (reviewed in Ebeid and Huh, 2017; reviewed in Groves and Fekete, 2012; reviewed in Munnamalai and Fekete, 2020). *Fgf10* can be detected in the Kölliker's organ as early as E11.5 (Fig. 1.2; Pauley et al., 2003; Pirvola et al., 2000). This ligand binds with high affinity to FGFR2b, which can be found in the outer sulcus as well as roof cells from the presumptive stria vascularis and Reissner's membrane by E13.5 (Hayashi et al., 2010; Pirvola et al., 2000). FGF10 is able to diffuse from the Kölliker's organ to these nonsensory regions where it has been proposed to promote BMP4 expression in the outer sulcus and to contribute to roof cell development (Hayashi et al., 2010; Pirvola et al., 2000; Urness et al., 2015). FGF9 and FGF20 can be detected in the presumptive Reissner's membrane at E11.5 and post-miotic prosensory domain at E13.5, respectively (Fig. 1.2; Hayashi et al., 2008b; Pirvola et al., 2004). Both ligands are thought to interact with FGFR1 (Hayashi et al., 2008b; Huh et al., 2012; Huh et al., 2015; Pirvola et al., 2002), which is broadly expressed throughout the cochlear epithelium around E13.5 before becoming restricted to the lateral compartment of the developing organ of Corti (Hayashi et al., 2008b; Hayashi et al., 2010; Pirvola et al., 2002). FGF9/20-FGFR1 signaling is important for prosensory cell proliferation and sensory cell specification (Hayashi et al., 2008b; Huh et al., 2015; Pirvola et al., 2002), and

FGF20-FGFR1 signaling is additionally critical for differentiation of lateral compartment sensory progenitors into oHCs and their associated SCs (Huh et al., 2012; Huh et al., 2015). *Fgf8* can first be detected in iHCs at the base of the developing cochlea around E16 (Jacques et al., 2007). While FGF8 is thought to have the potential to bind with FGFR1 and FGFR3 (Hayashi et al., 2007), the signaling molecule shows preferential binding with FGFR3 (Hayashi et al., 2007; Jacques et al., 2007). *Fgfr3* expression is restricted to the lateral compartment of the developing cochlear sensory epithelium starting around E15.5 (Hayashi et al., 2010). In Deiters' cell precursors, SPRY2, a member of the SPRY family of negative feedback regulators for receptor tyrosine kinases, antagonizes FGF8-FGFR3 signaling, thereby preventing these cells from adopting a pillar cell fate (Shim et al., 2005). In $FGFR3^{+}$ pillar cell precursors, SPRY1 is thought to downregulate *Spry2* expression, and consequently, promote their cell fate (Hayashi et al., 2007; Jacques et al., 2007; Mueller et al., 2002; Puligilla et al., 2007; Shim et al., 2005). In summary, FGF signaling promotes prosensory cell proliferation and sensory cell specification in addition to sensory patterning in the developing cochlea.

1.4.4 WNT Signaling

During WNT (Wingless-type MMTV integration site family) signaling, secreted WNT glycoproteins bind FZD receptors and co-receptors, and in turn, activate the signal transducing protein DVL. In the β-catenin-dependent canonical pathway, activated DVL sequesters a destruction complex composed of Axin, APC, and GSK3-β. In the absence of DVL activation, the destruction complex is free to phosphorylate β-catenin, marking the protein for degradation. Unphosphorylated β-catenin, however, accumulates and translocates into the nucleus where it associates with TCF/LEF transcription factors to regulate gene expression. Beyond the canonical pathway, WNT signaling also encompasses two major β-catenin-independent non-canonical pathways, one that requires calcium and another that does not. In the calcium-dependent pathway, DVL-triggered calcium release from the endoplasmic reticulum results in

the activation of calcium binding proteins that regulate the activity of the transcription factor NFAT. In the calcium-independent pathway, the activated DVL signals through GTPases RHOA and RAS, which activate serine/threonine protein kinases ROCK or JNK. Both canonical and non-canonical WNT signaling pathways play important roles during cochlear development (reviewed in Jansson et al., 2015).

Members of the WNT pathway are expressed throughout the developing cochlear epithelium and in patterns that are both unique and dynamic. By E12.5, *Wnt4* is expressed in the presumptive Reissner's membrane, *Wnt5a* is strongly expressed in the early stria vascularis and weakly in the Kölliker's organ, *Wnt7a* is expressed in the cochlear floor, *Wnt7b* is expressed throughout the cochlear epithelium, and *Fzd3* shows broad expression across the cochlear epithelium (Fig. 1.2; Bohnenpoll et al., 2014). While the majority of WNT inhibitors are expressed at higher levels during postnatal stages (Geng et al., 2016), FRZB and DKK3 are notable exceptions that can be detected in the outer sulcus and Kölliker's organ, respectively, shortly after patterning of the cochlear floor (Fig. 1.2; Geng et al., 2016; Qian et al., 2007).

During early cochlear development, the canonical WNT pathway is essential for prosensory cell proliferation and subsequent HC differentiation (Jacques et al., 2012). β -catenin in combination with TCF/LEF transcriptional co-activators has been shown to directly promote *Atoh1* expression in neural progenitor cells (Shi et al., 2010), and the co-activators are thought to similarly promote *Atoh1* expression in differentiating HCs (Jacques et al., 2012). During later stages of development, non-canonical WNT signaling directs the initial position of the HC stereocilia bundles and later refines their alignment (Cotanche and Corwin, 1991; Dabdoub et al., 2003; Denman-Johnson and Forge, 1999; reviewed in Jansson et al., 2015), steps that are critical for proper deflection of stereocilia bundles in response to sound. During the developmental window associated with HC bundle orientation refinement, *Wnt7a* is the most abundantly expressed WNT ligand and is restricted to pillar cells that are thought to secrete the signal to both iHCs and oHCs (Fig. 1.2; Dabdoub et al., 2003). Interesting, FZD receptors and

DVL signal transducing proteins are expressed asymmetrically within the HCs. FZD3, FZD6, and DVL1 are found on the medial face of HCs, while DVL2 and DVL3 are found on the lateral face (Najarro et al., 2020). In short, WNT signaling plays an important role in prosensory proliferation, HC differentiation, and HC stereocilia bundle orientation.

1.4.5 Hh Signaling

Unlike the aforementioned signals, which are intrinsic to the cochlea, SHH is an extrinsic factor important in cochlear development. The Hh (Hedgehog) ligand is released from the spiral ganglion and diffuses to the developing cochlea where it interacts with PTCH receptors, de-represses SMO, and promotes GLI-mediated transcription of target genes. Hh signaling decouples prosensory cell proliferation from sensory cell differentiation in the cochlea, enabling these processes to occur in opposing gradients along the length of the cochlear duct and during distinct temporal windows (reviewed in Qin and Bronner, 2025). More specifically, SHH suppresses HC differentiation (Bok et al., 2013; Driver et al., 2008; Tateya et al., 2013). SHH-induced Hh signaling activity in the developing cochlea decreases in a base-to-apex sweep that parallels the sweep of HC differentiation (Bok et al., 2013). In the absence of SHH, cochleae undergo premature cell cycle exit and sensory differentiation, which lead to reduced cochlear duct outgrowth (Bok et al., 2013; Tateya et al., 2013). Hh signaling is critical for proper coordination of proliferation and differentiation in the cochlea, and consequently, normal morphogenesis.

1.5 Early B Cell Factors

COE (Collier, OLF, EBF) proteins form a group of evolutionarily conserved helix-loop-helix transcription factors distinguished by a unique DNA binding domain that contains an atypical zinc finger motif referred to as a zinc knuckle (reviewed in Dubois and Vincent, 2001; Fields et al., 2008; reviewed in Liberg et al., 2002). In mammals, the EBF (Early B cell Factor)

family comprises four members (EBF1-4) that are known for their importance in developmental processes, including cell fate decisions, differentiation, and migration (reviewed in Liberg et al., 2002). In addition to their characteristic N-terminal DNA binding domains, EBFs are composed of a transcription factor immunoglobulin (TIG/IPT) domain, helix-loop-helix domain, and C-terminal transactivation domain (Hagman et al., 1995). Via interactions between their helix-loop-helix domains, EBFs form stable homodimers and bind a palindromic consensus DNA motif (5'-TCCCNNGGGA-3'; Hagman et al., 1993; Travis et al., 1993).

EBF1, the most extensively studied member of the EBF family, is best known for its roles in B cell progenitor proliferation and differentiation (Hagman et al., 1993; Lin and Grosschedl, 1995; Pongubala et al., 2008; Thal et al., 2009), during which it acts as both a transcriptional activator and repressor (Li et al., 2018; reviewed in Ramírez et al., 2010; Treiber et al., 2010). EBF1 also recruits BRG1, the catalytic subunit of the SWI/SNF (BAF) chromatin remodeling complex, via its C-terminal transactivation domain to facilitate the transition from progenitor to B-lineage-committed accessible chromatin (Wang et al., 2020; Zolotarev et al., 2022). In addition to immune cell development, EBF1 is known to regulate adipocyte differentiation (Jimenez et al., 2007), bone metabolism (Nelson et al., 2024; Nieminen-Pihala et al., 2021), and neurogenesis (Catela et al., 2019; Davis and Reed, 1996; Garel et al., 2000; Garel et al., 1999; Garel et al., 1997; Lobo et al., 2008; Wang and Reed, 1993; Wang et al., 1997). In the olfactory system, for example, EBF1, also called OLF1, promotes olfactory receptor neuron maturation (Cheng and Reed, 2007; Roby et al., 2012; Tsai and Reed, 1997; Tsai and Reed, 1998; Wang et al., 1997). Like EBF1, EBF2 and EBF3 have reported roles specifically in olfactory receptor neuron development (Wang et al., 2004; Wang et al., 1997) and more broadly in neuronal development within both the central and peripheral nervous systems (Baek et al., 2014; Catela et al., 2019; reviewed in Dubois and Vincent, 2001; Garel et al., 2000; Garel et al., 1997; Iwai et al., 2018; Yang et al., 2015). EBF2 also has reported roles in adipogenesis like EBF1 (Jimenez et al., 2007). The final member of the EBF family, EBF4, remains the least characterized and

has been linked to cytotoxic function in immune cells (Kubo et al., 2022). EBFs have diverse and overlapping roles in development.

1.5.1 Interactions Between EBFs and Signaling Pathways

EBFs participate in crosstalk with major signaling pathways. During B cell lineage specification, E2A proteins (E12 and E47) promote *Ebf1* expression (Greenbaum and Zhuang, 2002; Kee and Murre, 1998; Roessler et al., 2007; Smith et al., 2002). EBF1 then activates *Pax5* (Decker et al., 2009), and together these two transcription factors are thought to downregulate Notch signaling and repress transcription factor genes that specify alternative hematopoietic cell fates (Pongubala et al., 2008; Souabni et al., 2002; Thal et al., 2009). Downregulation of Notch signaling is likely an essential precursor for EBF1 activity, as Notch1 intracellular domain reduces EBF-binding activity (Smith et al., 2005). In addition to Notch, EBFs interact with the BMP pathway. EBF1 downregulates expression of downstream BMP effector genes, *Id2* and *Id3*, during B cell specification (Thal et al., 2009), and ID1 is reported to directly bind and suppress EBF2 transcriptional activity during adipogenesis (Patil et al., 2017). EBFs have documented interactions with the Notch and BMP pathway during development.

1.5.2 EBF1 Expression in the Inner Ear

The Bermingham-McDonogh lab has been looking for novel factors that regulate sensory development in the cochlea to identify potential novel targets for stimulating HC regeneration. One such factor is EBF1. The transcription factor is thought to function downstream of DLX5 (Sajan et al., 2011), which is important in inner ear morphogenesis (Johnson et al., 2018), and SOXC transcription factors (Sun et al., 2013; Wang et al., 2023), which are essential for establishing sensory competence in the developing cochlea (Gnedeva and Hudspeth, 2015; Wang et al., 2023). A previous bulk ATAC-seq study from our lab found enrichment of the EBF consensus binding motifs in the open chromatin of the prosensory cells

that give rise to HCs and SCs (Wilkerson et al., 2019). Consistent with EBF1's well-documented interactions with the Notch signaling pathway in developmental contexts (reviewed in Dubois and Vincent, 2001; Pongubala et al., 2008), we noted EBF motif enrichment within and around the loci of Notch-related genes like *Jag1*, *Lfng*, and *Hes1*. Subsequent single cell RNA-seq analyses revealed that *Ebf1* is expressed in the developing cochlear epithelium while *Ebf2-4* show little to no expression. To investigate the role of EBF1 in cochlear development, I generated *Ebf1* conditional knockout mice. In this dissertation, I describe the role of EBF1 in cochlear development. I characterize the conditional knockout phenotypes in Chapter 2, and Chapter 3 presents multiome sequencing that I used to identify and characterize EBF1's interactions with the signaling pathways important in cochlear development. Lastly, I summarize the impact of this work and possible future directions in Chapter 4.

CHAPTER 2: Deletion of the *Ebf1*, a Mouse Deafness Gene, Causes a Dramatic Increase in Hair Cells and Support Cells of the Organ of Corti

The contents of this chapter have been published in the following journal article:

Powers, K. G., Wilkerson, B. A., Beach, K. E., Seo, S. S., Rodriguez, J. S., Baxter, A. N., Hunter, S. E. and Bermingham-McDonogh, O. (2024). Deletion of the Ebf1, a mouse deafness gene, causes a dramatic increase in hair cells and support cells of the organ of Corti. *Development* **151**. doi: 10.1242/dev.202816

Contributions by authors to the contents of this chapter were as follows:

Conceptualization: K.G.P., B.A.W., O.B.Mc.D.; Methodology: K.G.P., B.A.W., K.E.B., S.S.S., J.S.R., A.N.B., S.E.H.; Validation: K.E.B., O.B.Mc.D.; Formal analysis: K.G.P., B.A.W., J.S.R., O.B.Mc.D.; Investigation: K.G.P., B.A.W., K.E.B., J.S.R., S.E.H., O.B.-M.; Resources: O.B.Mc.D.; Data curation: K.G.P., B.A.W., K.E.B., S.S.S., J.S.R., A.N.B., S.E.H., O.B.Mc.D.; Writing - original draft: K.G.P., B.A.W., O.B.Mc.D.; Writing - review & editing: K.G.P., B.A.W., O.B.Mc.D.; Visualization: K.G.P., B.A.W., K.E.B., S.S.S., J.S.R., A.N.B., O.B.Mc.D.; Supervision: O.B.Mc.D.; Project administration: O.B.Mc.D.; Funding acquisition: K.G.P., O.B.Mc.D.

2.1 Abstract

Following up on our previous observation that early B cell factor (EBF) sites are enriched in open chromatin of the developing sensory epithelium of the mouse cochlea, we investigated the effect of deletion of *Ebf1* on inner ear development. We used a Cre driver to delete *Ebf1* at the otocyst stage before development of the cochlea. We examined the cochlea at P1 and found that the sensory epithelium had doubled in size but the length of the cochlear duct was unaffected. We also found that deletion of *Ebf1* led to ectopic sensory patches in the Kölliker's organ. Innervation of the developing organ of Corti was disrupted with no obvious spiral bundles. The ectopic patches were also innervated. All the extra hair cells (HCs) within the sensory epithelium and Kölliker's organ contained mechanoelectrical transduction channels as indicated by rapid uptake of FM1-43. The excessive numbers of HCs were still present in the adult *Ebf1* conditional knockout (cKO) animal. The animals had significantly elevated auditory brainstem response thresholds, suggesting that this gene is essential for hearing development.

2.2 Introduction

The inner ear contains the sensory structures necessary for our sense of both hearing and balance. A single sensory structure mediates hearing, the organ of Corti, which is the sensory region of the cochlear duct. It consists of one row of inner hair cells (iHCs) and three rows of outer HCs (oHCs), all with attendant support cells (SCs) and an extremely regular arrangement along the ventral cochlear duct. The inner border cell (iBC) and inner phalangeal cell (iPhC) are associated with the iHC. iBC projections wrap around the medial face of iHCs, and iPhC projections wrap around the lateral face. Each oHC is associated with a single Deiters' cell (DC). In between these HC/SC groups there are two pillar cells (PCs); the one closest to the iHC is called the inner PC (iPC) and the one closest to the oHCs is called the outer PC (oPC). These PCs form the fluid-filled tunnel of Corti without which the animal cannot hear (Colvin et

al., 1996; Hayashi et al., 2007). The development, position, and arrangement of these HCs and SCs are dependent on various signaling molecules from multiple families of growth factors expressed in medial (neural) to lateral (abneural) gradients (reviewed in Driver and Kelley, 2020; reviewed in Groves and Fekete, 2012). For example, there is a strong expression of BMP4 at the lateral side, which likely restricts the sensory domain in this direction (Ohyama et al., 2010). However, what exactly restricts the development of sensory cells medially is not known. This study investigating the role of EBF1 in developing cochleae suggests that the expression of this transcription factor establishes the medial border of the sensory domain.

In our analysis of the epigenetic regulation of cochlear development we discovered an enrichment of EBF transcription factor binding motifs in the open chromatin of SOX2-EGFP prosensory cells (Wilkerson et al., 2019). Other transcription factors known to be important in sensory development were also found. This suggests that a member of the EBF family of transcription factors is likely to play a role in the development of the organ of Corti. We looked at single cell RNA-seq obtained from developing cochleae at the same ages as the ATAC-seq samples and discovered that EBF1 is likely the EBF family member involved. Indeed, the expression of *Ebf1* in the inner ear was first described by Davis and Reed (1996) and later revealed in the Allen Brain Atlas.

EBF1 is a member of the COE (Collier, OLF1, and EBF1-4) family of transcription factors. The EBFs are helix-loop-helix proteins containing an unusual Zn coordinating domain that binds to DNA. *Ebf genes* are expressed in many parts of the nervous system and frequently co-expressed with other family members. Mutations in a single *Ebf* gene can often be compensated for by another family member; thus, loss of function of a single *Ebf* gene reveals a phenotype if it is the only member of the family expressed. This appears to be the case in the developing cochlear epithelium, as there is little to no expression of *Ebf2*, *Ebf3*, and *Ebf4*.

In this study, we examine the effect of deleting *Ebf1* from the otic epithelium on the developing cochlea using a tissue-restricted Cre or a tamoxifen-inducible Cre. We find that there

is a dramatic increase of both iHCs and oHCs, and their attendant SCs in the mice with the conditional deletions. The mutant mice also have ectopic patches of sensory epithelia that develop in Kölliker's organ, suggesting that EBF1 is suppressing sensory development in this medial region. The expanded sensory domain is innervated, but the outer spiral bundles do not develop normally in the *Ebf1* mutant mouse. The ectopic HCs we see in the non-sensory Kölliker's organ are also innervated and are surrounded by SCs. Interestingly these extra iHCs and oHCs are retained in the adult cochlea; however, the mice are severely hearing impaired.

2.3 Results

Ebf1 is expressed in Kölliker's organ, prosensory cells, HCs, and SCs of the developing cochlea

Recent work from our lab identified enrichment of EBF-binding motifs in the open chromatin of cochlear prosensory cells collected at key developmental time points (Wilkerson et al., 2019). To investigate *Ebf* gene expression in the developing cochlear sensory epithelium, we performed single cell RNA-seq on SOX2-EGFP^{+} cells FAC-sorted from E12, E14, and E16 cochlear ducts. Clustering the cells after sequencing using Seurat allowed us to identify the various cell types present in the sample. We were able to capture the major cell types (prosensory cells, iHCs, oHCs, SCs, neurons, glia, Kölliker's organ cells, cycling cells, roof cells, mesenchymal cells, and outer sulcus cells) present during these three developmental time points (Fig. 2.1A). Our analysis of the SOX2-EGFP^{+} single cells revealed that *Ebf1* is expressed in the developing cochlear epithelium whereas *Ebf2*, *Ebf3*, and *Ebf4* show little to no expression (Fig. 2.1C). More specifically, *Ebf1* is strongly expressed in prosensory cells, iHCs, oHCs, SCs, neurons, Kölliker's organ cells, cycling cells, and mesenchymal cells (Fig. 2.1A, C). In situ hybridization of the E14.5 inner ear confirmed our single cell results. *Ebf1* transcript expression was detected in the ventral cochlear duct, spiral ganglion, and mesenchyme (Fig. 2.1B).

Our transcript analyses indicated that *Ebf1* is the primary contributor to EBF protein expression in the developing cochlear sensory epithelium (Fig. 2.1A-C). To further explore the timing and localization of EBF expression, immunolabeling was performed using a pan-EBF antibody. At E12.5, EBF protein is expressed in a band that overlaps with the medial edge of the expression domain for SOX2 (Fig. 2.1D, D'), a well-known prosensory marker (Kiernan et al., 2005b). At E14.5, EBF protein expression extends medially into Kölliker's organ and overlaps with the SOX2 domain (Fig. 2.1E-E''). By E16.5, MYO7a^{+} HCs can be seen in the base and middle of the cochlear sensory epithelium (Sahly et al., 1997). At this stage, EBF protein is most strongly expressed in the population of SOX2^{+} Kölliker's organ cells immediately medial to the iHC row (Fig. 2.1F-F'') and shows comparatively weak expression in HCs and SCs of the sensory domain (bracket in Fig. 2.1F''). Although the developing cochlea maintains strong expression of EBF proteins in Kölliker's organ by E18.5 (Fig. 2.1G-G''), expression is diminished in the sensory cells, particularly in iHCs (bracket in Fig. 2.1G''). We continue to see EBF immunolabeling in the DCs and iPhCs of the adult organ of Corti (see below).

Deletion of Ebf1 in the otic vesicle at E9.5 leads to dramatic expansion in the sensory domain of the cochlea and the formation of ectopic sensory patches in Kölliker's organ

To investigate the role of EBF1 in cochlear development, we generated a conditional knockout (cKO) mouse in which the *Slc26a9* promoter directs Cre-mediated excision of floxed *Ebf1* exons 6-16 (Vilagos et al., 2012). SLC26A9 is a chloride transporter present at E9.5 in the otic vesicle that gives rise to the inner ear epithelium (Urness et al., 2020). Unlike the *Ebf1* global knockout (KO), which is postnatal lethal (Nelson et al., 2019), *Slc26a9*$^{Ebf1\text{-}cKO}$ mice are fertile and survive into adulthood. The cochleae of mice with the conditional deletion lose EBF immunolabeling in the cochlear epithelium but maintain EBF expression in the mesenchyme (Fig. 2.S1), likely due to *Ebf3* and *Ebf4*, which show low expression levels in the otic epithelium in our single cell analyses (Fig. 2.1C).

To determine the effects of loss of EBF1 in the developing cochlea, we analyzed P1 cochlear wholemounts of control and *Slc26a9*$^{Ebf1\text{-}cKO}$ mice. We found a dramatic expansion of the sensory epithelium in the mutant mice (Fig. 2.2). Unlike control littermates with the expected single row of iHCs (vGLUT3^{+} and MYO7a^{+}) and three rows of oHCs (vGLUT3^{-} and MYO7a^{+}; Fig. 2.2E-G), mice with the conditional deletion possess three to five rows of iHCs medial to approximately six rows of oHCs (Fig. 2.2K-M). *Slc26a9*$^{Ebf1\text{-}cKO}$ cochlear ducts exhibit approximately threefold and twofold increases, respectively, in iHC and oHC counts by P1 (Fig. 2.2Q). *Slc26a9*$^{Ebf1\text{-}cKO}$ neonates also demonstrate a delayed base-to-apex sweep of vGLUT3 expression relative to littermate controls (Fig. 2.2A, B versus C, D), suggesting a developmental delay in cochlear maturation. However, the lengths of P1 *Slc26a9*$^{Ebf1\text{-}cKO}$ and littermate control cochlear ducts are not significantly different ($P > 0.05$, Welch's t-test, 4598.1 ± 493.6 μm for nine *Slc26a9*$^{Ebf1\text{-}cKO}$ mice and 4653.2 ± 349.7 μm for nine littermate controls from four litters; one duct per mouse).

To determine whether the extent of HC expansion varies along the length of the cochlear duct in the mutant mice, we quantified HC density in the base, middle, and apex of cochlear wholemounts. Compared with littermate controls, iHC and oHC densities are significantly greater in all regions of the *Slc26a9*$^{Ebf1\text{-}cKO}$ samples (Fig. 2.2R, S and Table 2.S1). Although the mutants show an overall increase in HC density across all regions, the increase was greatest at the base for both iHCs and oHCs (Table 2.S1). The increases in HCs are accompanied by defects in either stereocilia bundle or HC orientation. The supernumerary iHCs in the mutant are arranged on either side of the space presumably formed by the developing tunnel of Corti (Fig. 2.2K). Although we did not quantify the support cell increases, there was a clear expansion of the SOX2^{+} domain (Fig. 2.2H-J versus N-P)

In addition to an excess of sensory cells within the sensory domain, the *Slc26a9*$^{Ebf1\text{-}cKO}$ mice also possess ectopic sensory patches throughout their Kölliker’s organs (arrowheads in Fig. 2.2C, D). These ectopic patches resemble miniature vestibular organs, consisting of

vGLUT3^{+} HCs resting on a bed of SCs that do not express the markers characteristic of sensory domain SCs (magnified inset capturing the ectopic patch outlined in Fig. 2.2D and Fig. 2.S2). *Slc26a9$^{Ebf1\text{-}cKO}$* supernumerary and ectopic patch HCs have functioning mechanoelectrical transduction (MET) channels, as demonstrated by their uptake of FM1-43 dye (Fig. 2.S3).

Increases in HC numbers in the Slc26a9$^{Ebf1\text{-}cKO}$ mice are accompanied by increases in SCs

Supernumerary HCs are neighbored by supernumerary SCs (Fig. 2.2N-P), and mutant mice exhibit more nuclear layers in in Kölliker's organ than littermate controls (Fig. 2.3A, A' versus B, B'). We measured the areas of the developing sensory domain and Kölliker's organ in the base of mid-modiolar sections collected from P1 *Slc26a9$^{Ebf1\text{-}cKO}$* and littermate control mice. Anti-SOX2 antibody was used to visualize the developing sensory domain in the base of mid-modiolar sections collected from P1 *Slc26a9$^{Ebf1\text{-}cKO}$* and littermate control mice (Fig. 2.3). As expected, we found that the area of SOX2 expression was significantly greater in *Slc26a9$^{Ebf1\text{-}cKO}$* than littermate control sections ($P < 0.05$, 2534 ± 682 μm^2 for *Slc26a9$^{Ebf1\text{-}cKO}$* and 1751 ± 331 μm^2 for littermate controls; Table 2.S1). Similarly, we used a marker unique to Kölliker's organ, PRDM16, to assess changes in the overall size of this transient structure (Ebeid et al., 2022). We found that the area of PRDM16^{+} expression was significantly greater in *Slc26a9$^{Ebf1\text{-}cKO}$* than in littermate control sections ($P < 0.05$, 4391 ± 940 μm^2 for *Slc26a9$^{Ebf1\text{-}cKO}$* and 3146 ± 398 μm^2 for littermate controls; Table 2.S1). The Kölliker's appears to increase in size along with the sensory domain, in the mutant mice.

To better characterize the increase in SCs of the sensory domain, we used several markers to identify SC subtype-specific changes in patterning within the base of P1 mid-modiolar sections. In addition to anti-SOX2 antibody, anti-jagged1 (JAG1) antibody was used to examine overall SC expansion. At P1, JAG1 is expressed in sensory domain SCs and lateral Kölliker's organ cells, and SOX2 expression overlaps with JAG1 and extends more medially into Kölliker's organ. The expression domain of JAG1 is expanded in cochlear sections from the

mutant mice compared with littermate controls (Fig. 2.3C, C' versus D, D'). To determine which SC subtypes contribute to the observed SC expansion in the mutant mice, we used specific markers for iBCs, iPhCs, iPCs, oPCs, and DCs. When compared with littermate controls, the mutant mice exhibited an increase in anti-FABP7 labeled iBCs/iPhCs (arrows in Fig. 2.3E, E' versus F, F') and anti-PROX1 labeled PCs and DCs, (Fig. 2.3G, G' versus H, H'). Further analysis with anti-p75 and anti-CD44 antibodies, which label iPCs and oPCs (Hertzano et al., 2010; Knipper et al., 1996), respectively, indicates that increases in oPC and DC numbers likely account for the observed increases in PROX1^{+} nuclei. Although multiple CD44^{+} oPCs can be seen in *Slc26a9*$^{Ebf1\text{-}cKO}$ cochlear sections, only one p75^{+} (NGFR) iPC is typically seen (arrowheads in Fig. 2.3J-J'''). Cells lateral to the oHCs do not demonstrate changes in their numbers. FABP7 is expressed by Hensen's cells (HeCs) in addition to iBCs and iPhCs, and CD44 is expressed by Claudius cells (CCs) in addition to oPCs. Compared with littermate control cochlear sections, HeC and CC populations are unchanged in *Slc26a9*$^{Ebf1\text{-}cKO}$ cochlear samples (Fig. 2.3E, E', I, I''' versus F, F', J, J''').

To further investigate the effects of *Ebf1* deletion in patterning of medial SCs, we performed immunolabeling on P1 cochlear wholemounts. Anti-FABP7 labeling revealed that mice with a conditional deletion of *Ebf1* possess more than the typical two rows of iBCs/iPhCs (arrows in 2.4A-A''' versus B-B'''). In the mutant cochlea, FABP7^{+} iBCs/iPhCs reside next to the medial and/or lateral faces of supernumerary HCs that resemble iHCs in their cell shape and position along the medial-lateral axis (arrows in Fig. 2.4B-B'''). The occasional iHC can be observed in the oHC region (Fig. 2.2K and Fig. 2.4B-B'''). Even among the oHCs, this iHC continues to direct patterning of a FABP7^{+} iBCs/iPhCs (Fig. 2.4B-B'''). Like iBCs/iPhCs, *Slc26a9*$^{Ebf1\text{-}cKO}$ cochlear ducts possess more CD44^{+} oPCs than littermate controls. Although controls possess a single continuous row of oPCs lateral to the row of iPCs (Fig. 2.4C-C'', G-G'''), *Slc26a9*$^{Ebf1\text{-}cKO}$ samples exhibit at least two discontinuous rows of oPCs lateral to their iPCs (Fig. 2.4D-D''', H-H'''). Although the *Ebf1* deletion induces an increase in many types of SCs, it

does not appear to increase iPC numbers. p75^{+} iPCs are present in a single row in both littermate control and *Slc26a9*$^{Ebf1\text{-}cKO}$ cochlear ducts (Fig. 2.4C-C’’’, E-E’’’ versus D-D’’’, F-F’’’).

Loss of Ebf1 expression leads to prolonged prosensory cell proliferation and delayed sensory cell differentiation

The increase in sensory cell numbers after *Ebf1* deletion suggests that the proliferation of the sensory progenitors may be prolonged in the mutant mice. To assess whether loss of EBF1 leads to prosensory cell proliferation beyond the typical E12-E15 window (Ruben, 1967), we performed EdU labeling on pregnant dams carrying *Slc26a9*$^{Ebf1\text{-}cKO}$ and control littermates. EdU was administered twice a day for 3 days starting on E15.5, and cochlear wholemounts were analyzed at P1 (Fig. 2.5G). Although HCs and attendant SCs fail to incorporate EdU in control cochleae (Fig. 2.5A-B’), many HCs and SCs in the sensory domains of *Slc26a9*$^{Ebf1\text{-}cKO}$ are EdU^{+} (open arrowheads in Fig. 2.5C-D’). Quantitative analysis of EdU^{+} iHC and oHC density revealed that the cochleae of the mutant mice possess significantly more EdU^{+} HCs than samples from littermate controls (Fig. 2.5E, F and Table 2.S1). The increase in EdU^{+} HCs is present in the *Slc26a9*$^{Ebf1\text{-}cKO}$ samples throughout the extent of the cochlea, with more EdU^{+} oHCs in the apex followed by the base and middle of *Slc26a9*$^{Ebf1\text{-}cKO}$ cochlear ducts (Table 2.S1). These results suggest that prolonged cell proliferation in the prosensory cells likely contributes to the sensory expansion seen after *Ebf1* deletion.

The precise coordination of cell cycle exit and sensory cell differentiation are essential for cochlear development (Benito-Gonzalez and Doetzlhofer, 2014; reviewed in Driver and Kelley, 2020). To assess whether delayed cell cycle exit in *Slc26a9*$^{Ebf1\text{-}cKO}$ mice is accompanied by delayed differentiation, we measured the sweep of MYO7a expression at E16.5 (Fig. 2.S4), well after the onset of HC differentiation (Chen et al., 2002). The distance from the apex to the first MYO7a^{+} cell is significantly greater in *Slc26a9*$^{Ebf1\text{-}cKO}$ cochlear ducts than in control cochlear ducts. This difference is not due to impaired formation of the SOX2^{+} prosensory domain, which

suggests that the sweep of differentiation is delayed in *Slc26a9*$^{Ebf1\text{-}cKO}$ samples (Fig. 2.S4A'', B'', C). At E16.5, it is worth mentioning that the lengths of *Slc26a9*$^{Ebf1\text{-}cKO}$ and control cochlear ducts are significantly different, suggesting that convergent extension is delayed ($P < 0.01$, 3724 ± 120 μm for *Slc26a9*$^{Ebf1\text{-}cKO}$ and 4463 ± 287 μm for littermate controls; Table 2.S1). By P1, *Slc26a9*$^{Ebf1\text{-}cKO}$ and littermate control ducts are similar in length.

Supernumerary HCs and SCs survive in adult Slc26a9$^{Ebf1\text{-}cKO}$ *mice*

Our results on the developing cochlea show dramatic sensory expansion in mice with a conditional deletion in *Ebf1*; to assess whether this phenotype persists in adult mice, we performed immunolabeling on mid-modiolar cochlear sections collected from P60 *Slc26a9*$^{Ebf1\text{-}cKO}$ and littermate control mice. Much like *Slc26a9*$^{Ebf1\text{-}cKO}$ neonatal cochleae (Fig. 2.S1B, B'), adult *Slc26a9*$^{Ebf1\text{-}cKO}$ cochleae continue to express EBFs in their mesenchymal cells and show little to no EBF expression in the cochlear sensory epithelium (Fig. 2.6B, B'). Control littermates exhibit EBF expression in their SCs in addition to their mesenchymal cells (Fig. 2.6A, A'). To examine the effects of *Ebf1* deletion in SC survival and maturation in the adult mice, we looked at expression of several HC and SC markers. We found that in adult mutant mice, the increase in SC numbers persisted, and strikingly, the additional SCs appear to give rise to multiple tunnels of Corti (asterisks in Fig. 2.6D'', D''', F, F'''). To assess HC survival and maturation, we performed labeling using anti-vGLUT3 and anti-prestin antibodies. We found that there was a loss in oHCs in the base of a subset of adult *Slc26a9*$^{Ebf1\text{-}cKO}$ cochleae; however, supernumerary HCs appear to survive throughout the rest of the duct. Adult supernumerary vGLUT3^{+} iHCs are typically found medial to tunnels of Corti, although the occasional vGLUT3^{+} iHC can be seen in the PC region (open arrowhead in Fig. 2.6F, F'). Neurofilament (NF-M) labeling indicates that supernumerary iHCs and oHCs are innervated (Fig. 2.6F'''). Interestingly, *Slc26a9*$^{Ebf1\text{-}cKO}$ mice demonstrate significantly elevated auditory brainstem response (ABR) thresholds for all tested

stimulus frequencies except 60 kHz. These results suggest that adult *Slc26a9*$^{Ebf1\text{-}cKO}$ mice are deaf (Fig. 2.6G, H).

Loss of Ebf1 expression leads to aberrant innervation in the sensory domain and ectopic sensory patches are innervated

HCs are known to secrete neurotrophins that direct their innervation by spiral ganglion neurons (Fariñas et al., 2001; reviewed in Fritzsch et al., 1997). To determine whether supernumerary HCs are innervated, we performed immunolabeling with anti-NF-M antibodies. P1 littermate control mice demonstrate the typical innervation pattern. Numerous neuronal projections terminate on iHCs (arrowheads in Fig. 2.7A''), and the type II afferent projections turn towards the base, innervating multiple oHCs in the same row and forming three spiral bundles (Fig. 2.7A, A') (Liberman et al., 1990). Although fibers continue to terminate on *Slc26a9*$^{Ebf1\text{-}cKO}$ iHCs (arrowheads in Fig. 2.7B''), the spiral bundles are completely lost in the oHC region and the innervation appears disorganized (Fig. 2.7B, B'). In addition to fibers extending to supernumerary HCs in sensory domain, HCs in the ectopic sensory patches of Kölliker's organ are also innervated (Fig. 2.7C-C'').

Deletion of Ebf1 in the developing sensory epithelium at E11 leads to moderate expansion in the sensory domain

The *Slc26a9*$^{Ebf1\text{-}cKO}$ mice show the effects of the loss of the *Ebf1* gene at a very early stage of cochlear development (E9.5). To determine the role of EBF1 at later stages of development, we used an inducible Cre-mouse line: *Sox2*^{CreER}. This second Cre-line was crossed to *Ebf1*$^{fl/fl}$ mice, and then *Ebf1* deletion was induced with two tamoxifen treatments: one at E11 and another at E12. Owing to tamoxifen toxicity (Ved et al., 2019), we opted to analyze these litters at E18 (Fig. 2.8O). iHCs were distinguished from oHCs based on their position relative to the developing tunnel of Corti. At E18, *Sox2*$^{Ebf1\text{-}cKO}$ mice show extra iHCs and oHCs in

an apically-biased manner. In the apex, iHC density and oHC density are both significantly greater in *Sox2*$^{Ebf1\text{-}cKO}$ than *Sox2*^{CreER}-negative control samples. In the middle, iHC density is greater in *Sox2*$^{Ebf1\text{-}cKO}$ than that in *Sox2*^{CreER}-negative controls. *Sox2*$^{Ebf1\text{-}cKO}$ cochlear ducts show no difference in oHC density in the middle and no differences in HC density in the base (Fig. 2.8M, N and Table 2.S1). In *Sox2*$^{Ebf1\text{-}cKO}$ cochlear ducts, most of the extra iHCs are in a second row medial to the main row and instances of oHCs in a fourth row could be observed. Alignment of oHC rows is imperfect in *Sox2*$^{Ebf1\text{-}cKO}$ samples (Fig. 2.8G-I). Loss of EBF1 in the developing sensory epithelium at E11/12 does not significantly affect cochlear duct length ($P > 0.05$, Welch's t-test, 3592.3 ± 581.0 μm for seven *Sox2*$^{Ebf1\text{-}cKO}$ and 4042.6 ± 476.9 μm for 13 *Sox2*^{CreER}-negative controls, five litters; one duct per mouse). To discriminate between the effects of *Ebf1* deletion and *Sox2* haploinsufficiency on HC formation (Atkinson et al., 2018), we compared HC density in *Sox2*^{CreER} *Ebf1*$^{fl/fl}$ mice not treated with tamoxifen with that of *Sox2*^{CreER}-negative littermate controls treated with tamoxifen (13.0 ± 0.8 iHCs and 51.8 ± 2.8 oHCs per 100 μm in the base, 16.2 ± 0.4 iHCs and 53.0 ± 2.8 oHCs per 100 μm in the middle, 15.7 ± 0.5 iHCs and 49.3 ± 2.3 oHCs per 100 μm in the apex for three *Sox2*^{CreER} *Ebf1*$^{fl/fl}$ mice not treated with tamoxifen; one duct per mouse). No significant differences were observed in HC density of *Sox2*^{CreER} *Ebf1*$^{fl/fl}$ mice not treated with tamoxifen and the *Sox2*^{CreER}-negative control samples ($P > 0.05$, two-way ANOVA with Tukey's multiple comparison's test).

2.4 Discussion

The role of Ebf1 in neural development

EBF1 is best known for its role in B cell lineage development, but it also plays a role in nervous tissues. EBF1 has been shown to be necessary for striatal medium spiny neuron development and differentiation (Lobo et al., 2008). It has also been shown to play a role in dopaminergic neuron development with loss of these cells in the substantia nigra of *Ebf1*$^{-/-}$ mice

(Yin et al., 2009). In chick neural tube, early neurogenic genes such as *Ngn2* and *NeuroM* have been shown to activate *Ebf1*, allowing neuronal differentiation and migration to take place (Garcia-Dominguez et al., 2003). The olfactory system is the most closely related to the auditory system, and, in this system, *Ebf1* has roles in the regulation of genes in the odorant signaling cascade (Davis and Reed, 1996). Davis and Reed have described *Ebf1* expression in many areas of the nervous system, including the inner ear. In this study, we have systematically described the expression of *Ebf1* in the developing cochlea using immunohistochemistry, in situ hybridization, and single cell RNA-seq. Although many studies suggest that *Ebf1* plays a role after exit from the cell cycle, we observed expression in areas of the cochlear epithelium that are still in the cell cycle. However, our data are suggestive of a regulation of exit from the cell cycle, because we see a dramatic increase in cells that develop into sensory cells when *Ebf1* is deleted at the otocyst stage.

Expansion of the sensory domain in the developing cochlea of Ebf1-cKO mice

The most obvious phenotype in the *Slc26a9*$^{Ebf1\text{-}cKO}$ is the more than doubling of the sensory epithelium. This result suggests that *Ebf1* plays a role in either regulating proliferation of prosensory cells or in limiting the extent of the developing sensory epithelial domain. Sensory epithelium patterning in the cochlea can be subdivided into two key processes: prosensory domain establishment and sensory cell differentiation (reviewed in Brown and Groves, 2020). The prosensory domain is defined between E12 and E15 as prosensory cells undergo cell cycle exit in a wave that starts at the apex of the cochlea and sweeps to the base (Ruben, 1967). HC and SC differentiation proceeds in the opposite direction, starting at the base around E14 and reaching the apex during neonatal stages (Chen et al., 2002).

The development of the sensory epithelium is highly regulated and dependent on many signaling pathways (reviewed in Groves and Fekete, 2012). Changes in several pathways give rise to cochleae with extra HCs. BMP4 is produced by the cells on the lateral edge of the

developing organ of Corti, the development of which is dependent on low levels of BMP4 but inhibited by high levels. BMP4 is responsible, at least in part, for the sharp border at the lateral edge of the sensory epithelium (Ohyama et al., 2010). There is a gradient of WNTs and FGF10 from Kölliker's organ on the medial side of the sensory domain. The sensory domain itself is defined by expression of *Fgf20*, which is initially expressed in base and sweeps towards the apex ahead of MYO7a expression (Hayashi et al., 2008b). The Notch pathway is also involved in sensory epithelial patterning. During early development, it is responsible for inducing a sensory fate via signaling from JAG1 (Kiernan et al., 2006) expressed in Kölliker's organ and overlapping the region where iHCs will form (lateral induction). Later in development, the Notch pathway suppresses HC fate because of the early expression of Notch ligands by HCs, thus allowing the cells next to each HC to develop as SCs (lateral inhibition). There are numerous mutations in Notch, its ligands or effectors that will give extra HCs (reviewed in Basch et al., 2016a; Basch et al., 2016b; Kiernan et al., 2005a).

How does EBF1 fit with all these signaling mechanisms? It is clear from our data that there is a delay in cell cycle exit. Other labs have shown that prolonged prosensory cell proliferation leads to increases in both HCs and SCs (Chen and Segil, 1999; Jacques et al., 2012; Kiernan et al., 2005a; Tateya et al., 2011). A doubling in the width of the sensory epithelium could be accounted for by progenitors going through one more cell cycle. This, however, does not account for the more than doubling of the iHCs. We propose that EBF1 plays an early role in regulating exit from the cell cycle and a later role in maintaining the medial border of the sensory epithelium such that the cells closest to the sensory epithelium do not develop as HCs or SCs. The suppression of sensory epithelium formation also accounts for the ectopic sensory patches we see in the cochlea from *Slc26a9*$^{Ebf1\text{-}cKO}$ animals. This two-stage requirement for EBF1 activity is consistent with our finding that when *Ebf1* is eliminated at E11/12, we only find extra iHCs, whereas oHC numbers are unaffected.

In addition to extra HCs in the *Ebf1* conditional deletions, we also observed extra SCs. The extra HCs in mice with either conditional deletion (*Slc26a9*$^{Ebf1\text{-}cKO}$ or *Sox2*$^{Ebf1\text{-}cKO}$) appear to pattern their immediately adjacent SCs, possibly via a secreted factor. Such a factor may be *Fgf8*, which is uniquely expressed only by iHCs. Mutations that affect the FGF signaling pathway have been shown to lead to both defects in PC differentiation as well as extra oHCs (Hayashi et al., 2007; Shim et al., 2005). The extra iHCs in the *Ebf1*-cKOs should lead to a higher concentration of FGF8; previous studies have shown that overexpression of *Fgf8* in explant cultures will induce extra p75^{+} iPCs (Jacques et al., 2007). One might have anticipated that the mutant would have extra iPCs rather than the extra oPCs that we observe in the *Slc26a9*$^{Ebf1\text{-}cKO}$ mice. Mice with a *Fgfr3* mutation, which causes an overactive kinase activity of the receptor, also have extra oPCs (Mansour et al., 2013). In the *Fgfr3* mutants, it is thought that the receptor is activated by FGF10, which is abundantly expressed in Kölliker's organ.

Ectopic patches of sensory epithelium present in Kölliker's organ of Slc26a9$^{Ebf1\text{-}cKO}$

The number of ectopic sensory patches in Kölliker's organ is highly variable; however, every mutant cochlea examined had at least one. These are located throughout the cochlea and at various positions along the medial axis of Kölliker's organ. We have never seen complete conversion of Kölliker's organ to sensory epithelium, which suggests that there is more than one inhibitor of sensory development present. We also do not know what kind of HCs are in these ectopic patches. The surrounding cells express SOX2, suggesting that they are SCs, but they do not express any of the specific markers for medial SCs (iBCs, iPhCs, and PCs). The HCs do express *Slc17a8*, suggesting that these are either iHCs or vestibular HCs. They also show rapid uptake of FM1-43, indicating active MET channels. We have only examined adult cochleae from the *Ebf1* mutants as sections, so we cannot say at this stage whether these ectopic HCs are retained. It appears that the inner sulcus does form at least in the base.

Deafness

In the *Slc26a9*$^{Ebf1\text{-}cKO}$ animal, there are many defects in the sensory epithelium. We see extra iHCs, oHCs, iPhCs, oPCs, and DCs, as well as defective neural connections, any of which would dramatically change the response to sound of the animal. In the adults, we found that the extra HCs were retained, and the animal showed dramatic hearing loss. There are multiple potential reasons for this result, including the sheer weight of the extra cells causing mechanical disturbances to the propagation of sound waves along the basilar membrane. We also noticed defects in the tectorial membrane, which appeared thinner and more disorganized in the mutant animals, and defects in innervation.

In summary, we have identified EBF1 as a key factor for patterning the mammalian cochlea and deletion of *Ebf1* leads to deafness in mice. We also found expression of *Ebf1* in the vestibular system but see no vestibular phenotype in the cKO mice. Remaining questions relate to the mechanism of action of EBF1 in cochlear development. From what is known about this family, it could be acting as a transcriptional activator, repressor, or chromatin remodeler (reviewed in Ramírez et al., 2010). It may also have different mechanisms that are context dependent at the various stages of development. We are currently looking into the pathways that are mis-regulated when *Ebf1* is deleted in the developing inner ear. In a recent study, the expression of *Ebf1* was shown to be regulated by SOXC family. In a KO of *Sox4* and *Sox11* in the inner ear, the expression of *Ebf1* was dramatically downregulated along with other prosensory factors such as *Fgf20* (Hayashi et al., 2008b; Wang et al., 2023). In addition, EBF1 appears to be regulated by FGF; *Ebf1* is downregulated in the otic mesenchyme but appears to be upregulated in the epithelium at E12.5 in *Fgf9/20* double KO mice (Ebeid and Huh, 2020). The importance of *Ebf1* in cochlear development is underscored by a recent publication that also analyzed a KO and a cKO for *Ebf1* (Kagoshima et al., 2024). The results from this study are similar to ours, although different mutant mice are used. Their findings agree with those we

detail in this report and further support an important role for EBF1 in development of the organ of Corti and suggest its mutation might cause deafness in humans.

2.5 Materials and Methods

Mice

Mice were housed in either the University of Washington Department of Comparative Medicine or in the Medical University of South Carolina Division of Lab Animal Resources. All experiments were approved by the Institutional Animal Care and Use Committee of the University of Washington, as well as by the Medical University of South Carolina, and were performed in accordance with the standards outlined by the National Institutes of Health (NIH). Mice were euthanized in accordance with IACUC approved procedures and in line with NIH policies.

Ebf1$^{fl/fl}$ mice were obtained from Jackson labs on a C57BL/6 background (Strain #028104). *Sox2*^{CreER} mice obtained from Jackson labs on a mixed background of C57BL/6 and 129S4/SVJae (Strain #017593), and the *Slc26a9*$^{P2A\text{-}Cre}$ mice were obtained on a C57BL/6 background (Urness et al., 2020). To generate *Slc26a9*- and *Sox2*-conditional *Ebf1* knockout mice, *Slc26a9*$^{P2A\text{-}Cre}$ and *Sox2*^{CreER} mice were crossed with *Ebf1*$^{fl/fl}$ females to generate *Cre*$^{+}$ *Ebf1*$^{fl/+}$ progeny. Male *Cre*$^{+}$ *Ebf1*$^{fl/+}$ mice identified by genotyping (see below) were then crossed with *Ebf1*$^{fl/fl}$ mice to generate litters containing *Cre*$^{+}$ *Ebf1*$^{fl/fl}$ mice. *Cre*$^{+}$ *Ebf1*$^{fl/fl}$ mice identified by genotyping were bred with *Ebf1*$^{fl/fl}$ mice to generate *Cre*$^{+}$ *Ebf1*$^{fl/fl}$ and *Ebf1*$^{fl/fl}$ littermates for our phenotypic analyses. To induce Cre recombination, timed-pregnant dams carrying *Sox2*^{CreER} *Ebf1*$^{fl/fl}$ and *Ebf1*$^{fl/fl}$ embryos received tamoxifen diluted in corn oil (100 mg/kg; Sigma-Aldrich T5648) via oral gavage at E11 and at E12. *Sox2-EGFP* knock-in mice (Arnold et al., 2011) from Jackson labs (Strain #017592) were bred to generate time-pregnant litters. *Sox2-EGFP*$^{+}$ embryos were identified by epifluorescence and their cells were purified by FAC-sorting for

single cell analysis. Stages were verified by Theiler's criteria. Tail tips or ear punches were collected for genotyping.

Mice positive for *Sox-CreER* were genotyped with the following primer pair: TCCTTAGCGCCGTAAATCAA and TGCCAGGATCAGGGTTAAAG. Mice positive for *Slc26a9*$^{P2A\text{-}Cre}$ were genotyped using the following primer trio: GGAGGAACACAGTTCACAGT, GTGTCTGGTGTGGCTGATGACC and ATGGGTTCACCAGAGTCTCATC. *Ebf1*$^{fl/fl}$ mice were genotyped using two distinct primer pairs: (1) TGTGGCAACCGAAATGAG and CCTGTGAGCGACACAAAGC in addition to (2) ACGACTTCTTCAAGTCCGCC and TCTTGTAGTTGCCGTCGTCC. The first primer pair was designed to identify the presence of the wildtype *Ebf1* allele (Vilagos et al., 2012). The second primer pair was used to reveal the presence of the *EGFP* associated with the fusion protein encoded in the floxed *Ebf1* allele (Vilagos et al., 2012). Mice were identified as *Ebf1*$^{fl/fl}$ if they tested negative for wildtype *Ebf1* allele and positive for *EGFP*.

In situ hybridization

The hybridization was performed as described previously (Hayashi et al., 2007; Wilkerson et al., 2021). Briefly E14.5 heads were fixed in a modified Carnoy's solution overnight at 4 °C. Heads were then dehydrated using increasing concentrations of ethanol and left in 100% ethanol overnight at 4 °C. Heads were washed in xylene twice before embedding in low melt paraffin (Thermo Fisher Scientific, 23-021-401) and sectioning at 8 mm. Mouse *Ebf1* cDNA was obtained from the Allen Institute (Seattle, WA, USA). Digoxigenin (DIG)-labeled probes for *Ebf1* were generated using SP6 RNA polymerase (Promega P1085) and the following nested PCR primers: CTCAGTCACCACAAGCATGAAT, CACTTCATTCTCCCCTTCCATA, and GCGATTTAGGTGACACTATAGCATGGAGTCTTGTTTATAGTGGC. In situs were performed using the DIG-labeled *Ebf1* probes. The in situ product was visualized using NBT/BCIP (Sigma-

Aldrich B1911) and anti-DIG conjugated to secondary antibody (Roche, 11093274910). Tissue sections were imaged using a Zeiss Axioplan 2 microscope.

FACS and single cell RNA-seq

SOX2-GFP^{high+} cochlear duct cells were isolated as described previously (Wilkerson et al., 2019) from 10-12 cochleae gathered from one to two litters per stage. Libraries were prepared using the Chromium Single Cell 3' Library & Gel Bead Kit v3 (10x Genomics) according to the manufacturer's instructions. Reads were aligned to mm10 and filtered using 10X Genomics Cell Ranger, as described previously (Wilkerson et al., 2021). Briefly, E12, E14 and E16 samples were batch-corrected and normalized in Seurat 4 (Butler et al., 2018; Satija et al., 2015). Principal component, UMAP and clustering analysis (McInnes and Healy, 2018 preprint) was performed in Seurat; trajectory analysis was performed in Monocle 3 (Cao et al., 2019). Cell types were identified based on cluster-specific expression of known markers (see Fig. 2.1). Differential expression analysis was performed on raw counts using the FindMarkers function in Seurat.

Immunostaining

For embryonic stages, heads were fixed overnight at 4 °C. P1 and adult temporal bones were fixed in 4% paraformaldehyde (PFA) either for 30 min at room temperature or overnight at 4 °C. After fixation, heads and temporal bones were washed in PBS three times for 10 min on a nutator at room temperature. For wholemount tissue experiments, cochlear ducts were dissected from embryonic heads and P1 temporal bones. For tissue section experiments, the heads and temporal bones were then incubated in a sucrose series consisting of 5%, 10%, and 15% sucrose washes. Adult temporal bones and embryonic heads were incubated in an additional 25% sucrose and 30% sucrose wash, respectively. After incubating in OCT (Tissue-Tek 4583) at 4 °C, heads and temporal bones were embedded in OCT and cryosectioned at 12 µm.

Wholemount tissue was permeabilized with 0.5% TX-100 for experiments visualizing cell surface markers and 2% Triton X-100 for experiments visualizing nuclear or cytoplasmic markers. Before blocking, adult sections to be stained with rabbit anti-SOX2 antibody were treated with 1% SDS for 5 min. Sections and wholemount tissue were incubated in primary antibodies diluted in block overnight at room temperature. Sections and wholemount tissue were blocked in 10% serum (donkey or fetal bovine) with 0.1% and 0.5% Triton X-100, respectively. Wholemount tissue was washed for 15 min or 1.5 h three times in 0.1% and 0.5% Triton X-100 for sections and wholemount tissue, respectively. Wholemount tissue was subsequently incubated in block for another 1 h. Sections and wholemount tissue were incubated in secondary antibodies diluted in block for 50 min or overnight at room temperature. Antibody details are provided in Table 2.S2. All samples were imaged on a Zeiss LSM 880 confocal microscope.

FM1-43 uptake

To identify the presence of mechanoelectrical transduction (MET) channels in HCs, we treated freshly dissected P6 cochlear ducts with a styryl dye, FM1-43 FX (4 μM; Thermo Fisher Scientific F35355), for 30 s at room temperature. After removing the FM1-43 dye, the cochlear ducts were washed with HBSS three times. The cochlear wholemounts were imaged on a Zeiss LSM 880 confocal microscope.

Proliferation assay

To trace proliferation at embryonic stages, we administered 5-ethynyl-2’-deoxyuridine (EdU; 50 mg/kg; Invitrogen A10044) reconstituted in sterile PBS to pregnant dams via intraperitoneal injection twice a day (separated by 8 h) starting on E15 and ending on E17. Click-iT Alexa-Fluor-647 (Invitrogen C10430) was used to detect incorporated EdU in P1

cochlear ducts using the manufacturer's protocol. The EdU-labeled cochlear wholemounts were imaged on a Zeiss LSM 880 confocal microscope.

Morphometrics

To quantify HCs in *Slc26a9*$^{Ebf1\text{-}cKO}$ (*Slc26a9*$^{P2A\text{-}Cre}$ *Ebf1*$^{fl/fl}$) and control (*Ebf1*$^{fl/fl}$) littermates, anti-MYO7a^{+} HCs were counted using the point tool and ROI Manager in Image J/Fiji. iHCs were distinguished from oHCs based on their comparatively strong expression of vGLUT3 (SLC17A8) protein and cell shape. Just as the oHCs taper from three rows in the base to two rows in the hook region of *Ebf1*$^{fl/fl}$ control cochleae, a reduction in the number of oHC rows can be seen in the hooks of *Slc26a9*$^{Ebf1\text{-}cKO}$ cochleae. Counts were made starting in the base of each cochlea up to the point in the apex where anti-vGLUT3^{+} iHCs were no longer visible. To measure cochlear duct length, we used the segmented line tool to generate a line composed of 50 µm segments along the space between the iHCs and oHCs. We chose to use this space rather than the row of iPC nuclei (as was done for the *Sox2*-conditional model) because iPCs cannot be identified based on the unique shape of their nuclei in *Slc26a9*$^{Ebf1\text{-}cKO}$ mice. The segmented line tool was also used to measure the sweep of differentiation in embryonic cochlear wholemounts. We measured from the apex of the cochlear epithelium to the first SOX2^{+} cell in the apex and along medial edge of the strongly SOX2^{+} prosensory domain to the first MYO7a^{+} cell in the apex. For all regional analyses in the cochlea, HC density was measured in ~400 µm samples in the base, middle and apex. Basal measurements were made starting immediately above the hook. Apical measurements were made in the most apical region of the duct where a space was still evident between the iHCs and oHCs. Middle measurements were made at the approximate midpoint for the duct. For EdU^{+} counting in HCs, EdU^{+} iHCs were distinguished from EdU^{+} oHCs based on vGLUT3 protein expression and cell shape.

To quantify HCs in *Sox2*$^{Ebf1\text{-}cKO}$ (*Sox2*^{CreER} *Ebf1*$^{fl/fl}$ treated with tamoxifen) mice, littermate controls (*Ebf1*$^{fl/fl}$ treated with tamoxifen), and *Sox2*^{CreER} *Ebf1*$^{fl/fl}$ mice not treated with tamoxifen,

anti-MYO7a^{+} HCs were counted using the point tool and ROI Manager in Image J/Fiji. The hook region was excluded from counting and length measurements. Counts were made starting in the base of each cochlea, immediately above the hook, up to the point in the apex where iHCs were missing and intermittent (i.e., ~10% distance from the apex in E18). To quantitate HC density, the length of the counted region was measured using the segmented line tool to measure between iHCs and oHCs, along the zipper-like row of anti-SOX2^{+} PC nuclei. To measure total cochlear duct length, the segmented line tool was used to draw a line along the PC region. For regional analysis of iHC density in the cochlea, HC density was measured in ~300 μm samples in the base, middle and apex. Basal measurements were made starting immediately above the hook (90-100% distance from the apex). Apical measurements were made from the point in the apex where iHCs were missing and intermittent, extending toward the base (10-20% distance from the apex). Middle measurements were made at ~40-50% distance from the apex. For regional analysis of oHC density in the cochlea, HC density was measured in ~100 μm samples in the base, middle and apex. oHC differentiation slightly lags iHC differentiation at E18, so apical oHC counts were made at ~20-30% distance from the apex in regions containing three or more rows of oHCs. Basal and middle oHC counts were made in approximately the same regions as the iHC counts in each image.

Auditory brainstem response

Mice were anesthetized by intraperitoneal injection of ketamine (90 mg/kg) and xylazine (10 mg/kg). Subcutaneous electrodes were placed at the cranial vertex for recording, behind the pinna on the stimulus side for reference and behind the contralateral pinna for grounding. Mice were placed in a sound-attenuating chamber and then calibrated tone pips (at 6, 12, 18, 24, 32 45 and 60 kHz; 500 responses at 21/s) and broadband click stimuli (300 responses, at 42.6/s) were presented and the responses recorded from 0-90 dB SPL (5 dB steps) using an RZ6 system (Tucker Davis Technologies). ABR thresholds were determined manually by experienced

readers as the minimum sound level, eliciting identifiable ABR waveforms compared with the 0 dB level.

Experimental design and statistical analyses

The number of animals analyzed per genotype and/or treatment group is listed under sample size in the figure legend for each experiment as well as in Table 2.S1. Biological replicates were analyzed in expression experiments. Male and female mice were used for all experiments.

Graphs were created in GraphPad Prism. Mean total HC counts, HC and EdU^+ HC densities, and sweep of differentiation are shown as bar graphs with standard deviation error bars. Mean ABR thresholds are shown as a line graph with standard deviation error bars. Significance is indicated as follows: * $P < 0.05$, ** $P < 0.01$, *** $P < 0.001$, and **** $P < 0.0001$.

For duct length, total HC counts, PRDM16 and SOX2 expression areas, and sweep of differentiation, statistically significant differences between genotypes were identified using Welch's t-tests. Two-way ANOVA with Holm-Šídák's multiple comparisons test was used to test statistically significant differences in HC and EdU^+ HC density between $Slc26a9^{Ebf1\text{-}cKO}$ and littermate control samples for each region analyzed (base, middle, and apex). To test for statistically significant differences between regions in these genotypes, two-way repeated measures ANOVA was performed with the same multiple- comparisons correction. Two-way ANOVA with Holm-Šídák's multiple comparisons test was also used to determine statistically significant differences in ABR thresholds between adult $Slc26a9^{Ebf1\text{-}cKO}$ and control littermates for each stimulus frequency. Two-way ANOVA with Tukey's multiple comparisons test was used to test for statistically significant differences in HC density between samples from $Sox2^{Ebf1\text{-}cKO}$ mice, littermate controls treated with tamoxifen, and $Sox2^{CreER}$ $Ebf1^{fl/fl}$ mice not treated with tamoxifen. To test for statistically significant differences between regions within these

genotypes, two-way repeated measures ANOVA was performed with the same multiple-comparisons correction (Table 2.S1).

2.6 Acknowledgements

We thank Dr. Suzanne Mansour for suggesting the *Slc26a9*$^{P2A\text{-}Cre}$ mice, members of the Reh lab for helpful critiques on experiments, and Drs. Reh, Pavlou, and Kaplan for comments on this manuscript. We thank Connor Finkbeiner for help with single cell RNA-seq bioinformatics and Erica Lee for technical assistance.

2.7 Figures

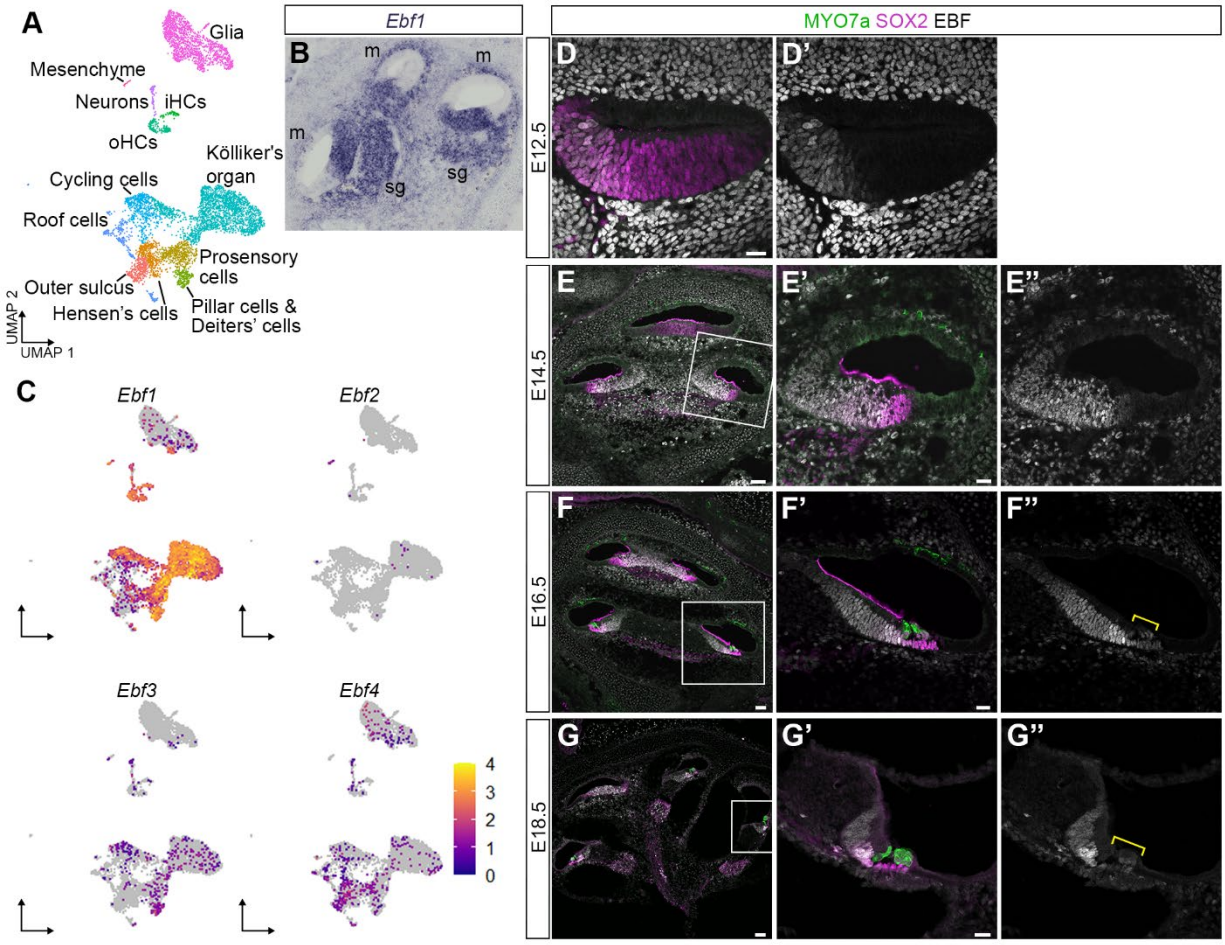

Figure 2.1. Ebf1 expression in the developing cochlea.

(A) A uniform manifold approximation and projection (UMAP) plot of SOX2-EGFP FAC-sorted single cells pooled from E12, E14, and E16 cochlear ducts. Cell types were identified based on marker gene expression. **(B)** In situ hybridization shows robust *Ebf1* expression in the ventral cochlear duct in addition to the spiral ganglion (sg) and adjacent mesenchyme (m) by E14.5. **(C)** Feature plots of pooled E12, E14, and E16 single cells highlighting *Ebf1-4* expression. **(D-G")** Confocal images of E12.5, E14.5, E16.5, and E18.5 C57BL/6 cochlear sections immunolabeled with pan-EBF antibody. **(E'-G")** Zoomed views of base in cochlear sections (outlined in E-G). **(D, D')** At E12.5, EBF protein expression overlaps with the medial domain for SOX2 expression. **(E', E")** In the base of E14.5 cochleae, EBF expression overlaps with SOX2 and extends

medially into Kölliker’s organ. **(F’, F”)** In the base of E16.5 cochleae, EBFs are most strongly expressed in the lateral edge of Kölliker’s organ and show reduced expression in HCs, SCs, and the developing inner sulcus. **(G’, G”)** In the base of E18.5 cochlea, EBFs maintain strong expression in the lateral edge of Kölliker’s organ medial to the iHC. EBFs appear to be downregulated in the SCs and HCs (brackets in F’’ and G’’), particularly iHCs. Scale bars: 20 μm for D,D′,E′,E″,F′,F″,G′,G″; 50 μm for E,F,G.

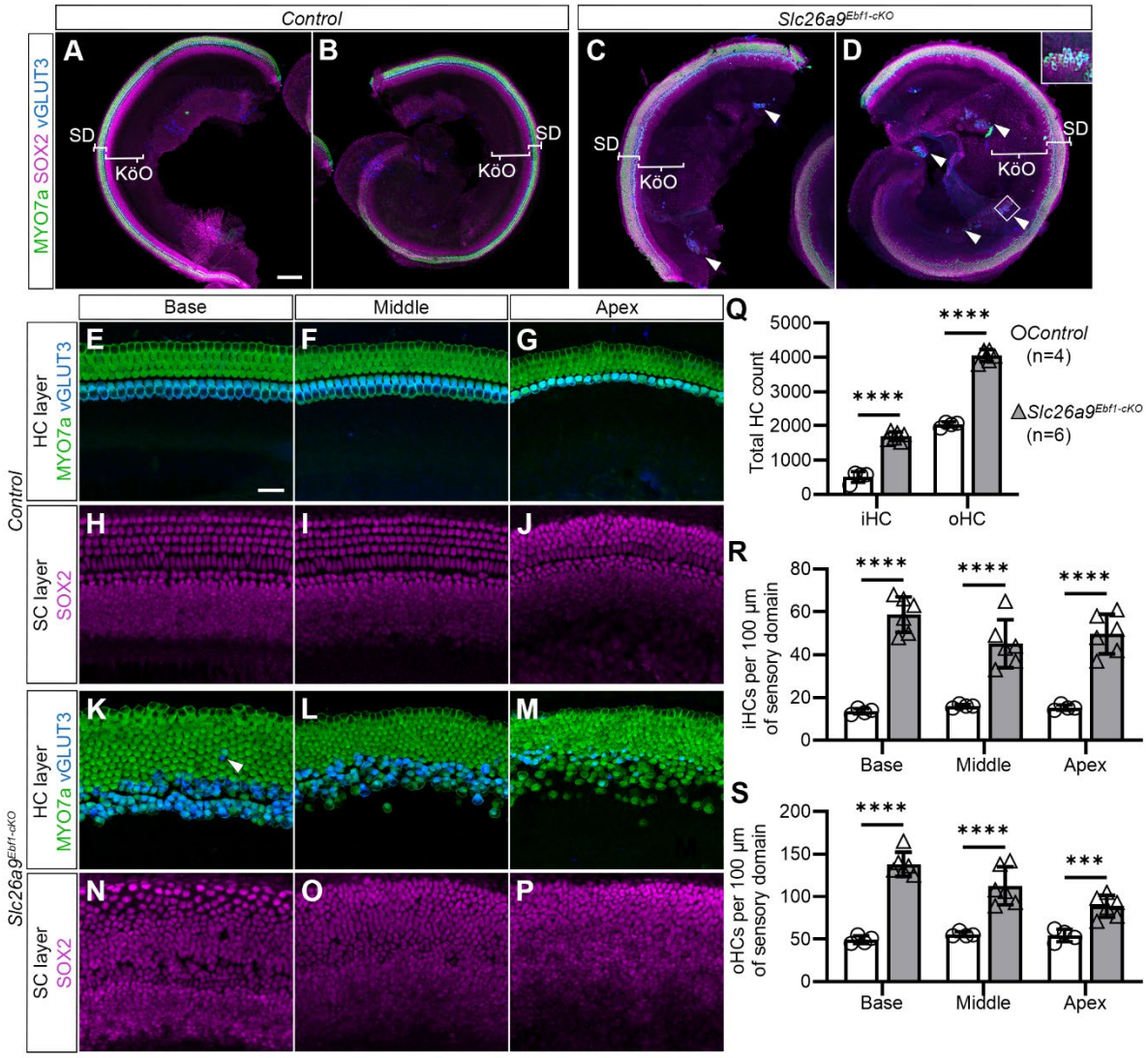

Figure 2.2. Deletion of Ebf1 in the otic vesicle at E9.5 leads to dramatic sensory expansion.

(A, B) Confocal images of basal and apical turns from a P1 littermate control cochlear wholemount. Within the sensory domain (SD), control cochleae exhibit a single row of iHCs (vGLUT3^{+} and MYO7a^{+}) medial to three rows of oHCs (vGLUT3^{-} and MYO7a^{+}). **(C, D)** Confocal images of basal and apical turns from a *Slc26a9$^{Ebf1\text{-}cKO}$* P1 cochlear wholemount. In addition to three to five discontinuous rows of iHCs medial to approximately six rows of oHCs in the sensory domain, *Slc26a9$^{Ebf1\text{-}cKO}$* mice exhibit ectopic sensory patches (arrowheads) throughout Kölliker's organ (KöO). **(E-J)** Confocal images of the HC and SC layers in the base, middle, and

apex of a P1 control cochlear wholemount. **(K-P)** Confocal images of the HC and SC layers in the base, middle, and apex of a P1 *Slc26a9*$^{Ebf1\text{-}cKO}$ cochlear wholemount. A 'confused' iHC (arrowhead) can occasionally be seen in the oHC region of *Slc26a9*$^{Ebf1\text{-}cKO}$ cochlear ducts. **(Q)** The mean (± s.d.) total iHC and oHC counts in *Slc26a9*$^{Ebf1\text{-}cKO}$ P1 mice are significantly greater than those for littermate controls (Table 2.S1). **(R)** Compared with littermate control P1 mice, mean (± s.d.) iHC density in *Slc26a9*$^{Ebf1\text{-}cKO}$ mice is significantly greater in the base, middle, and apex (Table 2.S1). **(S)** Compared with littermate control P1 mice, mean (± s.d.) oHC density in *Slc26a9*$^{Ebf1\text{-}cKO}$ mice is significantly greater in the base, middle, and apex (Table 2.S1). Sample size: four control and six *Slc26a9*$^{Ebf1\text{-}cKO}$ mice from two litters, one duct per mouse. Scale bars: 100 μm for A-D; 20 μm for E-P).

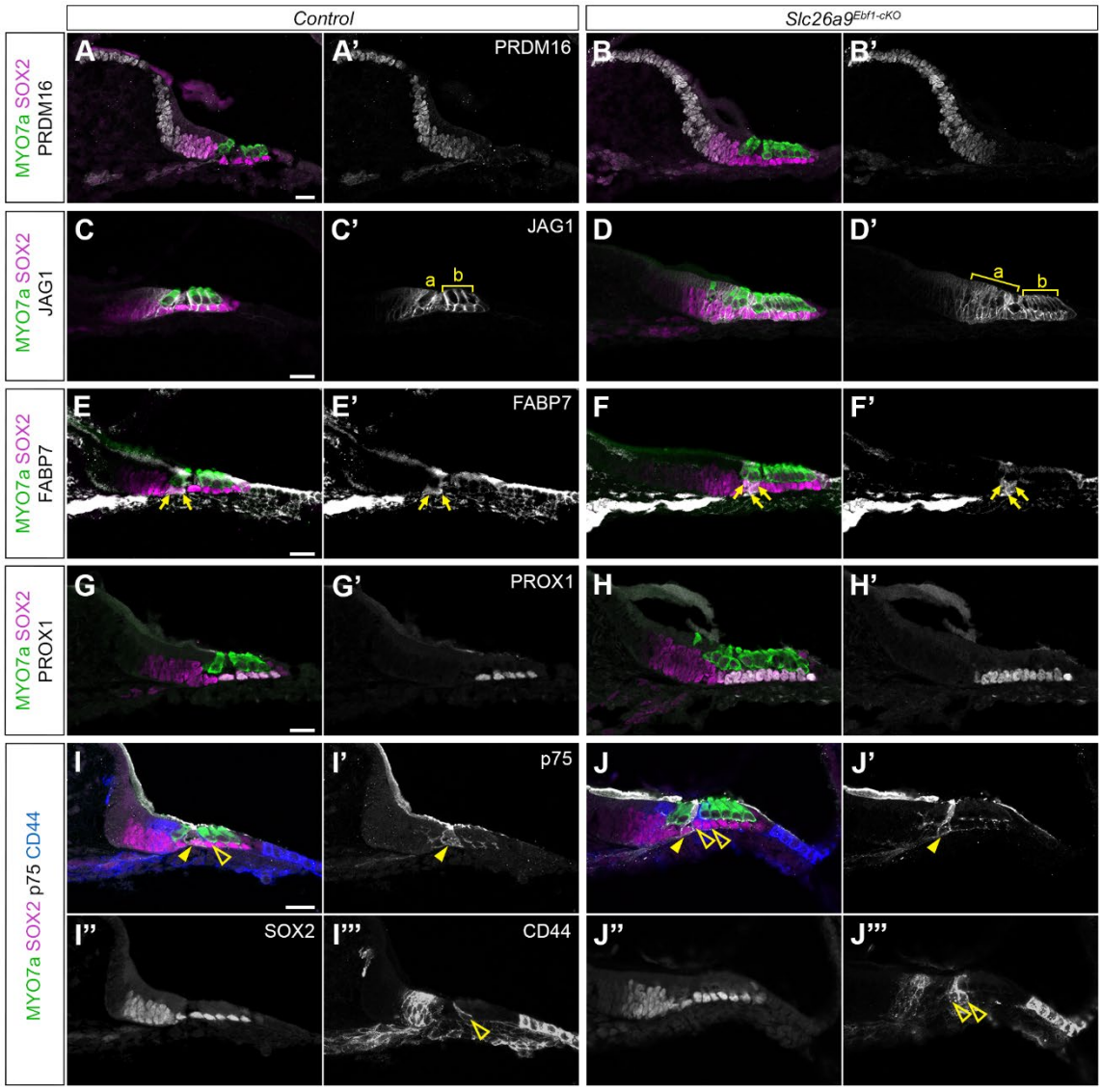

Figure 2.3. Slc26a9$^{Ebf1\text{-}cKO}$ mice demonstrate increases in SC subtypes.

(A-J''') Sections capturing the base of P1 control and *Slc26a9*$^{Ebf1\text{-}cKO}$ cochleae. **(A-B')** Significantly more PRDM16^{+} nuclei reside in Kölliker's organs in *Slc26a9*$^{Ebf1\text{-}cKO}$ cochleae compared with littermate controls. **(C-D')** JAG1^{+} SCs are increased in *Slc26a9*$^{Ebf1\text{-}cKO}$ cochlear sections and continue to extend projections around iHCs (bracket a) and oHCs (bracket b). **(E-F')** A pair of FABP7^{+} iBCs/iPhCs (yellow arrows) are seen in control cochlear sections. More than two FABP7^{+} iBCs/iPhCs are present in *Slc26a9*$^{Ebf1\text{-}cKO}$ cochlear sections. **(G-H')** *Slc26a9*$^{Ebf1\text{-}cKO}$ cochleae demonstrate increases in PROX1^{+} PC and DC nuclei. **(I-J''')** A single

p75^{+} iPC (closed yellow arrowhead) can be observed in both control and *Slc26a9*$^{Ebf1\text{-}cKO}$ cochlear sections. Multiple CD44^{+} oPCs (open yellow arrowheads) are present in *Slc26a9*$^{Ebf1\text{-}cKO}$ cochlear sections, whereas only a single oPC is observed in littermate controls. The expression domain of SOX2 protein shows dramatic expansion in the *Slc26a9*$^{Ebf1\text{-}cKO}$ cochleae compared with littermate controls. Scale bars: 20 μm (bars in A,C,E,G,I apply to A-B′,C-D′,E-F′,G-H′ and I-J‴, respectively).

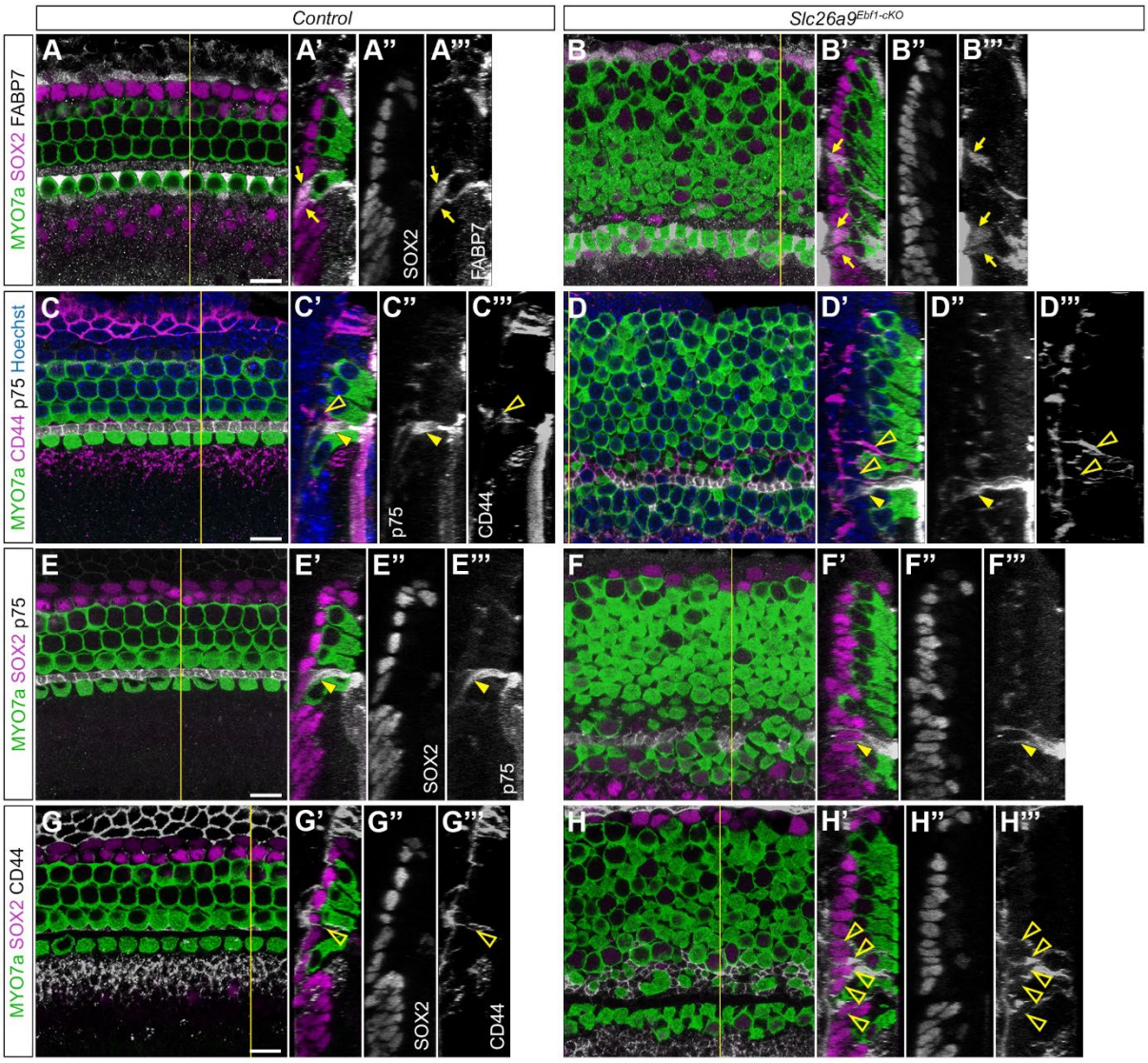

Figure 2.4. Supernumerary iHCs continue to direct SC patterning.

(A-H) Single xy plane confocal images of basal region of P1 control and *Slc26a9*$^{Ebf1\text{-}cKO}$ cochlear wholemounts. **(A'-H')** Orthogonal projections of the yz plane (yellow lines in xy plane images) for the control and *Slc26a9*$^{Ebf1\text{-}cKO}$ cochlear wholemounts. **(A-B''')** FABP7^{+} iBCs/iPhCs (yellow arrows) are arranged in two rows in control cochleae. iBCs form a single row on the medial side of the iHCs and iPhCs form a single row on the lateral side. Supernumerary iHCs in *Slc26a9*$^{Ebf1\text{-}cKO}$ cochleae appear to be adjacent to at least one FABP7^{+} iBC/iPhC. These supernumerary FABP7^{+} iBCs/iPhCs are present in two to six discontinuous rows. **(C-F''')** p75^{+} iPCs (closed yellow arrowheads) are arranged in a single, continuous row in control cochleae. Although p75^{+}

iPCs are still arranged in a single row in *Slc26a9*$^{Ebf1\text{-}cKO}$ cochleae, this row is interrupted by supernumerary HCs. **(C-D‴, G-H‴)** CD44^{+} oPCs (open yellow arrowheads) are arranged in a single continuous row in control cochleae. These cells, by contrast, are arranged in at least two discontinuous rows in *Slc26a9*$^{Ebf1\text{-}cKO}$ cochleae. Scale bars: 10 μm (bars in A,C,E,G apply to A-B‴,C-D‴,E-F‴ and G-H‴, respectively).

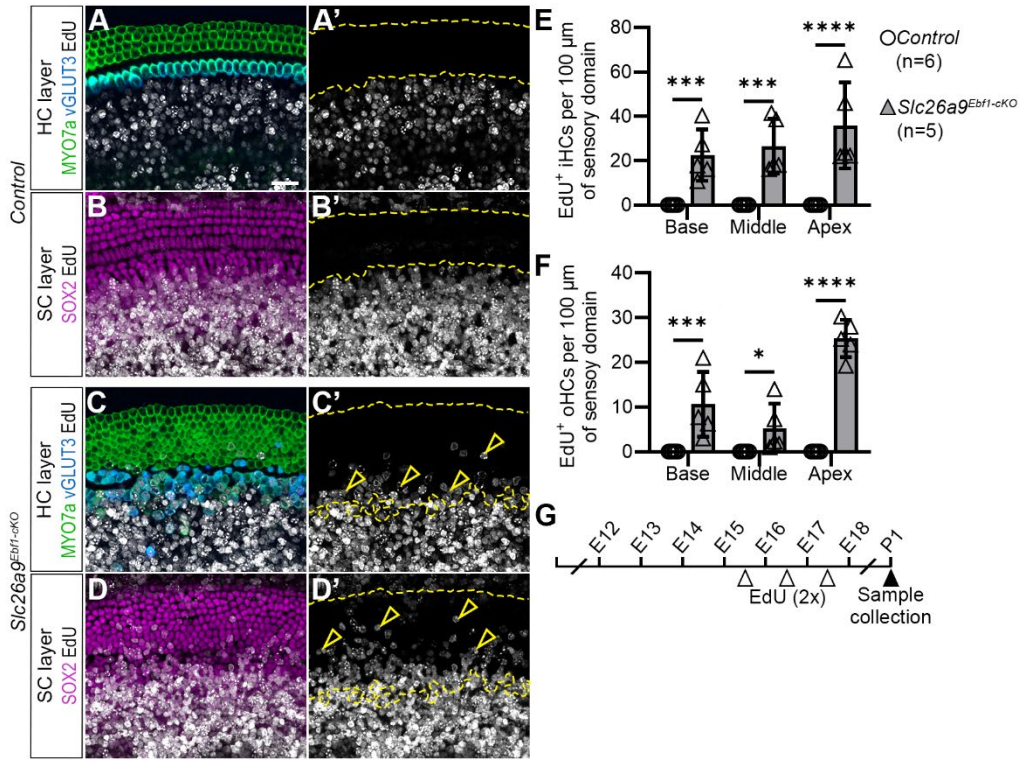

Figure 2.5. Prolonged prosensory cell proliferation in Slc26a9$^{Ebf1\text{-}cKO}$ cochleae.

(A-D') Confocal images of the HC and SC layers in the middle of EdU labeled P1 control and *Slc26a9*$^{Ebf1\text{-}cKO}$ cochlear wholemounts. **(A-B')** Control HCs and underlying SCs (dashed yellow lines) lack EdU labeling. **(C-D')** *Slc26a9*$^{Ebf1\text{-}cKO}$ HCs and underlying SCs are EdU^{+} (open yellow arrowheads in C' and D'). **(E)** Compared with littermate control P1 mice, mean (± s.d.) EdU^{+} iHC density in *Slc26a9*$^{Ebf1\text{-}cKO}$ mice is significantly greater in the base, middle, and apex (Table 2.S1). **(F)** Compared with littermate control P1 mice, mean (± s.d.) EdU^{+} oHC density in *Slc26a9*$^{Ebf1\text{-}cKO}$ mice is significantly greater in the base and apex (Table 2.S1). **(G)** Mice used in proliferation experiments were treated with EdU twice a day for 3 days (E15.5-E17.5) and collected at P1. Sample size: six control and five *Slc26a9*$^{Ebf1\text{-}cKO}$ mice from two litters, one duct per mouse. Scale bars: 20 µm (bar in A applies to all panels).

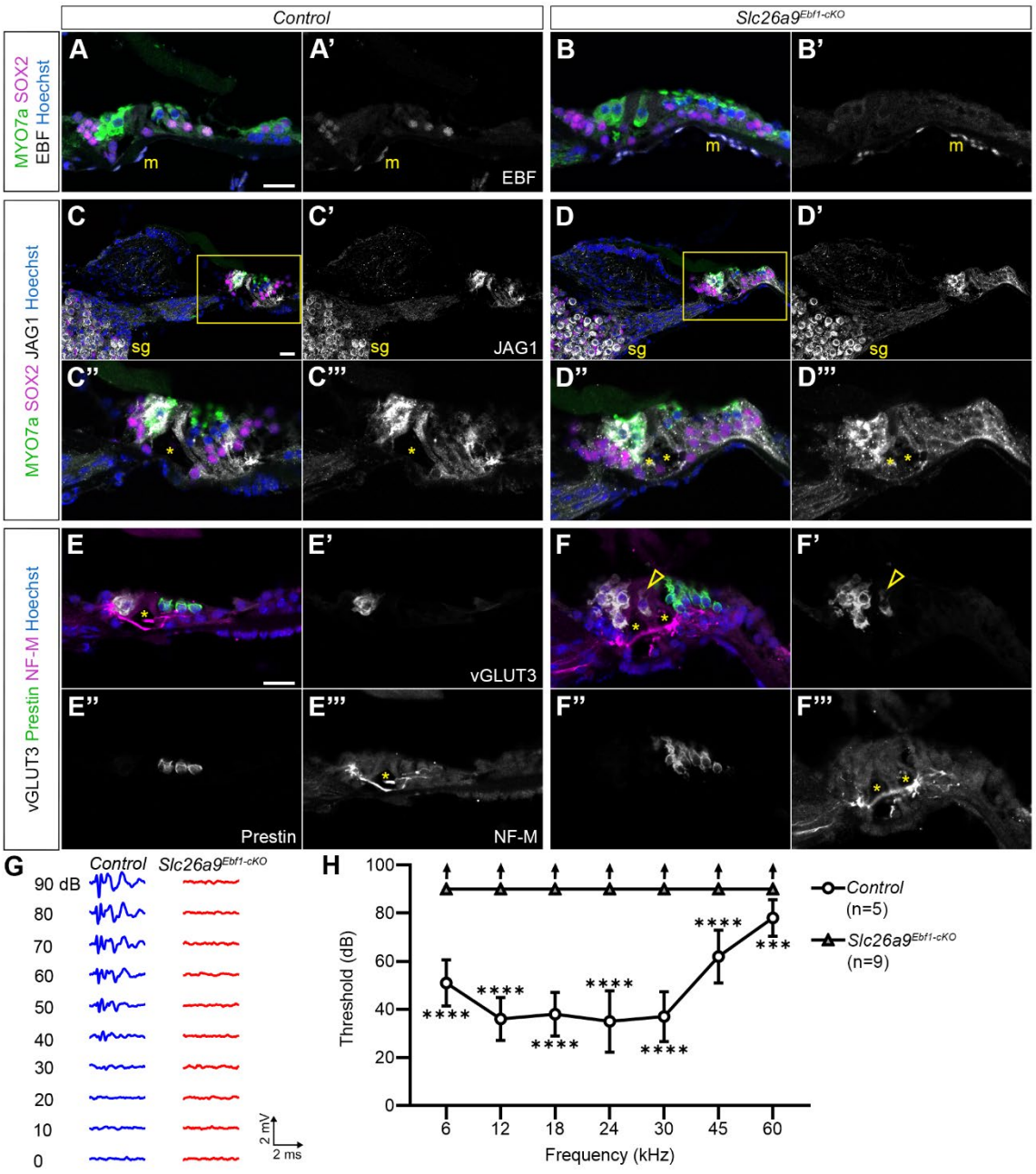

Figure 2.6. Supernumerary HCs and SCs are present in adult Slc26a9$^{Ebf1\text{-}cKO}$ mice, which are deaf.

(A-F''') Sections capturing the middle of P60 control and *Slc26a9*$^{Ebf1\text{-}cKO}$ cochleae. **(C''-D''')** Zoomed views of the organ of Corti (outlines in C and D). **(A-B')** EBF expression is maintained in the SC and mesenchymal cell nuclei of adult control cochleae. EBF expression is not evident in the sensory epithelium of *Slc26a9*$^{Ebf1\text{-}cKO}$ cochleae but can still be seen in the mesenchyme

(m). **(C-F’’’**) Although the expected single tunnel of Corti is observed in controls, multiple tunnels of Corti (asterisks) are present in *Slc26a9*$^{Ebf1\text{-}cKO}$ cochlear sections. **(C-D’)** JAG1 expression is present in the spiral ganglion (sg) and in SCs of control and *Slc26a9*$^{Ebf1\text{-}cKO}$ cochleae. **(C’’-D’’’)** JAG1^{+} supernumerary SCs persist in *Slc26a9*$^{Ebf1\text{-}cKO}$ cochlear sections. **(E-F’’’)** *Slc26a9*$^{Ebf1\text{-}cKO}$ supernumerary iHCs are vGLUT3^{+} and supernumerary oHCs are prestin^{+}. The occasional vGLUT3^{+} iHC can be seen in the PC region (open yellow arrowheads). NF-M^{+} neuronal projections extend to supernumerary iHCs and oHCs in adult samples. **(G)** Example control and *Slc26a9*$^{Ebf1\text{-}cKO}$ ABR waveforms generated in response to broadband click stimulus. **(H)** P50-P74 *Slc26a9*$^{Ebf1\text{-}cKO}$ mice demonstrate elevated ABR thresholds compared with littermate controls (Table 2.S1). Sample size: five controls (one female and four males) and nine *Slc26a9*$^{Ebf1\text{-}cKO}$ mice (six females and three males). Scale bars: 20 μm in A-C (bars apply to A-A‴, B-B‴ and C-C‴, respectively); 9 μm in C″,C‴ and D″,D‴.

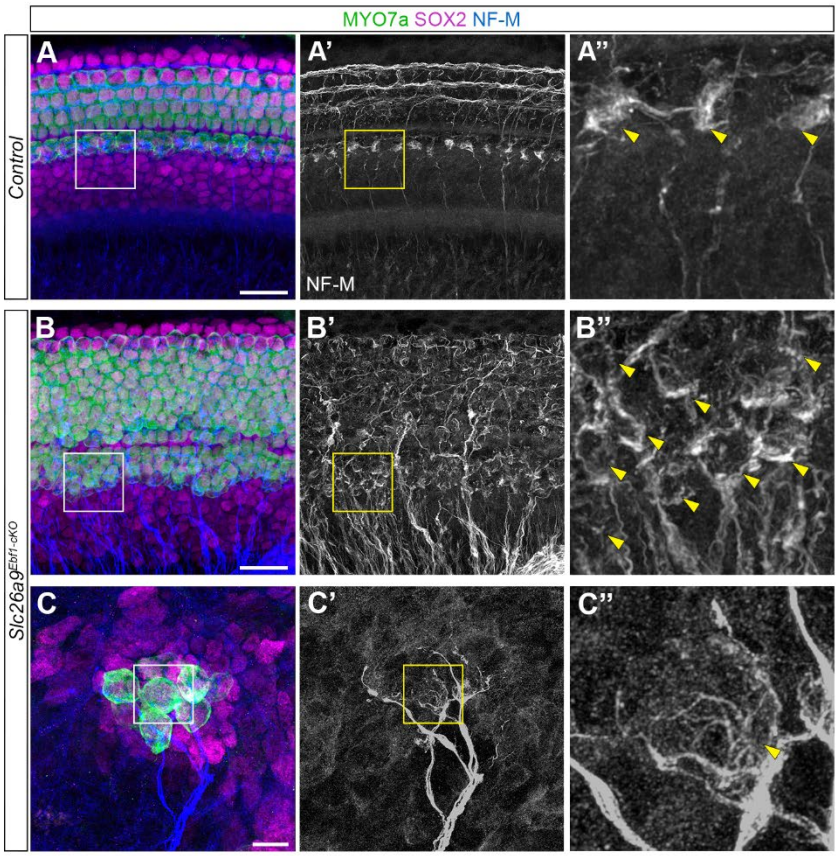

Figure 2.7. Aberrant innervation of Slc26a9$^{Ebf1\text{-}cKO}$ HCs.

(A-B') The basal region of P1 control and *Slc26a9*$^{Ebf1\text{-}cKO}$ cochlear wholemounts. **(C, C')** An ectopic sensory patch near the apex of a *Slc26a9*$^{Ebf1\text{-}cKO}$ cochlear wholemount. **(A'', B'')** Zoomed views of NF-M^{+} neuronal projections extending to and from the control and *Slc26a9*$^{Ebf1\text{-}cKO}$ iHC regions (outlined in A-B'). **(C'')** Zoomed view of NF-M^{+} neuronal projections extending to and from ectopic HCs (outlined in C and C'). **(A-A'')** Numerous fibers terminate on control iHCs (closed yellow arrowheads in A''). Neuronal projections innervate multiple oHCs within the same row, forming three spiral bundles in control cochleae. **(B-B'')** Fibers continue to terminate on supernumerary HCs (closed yellow arrowheads in B''). Organization of spiral bundles is lost in *Slc26a9*$^{Ebf1\text{-}cKO}$ cochleae. **(C- C'')** HCs in ectopic sensory patches are innervated (closed yellow arrowhead in C''). Scale bars: 20 μm for A-B′; 10 μm C,C′; 4.6 μm in A″,B″; 2.3 μm in C″ (bars in A-C apply to A-A″, B-B″ and C-C″, respectively).

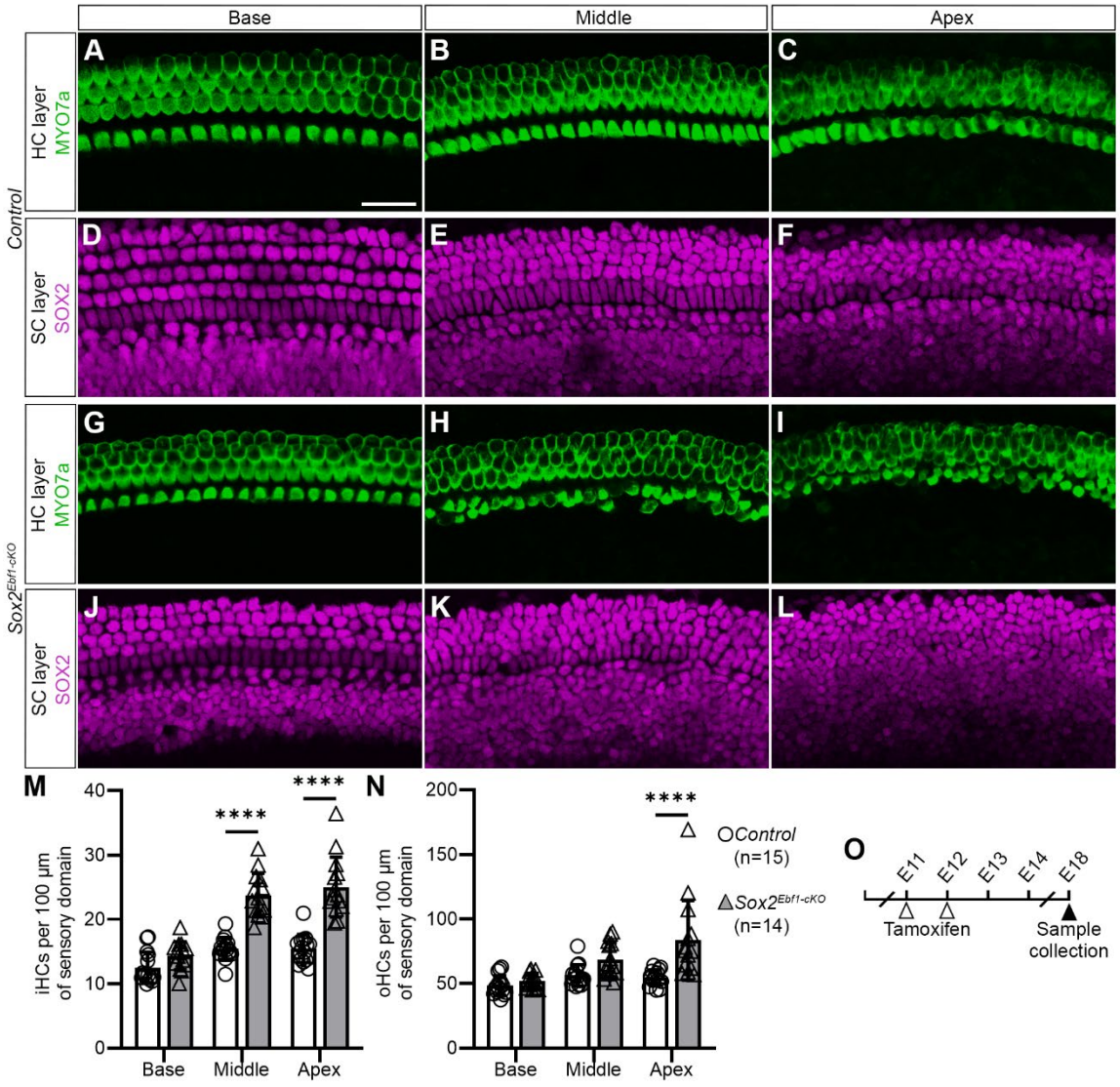

Figure 2.8. Deletion of Ebf1 in the prosensory domain at E11 and E12 leads to moderate sensory expansion.

(A-F) Confocal images of the HC and SC layers the base, middle, and apex of an E18 *Sox2*^{CreER}-negative control cochlear wholemount after tamoxifen injection at E11 and E12. **(G-L)** Confocal images of the HC and SC layers in the base, middle, and apex of an E18 *Sox2*$^{Ebf1\text{-}cKO}$ cochlear wholemount. **(M)** Compared with E18 *Sox2*^{CreER}-negative littermate controls, mean (± s.d.) iHC density in *Sox2*$^{Ebf1\text{-}cKO}$ mice is significantly greater in the middle and apex (Table 2.S1). **(N)** Compared with E18 *Sox2*^{CreER}-negative littermate controls, mean (± s.d.) oHC density in

Sox2$^{Ebf1\text{-}cKO}$ mice is significantly greater in the apex (Table 2.S1). **(O)** *Sox2*^{CreER} *Ebf1*$^{fl/fl}$ and *Ebf1*$^{fl/fl}$ littermates were treated with tamoxifen at E11 and E12 before being collected for analysis at E18. Sample size: 15 *Sox2*^{CreER}-negative controls and 14 *Sox2*$^{Ebf1\text{-}cKO}$ mice from six litters, one duct per mouse. Scale bars: 50 μm (bar in A applies to all panels).

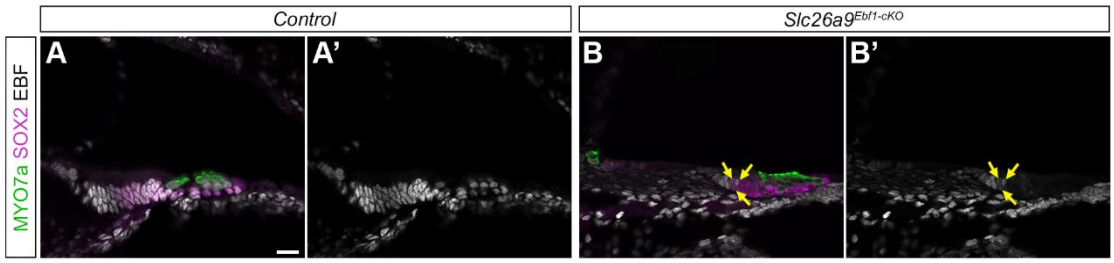

Figure 2.S1. EBF expression is reduced in Slc26a9$^{Ebf1\text{-}cKO}$ cochleae.

(A-B') Sections capturing the base of P1 control and *Slc26a9$^{Ebf1\text{-}cKO}$* cochleae. **(A, A')** EBF expression is present in HCs, SCs, Kölliker's organ cells, mesenchymal cells, and Schwann cells of control cochleae. **(B, B')** *Slc26a9$^{Ebf1\text{-}cKO}$* cochleae lack EBF expression in the HCs and SCs of the sensory domain but EBF^{+} cells can occasionally be observed in Kölliker's organ (yellow arrows). Scale bars: 20 μm for A (same for A', B, and B').

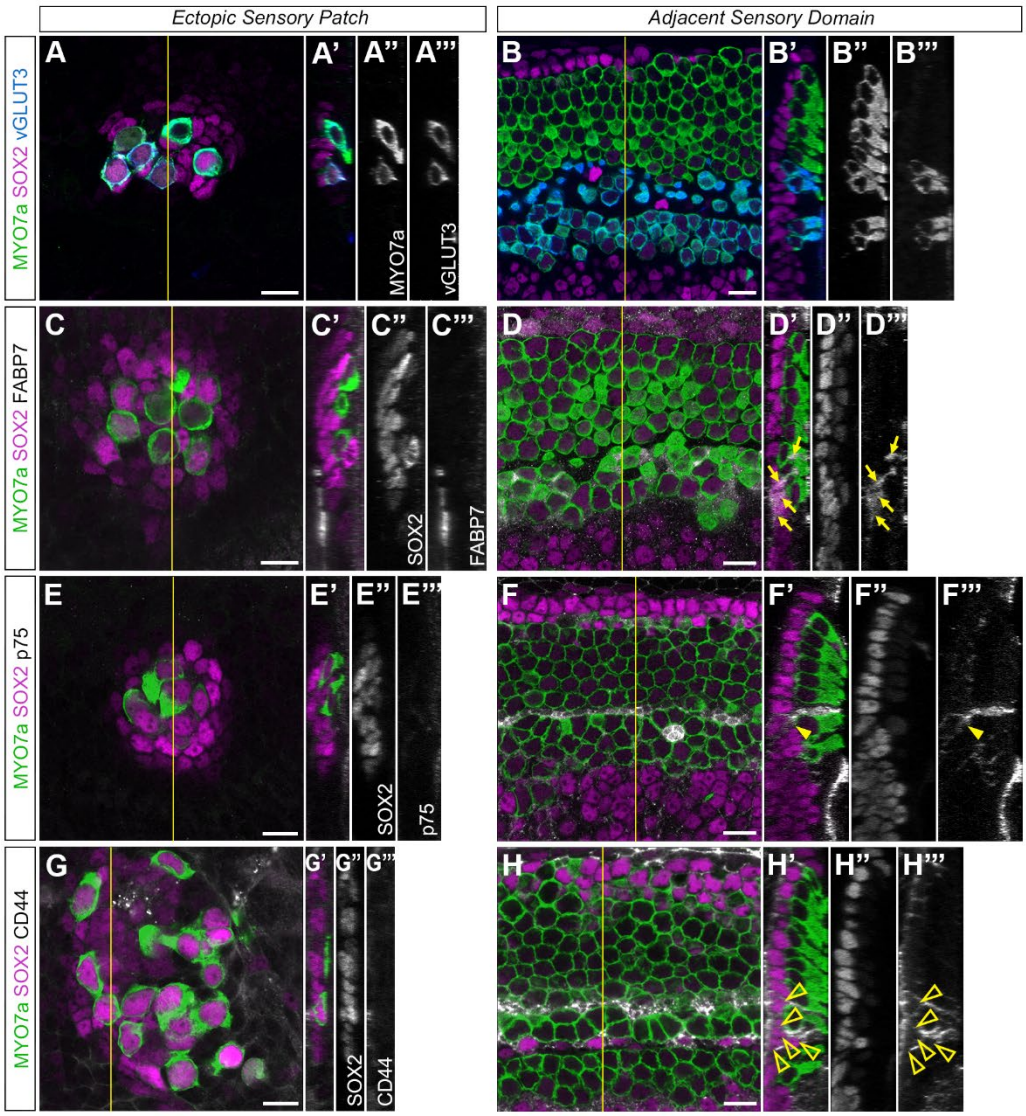

Figure 2.S2. HCs in ectopic sensory patches express vGLUT3 while their associated SCs fail to express markers associated with SC subtypes.

(A-H) Single xy plane confocal images of ectopic sensory patches and the sensory domains adjacent to these patches in P1 *Slc26a9*$^{Ebf1\text{-}cKO}$ cochlear wholemounts. **(A'-H')** Orthogonal projections of the yz plane (yellow line in xy plane images) of ectopic sensory patches and the adjacent sensory domains. **(A-B''')** HCs in ectopic sensory patches are vGLUT3^{+}. vGLUT3^{+} iHCs can be seen on either side of the PC region in the *Slc26a9*$^{Ebf1\text{-}cKO}$ sensory domain. **(C-D''')** SCs in ectopic sensory patches do not express FABP7. FABP7^{+} iBCs and iPhCs can be seen in the neighboring portion of the *Slc26a9*$^{Ebf1\text{-}cKO}$ sensory domain. **(E-F''')** SCs in ectopic sensory

patches do not express p75. $p75^{+}$ iPCs can be seen in neighboring portion of the *Slc26a9*$^{Ebf1\text{-}cKO}$ sensory domain. **(G-H”’)** SCs in ectopic sensory patches do not express CD44. $CD44^{+}$ oPCs can be seen in neighboring portion of the *Slc26a9*$^{Ebf1\text{-}cKO}$ sensory domain. Scale bars: 10 μm for A (same for A’-A”’), B (same for B’-B”’), C (same for C’-C”’), D (same for D’-D”’), E (same for E’-E”’), F (same for F’-F”’), G (same for G’-G”’), and H (same for H’-H”’).

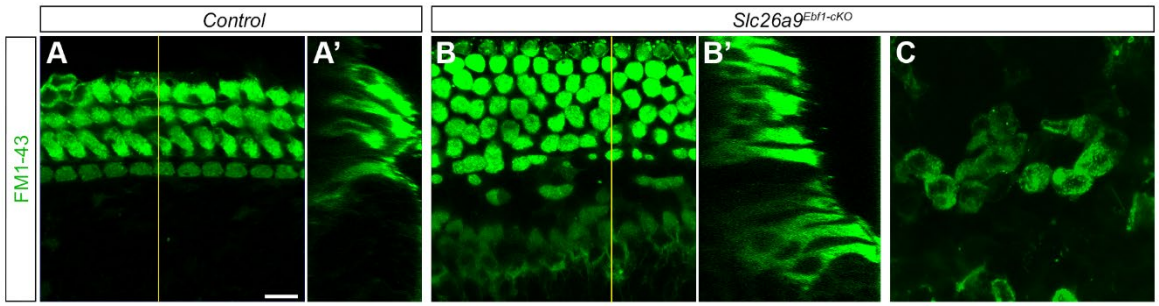

Figure 2.S3. Supernumerary HCs in the sensory domain and HCs in the ectopic sensory patches label with FM1-43 dye.

(A, B) Single xy plane confocal images of middle region of P6 control and *Slc26a9*$^{Ebf1\text{-}cKO}$ cochlear wholemounts. **(A', B')** Orthogonal projections of the yz plane (yellow line in xy plane images) for the control and *Slc26a9*$^{Ebf1\text{-}cKO}$ cochlear wholemounts. **(A, A')** FM1-43 labeling in the sensory domain of a control cochlear wholemount. **(B-C)** FM1-43 labeling in the sensory domain and an ectopic sensory patch of a *Slc26a9*$^{Ebf1\text{-}cKO}$ cochlear wholemount. Scale bars: 10 μm for A (same for A' and B-C).

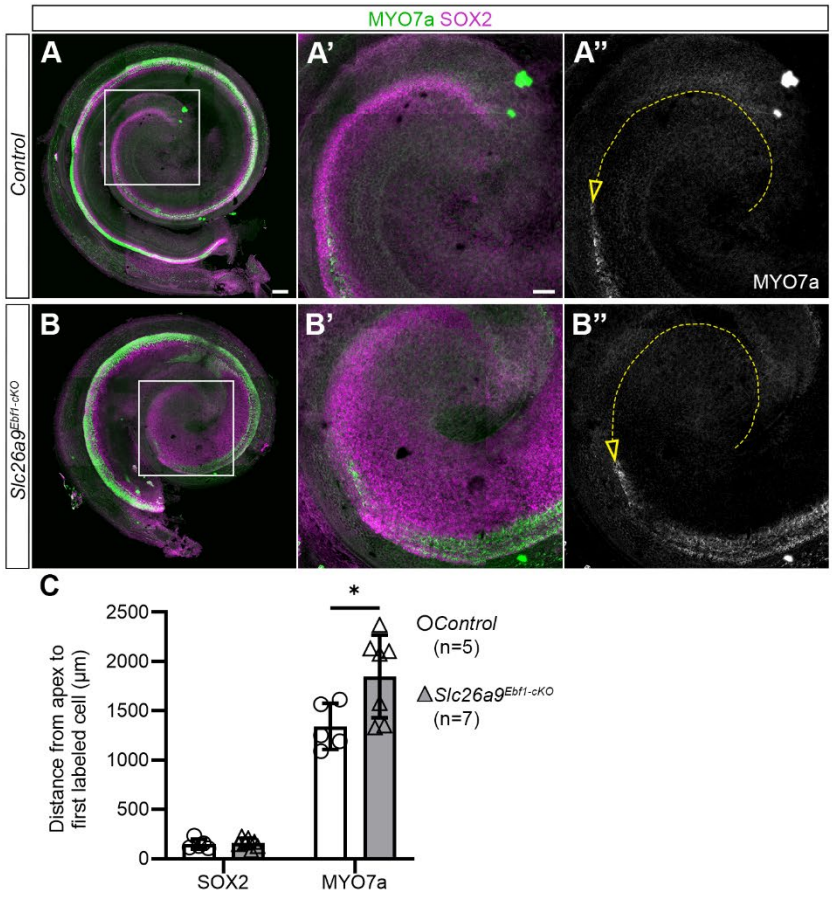

Figure 2.S4. Delayed sensory cell differentiation in embryonic Slc26a9$^{Ebf1\text{-}cKO}$ cochleae.

(A-B) E16.5 control and *Slc26a9*$^{Ebf1\text{-}cKO}$ cochlear wholemounts. **(A'-B'')** Zoomed views of apex in the control and *Slc26a9*$^{Ebf1\text{-}cKO}$ cochlear wholemounts (boxes in A and B). **(A'', B'')** The sweep of differentiation was quantified in cochlear wholemounts by measuring the distance (yellow dashed line in A'' and B'') from the apex of the cochlear epithelium to the first cell that expressed either SOX2 or MYO7a (open yellow arrowhead). **(C)** Compared with cochleae from E16.5 control littermates, the base-to-apex sweep of MYO7a expression is significantly delayed in *Slc26a9*$^{Ebf1\text{-}cKO}$ cochleae (Table 2.S1). Sample size: five control and seven *Slc26a9*$^{Ebf1\text{-}cKO}$ mice from two litters, one duct per mouse. Scale bars: 100 μm for A (same for B) and 50 μm for A' (same for A'', B', and B'').

Table 2.S1. Statistical analyses

Comparison	*Parameter*	*Sample size*	*Statistical test*	*Significant p-values*
P1 *Slc26a9*$^{Ebf1\text{-}cKO}$ vs. littermate control	Total HC count	6 *Slc26a9*$^{Ebf1\text{-}cKO}$ and 4 control mice from 2 litters, 1 duct per mouse	Welch's t-test, two-tailed	iHCs: $p < 0.0001$ oHCs: $p < 0.0001$
P1 *Slc26a9*$^{Ebf1\text{-}cKO}$ vs. littermate control	HC density	6 *Slc26a9*$^{Ebf1\text{-}cKO}$ and 4 control mice from 2 litters, 1 duct per mouse	Two-way ANOVA with Holm-Šídák's multiple comparisons test	iHCs: $p < 0.0001$ for all regional comparisons oHCs: $p < 0.0001$ for base and middle, $p = 0.0008$ for apex
P1 *Slc26a9*$^{Ebf1\text{-}cKO}$ vs. littermate control	Area of marker expression	6 *Slc26a9*$^{Ebf1\text{-}cKO}$ and 6 control mice from 4 litters, 1 tissue section per mouse	Welch's t-test, two-tailed	SOX2: $p = 0.0382$ PRDM16: $p = 0.0213$
P1 *Slc26a9*$^{Ebf1\text{-}cKO}$ vs. littermate control	EdU$^+$ HC density	5 *Slc26a9*$^{Ebf1\text{-}cKO}$ and 6 control mice from 2 litters, 1 duct per mouse	Two-way ANOVA with Holm-Šídák's multiple comparisons test	EdU$^+$ iHCs: $p = 0.0009$ for base, $p = 0.0003$ for middle, $p < 0.0001$ for apex EdU$^+$ oHCs: $p = 0.0002$ for base, $p = 0.0331$ for middle, $p < 0.0001$ for apex
Regions within P1 *Slc26a9*$^{Ebf1\text{-}cKO}$	HC density	6 *Slc26a9*$^{Ebf1\text{-}cKO}$ mice from 2 litters, 1 duct per mouse	Two-way repeated measures ANOVA with Holm-Šídák's multiple comparisons test	iHCs: $p = 0.0084$ for base vs. middle, $p = 0.0084$ for base vs. apex oHCs: $p = 0.0096$ for base vs. middle, $p = 0.0013$ for base vs. apex, $p = 0.0108$ for middle vs. apex
Regions within P1 *Slc26a9*$^{Ebf1\text{-}cKO}$	EdU$^+$ HC density	5 *Slc26a9*$^{Ebf1\text{-}cKO}$ and 6 control mice from 2 litters, 1 duct per mouse	Two-way repeated measures ANOVA with Holm-Šídák's multiple comparisons test	EdU$^+$ oHCs: $p = 0.0261$ for base vs. middle, $p = 0.0392$ for base vs. apex, $p = 0.0261$ for middle vs. apex
E16.5 *Slc26a9*$^{Ebf1\text{-}cKO}$ vs. littermate control	Base-to-apex sweep of marker expression	7 *Slc26a9*$^{Ebf1\text{-}cKO}$ and 5 control mice from 2 litters, 1 duct per mouse	Welch's t-test, two-tailed	$p = 0.0242$
E16.5 *Slc26a9*$^{Ebf1\text{-}cKO}$ vs. littermate control	Duct length	7 *Slc26a9*$^{Ebf1\text{-}cKO}$ and 5 control mice from 2 litters, 1 duct per mouse	Welch's t-test, two-tailed	$p = 0.0029$
P50-74 *Slc26a9*$^{Ebf1\text{-}cKO}$ vs. littermate control	ABR thresholds	9 *Slc26a9*$^{Ebf1\text{-}cKO}$ (6 females and 3 males) and 5 control (1 female and 4 males) mice from 3 litters	Two-way ANOVA with Holm-Šídák's multiple comparisons test	$p < 0.0001$ for 6, 12, 18, 24, 30, and 45 kHz, $p < 0.0004$ for 60 kHz
E18 *Sox2*$^{Ebf1\text{-}cKO}$ vs. *Sox2*^{CreER}-negative littermate control	HC density	14 *Sox2*$^{Ebf1\text{-}cKO}$ and 15 *Sox2*^{CreER}-negative control mice from 6 litters, 1 duct per mouse	Two-way ANOVA with Tukey's multiple comparisons test	iHCs: $p < 0.0001$ for middle and apex oHCs: $p < 0.0001$ for apex
Regions within E18 *Sox2*$^{Ebf1\text{-}cKO}$	HC density	14 *Sox2*$^{Ebf1\text{-}cKO}$ from 6 litters, 1 duct per mouse	Two-way repeated measures ANOVA with Tukey's multiple comparisons test	iHCs: $p < 0.0001$ for base vs. middle and base vs. apex oHCs: $p = 0.0001$ for base vs. middle, $p = 0.0026$ for base vs. apex
Regions within E18 *Sox2*^{CreER}-negative controls	HC density	15 *Sox2*^{CreER}-negative control mice from 6 litters, 1 duct per mouse	Two-way repeated measures ANOVA	iHCs: $p < 0.0001$ fir base vs. middle, $p = 0.0001$ for base vs. apex oHCs: $p < 0.0001$ for base vs. middle, $p = 0.0049$ for base vs. apex

Table 2.S2. Antibodies used for immunostaining				
Antigen	***Host***	***Dilution***	***Cat. No.***	***Vendor***
CD44	Rat	1:600	14-0441-82	Thermo fisher
EBF	Mouse	1:200	sc137065-af647	Santa Cruz
FABP7	Rabbit	1:1000	ab32423	Abcam
JAGGED1	Rabbit	1:125	2620	Cell signaling
MYO7a	Rabbit	1:1000	25-6790	Proteus
MYO7a	Guinea pig	1:1000	n/a	Stefan Heller
Neurofilament	Chicken	1:200	ab134458	Abcam
Prestin	Goat	1:200	sc22692	Santa Cruz
PROX1	Rabbit	1:1000	ab5475	Chemicon
SOX2	Goat	1:200	af2018	R&D systems
SOX2	Rabbit	1:200	ab97959	Abcam
vGLUT3	Rabbit	1:300	135203	Synaptic systems

CHAPTER 3: EBF1 Regulates Sensory Establishment in the Cochlea by Positioning the Medial Boundary of the Prosensory Domain and Restricting Proliferation of the Sensory Progenitor Population

The contents of this chapter have been submitted to Development for publication with the following authors: Kathryn G. Powers, Joshua Hahn, Juliette Wohlschlegel, and Olivia Bermingham-McDonogh

Contributions by authors to the contents of this chapter were as follows: Conceptualization: K.G.P., O.B.Mc.D.; Methodology: K.G.P., J.W.; Validation: K.G.P, J.H., O.B.Mc.D.; Formal analysis: K.G.P., J.H.; Investigation: K.G.P., J.H., O.B.Mc.D.; Resources: O.B.Mc.D.; Data curation: K.G.P., J.W.; Writing - original draft: K.G.P., O.B.Mc.D.; Writing - review & editing: K.G.P., J.H, J.W., O.B.Mc.D.; Visualization: K.G.P., J.H.; Supervision: O.B.Mc.D.; Project administration: O.B.Mc.D.; Funding acquisition: K.G.P., O.B.Mc.D.

3.1 Abstract

In our previous study, we reported that *Ebf1* excision throughout the inner ear epithelium and before the onset of cochlear development leads to dramatic sensory expansion in the cochlea by neonatal stages. *Ebf1* conditional knockout cochleae possess over twice as many sensory cells as littermate controls and develop ectopic sensory patches in their Kölliker's organs. To better understand the mechanism behind EBF1's role in restricting sensory establishment, we performed multiome sequencing in our current study. EBF1 is a transcription factor best known for its importance in B cell lineage specification, during which it acts as both an activator and a repressor. Our results indicate that EBF1 prevents the Kölliker's organ cells from being recruited to the prosensory domain by promoting expression of *Prdm16* and repressing expression of *Jag1* and *Sox2*. We also found that EBF1 may promote cell cycle exit by repressing *Ccnjl* expression. In summary, medial expansion of the prosensory domain, together with delayed cell cycle exit in the developing cochlear epithelium, underlies the robust increase in sensory cells seen in *Ebf1* conditional knockouts.

3.2 Introduction

The sensory region of the cochlea, called the organ of Corti, contains both hair cells (HCs) and support cells (SCs). This region develops from an unpatterned epithelium through a process dependent on BMP, FGF, WNT, Hh, and Notch signaling (reviewed in Brown and Groves, 2020; reviewed in Ebeid and Huh, 2017; Hayashi et al., 2007; Hayashi et al., 2008b; Mansour and Urness, 2025; Munnamalai and Fekete, 2016; Ohyama et al., 2010; Riccomagno et al., 2002). A complex gradient of factors determines the medial and lateral borders of this sensory region. While the signals that establish the medial boundary of the prosensory domain are not well defined, BMP4 is thought to be critical in specifying the lateral boundary (Ohyama et al., 2010). BMP4 is expressed in the outer sulcus and patterns the cochlea in a dose-

dependent manner. High BMP4 inhibits prosensory domain formation while low BMP4 concentrations appear necessary for prosensory specification (Ohyama et al., 2010). Following cochlear patterning and sensory differentiation, the organ of Corti consists of one row of inner HCs (iHCs) and three rows of outer HCs (oHCs). Each iHC is surrounded by inner phalangeal cells, and each oHC has an associated Deiters' cell. In between the rows of iHCs and oHCs are two rows of pillar cells (inner and outer) that differentiate with prominent microtubule bundles crosslinked with actin to form the tunnel of Corti (Fig. 3.1; Tolomeo and Holley, 1997; Tucker et al., 1999). The sensory epithelium (SE) lies above the basilar membrane, which vibrates in response to sound, allowing the stereocilia on the tops of the HCs to deflect and thereby initiate the mechanotransduction that leads to neurotransmitter release from the iHCs. The signal is then relayed to the brain by the spiral ganglion neurons that synapse onto the HCs.

We first became interested in EBFs (Early B cell Factors) following a bulk ATAC sequencing study. In addition to detecting enrichment of motifs associated with transcription factors already known to be important in cochlear development, we identified EBF-binding motifs as being enriched in the open chromatin of cochlear prosensory and sensory cells (Wilkerson et al., 2019). A complementary single cell RNA sequencing study revealed that *Ebf1* is strongly expressed in the developing cochlear SE while the other members of the *Ebf* family, *Ebf*2-*4*, show little to no expression (Powers et al., 2024). Thus, we chose to look at cochlear development in a conditional knockout (cKO) mouse for *Ebf1*.

EBFs contain an unusual zinc finger DNA binding domain, an IPT/TIG domain, a helix-loop-helix domain, and a transactivation region (Hagman et al., 1995). They typically form stable dimers via the HLH domain and bind a palindromic consensus DNA motif (5'-TCCCNNGGGA-3'; Hagman et al., 1993; Travis et al., 1993) to regulate cell fate decisions, differentiation, and migration (reviewed in Liberg et al., 2002). EBF1 is the most extensively studied member of the EBF family, and the transcription factor has well-documented roles in a diverse range of developmental processes, including adipocyte differentiation (Jimenez et al., 2007) and

neurogenesis (Catela et al., 2019; Davis and Reed, 1996; Garel et al., 1997; Lobo et al., 2008; Wang and Reed, 1993; Wang et al., 1997). Notably, EBF1, also known as OLF1, is important in olfactory development where it regulates the transition from differentiation to maturation in olfactory receptor neurons (Cheng and Reed, 2007; Roby et al., 2012). As its name implies, however, EBF1 is best known for its roles in B cell progenitor proliferation and differentiation, during which it acts as both an activator and repressor (Li et al., 2018; reviewed in Ramírez et al., 2010; Treiber et al., 2010). EBF1 is required for activation of *Pax5* expression (Decker et al., 2009), and the two transcription factors are thought to work together to promote B cell specification by downregulating Notch signaling and repressing genes that specify alternative hematopoietic cell fates (Pongubala et al., 2008; Souabni et al., 2002; Thal et al., 2009). EBF1 also facilitates the transition from progenitor to B-cell-lineage-committed accessible chromatin by recruiting BRG1, the catalytic subunit of the SWI/SNF (BAF) chromatin remodeling complex, via its C-terminal transactivation domain (Wang et al., 2020; Zolotarev et al., 2022). EBF1 integrates activation, repression, and chromatin remodeling to ensure proper B cell programming.

We previously reported the cochlear phenotype of an *Ebf1*-cKO mouse, which uses the *Slc26a9* promoter to direct Cre-mediated excision of *Ebf1* throughout the inner ear epithelium at the otocyst stage. In the developing mouse cochlea, *Ebf1* is strongly expressed in both the epithelium and the surrounding mesenchyme. Briefly, the *Ebf1*-cKO phenotype involves an increase in early proliferation of the precursor cells such that the SE is doubled in size. We also saw a further increase in iHCs, suggesting that EBF1 is also important in regulating the medial border of the developing organ of Corti (Powers et al., 2024). In this study, we advance our understanding of this mutant by investigating how EBF1 shapes both the transcription and open chromatin landscapes of cells within the developing cochlea. By characterizing EBF1-binding motif accessibility within differentially expressed genes in cell-type-matched populations in the *Ebf1*-cKO and control littermate datasets, we were able to identify EBF1's dual role as a

transcriptional activator and repressor during critical stages of cochlear development. Instead of the expected decrease in chromatin accessibility from lost BRG1 interactions, we observed an overall increase, which we attribute to EBF1's indirect upregulation of *Sox2*. Within the Kölliker's organ, the transient epithelial structure that gives rise to the inner sulcus of the cochlea, EBF1 seems to be required to promote *Prmd16* expression and repress *Jag1* and *Sox2* expression, and thus, prevent Kölliker's organ cells from taking on a prosensory fate. We also found that EBF1 may directly regulate cell cycle exit in the developing cochlear epithelium by repressing *Ccnjl* expression. Loss of EBF1's interactions with these transcriptional targets leads to prolonged proliferation that is accompanied by an increase in the size of the sensory progenitor pool.

3.3 Results

Ebf1 excision leads a medial shift in the boundary separating the prosensory domain from Kölliker's organ as early as E14.5

We previously reported that at neonatal stages, *Ebf1*-cKO cochleae exhibit dramatic sensory expansion, with more than twofold increases in HCs and SCs within the differentiated SE as well as ectopic sensory patches within the Kölliker's organ (Powers et al., 2024). To investigate whether changes in prosensory domain establishment contribute to this expansion, immunostaining was performed at E14.5, a developmental stage when the cochlear floor is patterned along the medial-lateral axis into the Kölliker's organ, prosensory domain, and outer sulcus (Ohyama et al., 2010). Because *Ebf1* is strongly expressed in the developing cochlear epithelium, while *Ebf2-4* show little to no expression (Powers et al., 2024), a pan-EBF antibody was used to label EBF1. Anti-SOX2 and anti-PRMD16 antibodies were used to label the prosensory domain and Kölliker's organ, respectively. SOX2 is a transcription factor necessary for sensory development in the cochlea (Dabdoub et al., 2008; Kiernan et al., 2005b), and

PRDM16 is a transcription factor important in the development of the Kölliker's organ (Ebeid et al., 2022; Zhang et al., 2025). At E14.5, EBF1 is strongly expressed in the PRDM16^{+} Kölliker's organ and weakly expressed in the SOX2^{high+} prosensory domain of control cochleae. By contrast, *Ebf1*-cKO littermate cochleae exhibit a much smaller PRDM16^{+} Kölliker's organ and a much larger SOX2^{high+} prosensory domain (Fig. 3.2A). Interestingly, the few PRDM16^{+} Kölliker's organ cells that remain in the *Ebf1*-cKO cochleae appear to show weak EBF labeling. This *Ebf* expression could be the result of residual *Ebf1* expression or from *Ebf3* and *Ebf4*, which show modest levels of expression in the Kölliker's organ at this developmental timepoint (Powers et al., 2024).

To enable investigation of EBF1-dependent changes in cochlear patterning at the single cell level, multiome sequencing, which combines single nucleus RNA sequencing (snRNA-seq) and single nucleus ATAC sequencing (snATAC-seq), was performed at E14.5. Multiome sequencing makes it possible to examine shifts in the distribution of cell types across the entire cochlear epithelium and to control for patterning differences caused by delayed convergent extension in *Ebf1*-cKO embryonic cochlear ducts (Powers et al., 2024). The multiome datasets were generated from nuclei isolated from six control and six *Ebf1*-cKO cochlear ducts collected from one litter of four control and four *Ebf1*-cKO mice. The epithelial cells were separated from the non-epithelial cells (Fig. 3.S1) and clustering was performed on the epithelial cells using the control and *Ebf1*-cKO snRNA-seq data (Fig. 3.S2). As expected, snATAC-seq analysis of the *Ebf1*-cKO relative to control cochleae shows reduced predicted EBF1-binding activity in their Kölliker's organ cells and prosensory cells (Fig. 3.S3A). Surprisingly, however, snRNA-seq *Ebf1* transcript levels appear comparable between *Ebf1*-cKO and control cochleae (Fig. 3.S3B). This result can be attributed to both a poly-A stretch at the transcription start site of *Ebf1* transcripts that enables capture via poly(dT) priming and the design of the *Ebf1*-floxed allele (Vilagos et al., 2012). Exons 6-16 of *Ebf1* are excised in *Ebf1*-cKOs, leaving a sequence that encodes a fusion protein containing the EBF1 zinc coordination motif and GFP. While coverage near the *Ebf1*

transcription start site is similar for *Ebf1*-cKO and control samples (Fig. 3.S3C), coverage in exons 6-16 is significantly reduced in the *Ebf1*-cKO (Fig. 3.S3D), consistent with their successful excision in the *Ebf1*-cKOs.

The distribution of epithelial cells in *Ebf1*-cKO and control snRNA-seq UMAPs (Fig. 3.2B, C) recapitulate the phenotype seen in the stage-matched embryonic immunostaining experiment (Fig. 3.2A). Like *Sox2*, *Hey2* is expressed by prosensory cells (Hayashi et al., 2008a); however, *Hey2* expression is more restricted to just the prosensory domain (Fig. 3.S2). In the E14.5 control cochleae, the *Prdm16*$^{high+}$ Kölliker's organ accounts for 16.9% of epithelial cells while the *Hey2*$^{+}$ prosensory cells represent 21.4%. In E14.5 *Ebf1*-cKO cochleae, the relative number of Kölliker's organ cells drops by more than half to 7.6% and prosensory cells increases to 27.3%, while the percentages for the other epithelial cell types remain largely unchanged compared with the littermate controls (Fig. 3.2C-E). In summary, both the E14.5 immunostaining and multiome sequencing experiments demonstrate that loss of EBF1 during cochlear patterning leads to the co-option of Kölliker's organ cells into the prosensory domain.

Ebf1 excision leads to delayed cell cycle exit as late as E16.5 in the developing cochlear epithelium

In the developing cochlea, the prosensory domain is defined between E12 and E15 as prosensory cells undergo cell cycle exit in a wave that starts at the apex and progresses towards the base (Chen and Segil, 1999; Ruben, 1967). These prosensory cells subsequently differentiate into HCs and SCs in a wave that proceeds in the opposite direction, starting at the base around E14 and reaching the apex during neonatal stages (Chen et al., 2002). To assess how the changes in cochlear patterning observed at E14.5 impact development at later stages when HC and SC differentiation is well underway, immunostaining was performed at E16.5. Much like at E14.5, EBF1 is strongly expressed in the Kölliker's organ and weakly expressed in the developing SE, and the expanded *Ebf1*-cKO SOX2^{high+} developing SE is adjacent to a

smaller PRDM16^{+} Kölliker's organ (Fig. 3.3A). Interestingly, the *Ebf1*-cKO PRDM16 expression domain appears less diminished at this later stage, suggesting compensatory pathways may begin to counteract loss of *Ebf1* by E16.5 and allow for the Kölliker's organ to reestablish by neonatal stages (Powers et al. 2024).

Multiome sequencing was performed at E16.5 to investigate how loss of *Ebf1* impacts cochlear patterning, cell cycle exit, and differentiation at the single cell level. The E16.5 multiome datasets were generated from six control and six *Ebf1*-cKO cochlear ducts from one litter of four control and three *Ebf1*-cKO mice. *Ebf1*-cKO and control epithelial cells were separated from the non-epithelial populations (Fig. 3.S4), and clustering was performed on the epithelial subset using the snRNA-seq data (Fig. 3.S5). In the E16.5 control cochleae, the Kölliker's organ accounts for 41.9% of epithelial cells while the developing SE, inner HCs (iHCs), outer HCs (oHCs), and early lateral SCs account for 11.9%. In E16.5 *Ebf1*-cKO cochleae, the relative number of Kölliker's organ cells drops by about a third to 28.3% and the relative number of developing SE and differentiated sensory cells approximately doubles to 22.3% (Fig. 3.3B, C). In addition to capturing the recruitment of Kölliker's organ cells to the developing SE observed in the stage-matched embryonic immunostaining experiment, the E16.5 snRNA-seq data highlight an increase in the relative number of *Top2a*$^{+}$ and *Mki67*$^{+}$ cycling cells in *Ebf1*-cKO compared with control cochleae (Fig. 3.3C-E). Cycling cells represent 3.0% of the control epithelial cells and 9.3% of the *Ebf1*-cKO epithelial cells (Fig. 3.3C). This result agrees with our previous finding that proliferation of *Ebf1*-cKO prosensory cells persists beyond E15 (Powers et al., 2024). Since the relative number of cycling cells at E14.5 is comparable between *Ebf1*-cKO and control cochleae (Fig. 3.2C), the increase detected at E16.5 is likely due to delayed cell cycle exit. EBF1 regulates sensory development in the cochlea by both positioning the medial boundary of the prosensory domain and restricting the proliferative capacity of the sensory progenitor population.

EBF1 likely regulates Prdm16, Sox2, and Jag1 expression to prevent Kölliker's organ cells from adopting a prosensory cell fate

To investigate the mechanism underlying EBF1's role in cochlear patterning at E14.5, R packages Seurat and Signac were used to perform multiomic analyses involving both snRNA-seq and snATAC-seq data from *Ebf1*-cKO and control littermates. Differentially expressed genes in Kölliker's organ cells were identified to uncover potential EBF1 targets that explain the transcription factor's role in preventing their recruitment to the prosensory domain (Table 3.S1). *Ebf1* excision leads to an overall increase in chromatin accessibility in Kölliker's organ cells, with 510 ATAC peaks more accessible and only five peaks less accessible in *Ebf1*-cKOs relative to controls (Fig. 3.4A). Consistent with the E14.5 immunostaining results (Fig. 3.2A), *Prdm16* is among the 51 downregulated genes and *Sox2* is among the 106 upregulated genes in *Ebf1*-cKO compared with control Kölliker's organ cells (Fig. 3.4B). This shift is accompanied by upregulation of additional established prosensory markers, including *Hey2* and *Fgf20* (Hayashi et al., 2008a; Hayashi et al., 2008b). Interestingly, *Jag1* expression is also elevated in *Ebf1*-cKO Kölliker's organ cells. JAG1 (Jagged-1), a Notch ligand important in prosensory specification, is initially expressed throughout the cochlear floor at E12.5 and becomes restricted to the Kölliker's organ by E13.5 (Basch et al., 2016b; Kiernan et al., 2006; Ohyama et al., 2010). JAG1 expression then shifts to the differentiating prosensory domain before ultimately being expressed in differentiated SCs by E16.5 (Basch et al., 2016b; Murata et al., 2006). As JAG1 shifts from the Kölliker's organ to the prosensory domain, its expression domain becomes restricted to a column of cells along the medial boundary of the prosensory domain at E14.5. Loss of EBF1 leads to a marked, medial expansion of the JAG1 expression domain (Fig. 3.4C, D). Like the dysregulation of *Prdm16* and *Sox2* expression, the upregulation of *Jag1* in the receding *Ebf1*-cKO Kölliker's organ suggests it may be direct or indirect target of EBF1, essential for proper cochlear patterning.

After identifying potential EBF1 targets with the snRNA-seq data, the snATAC-seq data was used to look for evidence of direct regulation by EBF1. Differentially accessible chromatin regions within and 500 kb proximal to the gene loci were screened for both EBF1-binding motifs and a strong correlation with RNA expression using the 'LinkPeaks' function in Signac. Given that EBF1 is known to act as an activator as well as a repressor during B cell lineage specification (Li et al., 2018; reviewed in Ramírez et al., 2010; Treiber et al., 2010), the snRNA-seq and snATAC-seq data were analyzed together to determine EBF1's mode of regulation at each target locus. EBF1-dependent changes in chromatin accessibility are consistently more pronounced in Kölliker's organ cells than prosensory cells, and *Ebf1* excision in the cochlear epithelium causes the open chromatin of Kölliker's organ cells to take on a more prosensory-like pattern (Fig. 3.4E-G). Two open chromatin regions were identified that strongly correlate with *Prdm16* RNA expression and that contain EBF1 motifs, and both regions are less accessible in *Ebf1*-cKO than control Kölliker's organ cells (Fig. 3.4E). Taken together with our finding that *Ebf1* excision leads to downregulation of *Prdm16*, this decrease in chromatin accessibility suggests that EBF1 is needed to promote *Prdm16* expression in Kölliker's organ cells. Examination of open chromatin regions linked with *Jag1* RNA expression reveals regions containing EBF1 motifs that show subtle changes and appear more accessible in the *Ebf1*-cKO Kölliker's organ cells (Fig. 3.4F). These open chromatin regions also contain PRDM16 motifs. Given that *Ebf1*-cKOs show upregulation of *Jag1* in their Kölliker's organ cells, PRDM16 may interact with EBF1 to repress *Jag1* expression. Although we did not find any open chromatin regions near the *Sox2* locus that both contained EBF1 motifs and were linked to expression of the gene, we did detect a distal region (~500 kb from the transcription start site) containing a PRDM16 motif and associated with *Sox2* RNA expression (Fig. 3.4G). This region is more accessible in the *Ebf1*-cKO Kölliker's organ cells (Fig. 3.4G'). As *Ebf1* excision leads to an upregulation of *Sox2* in Kölliker's organ cells, this finding suggests that PRDM16 directly represses *Sox2* expression in these cells. In summary, our analyses indicate EBF1 is necessary

to promote *Prdm16* expression and possibly to co-repress *Jag1* expression with PRDM16. PRDM16, in turn, appears to be necessary to repress *Sox2* expression. EBF1's regulation of these targets in the Kölliker's organ likely helps prevent the cells from assuming a prosensory identity.

Gene ontology (GO) term enrichment analysis using our snATAC-seq data revealed that the top two dysregulated terms in the Kölliker's organ cells of E14.5 *Ebf1*-cKOs compared with controls were *Negative Regulation of Notch Signaling* and *Regulation of Notch Signaling* (Fig. 3.S6A). Consistent with this finding, receptor-ligand analysis of the Notch pathway at E14.5 using CellChat shows that Notch signaling levels in *Ebf1*-cKO Kölliker's organ cells increase dramatically and resemble those seen in prosensory cells (Fig. 3.S6B). This increase in Notch signaling is likely driven by the upregulation of *Jag1* observed in *Ebf1*-cKOs, as we do not find significant expression differences between *Ebf1*-cKO and control cochleae in other Notch-ligand genes (Fig. 3.S6C) and our multiomic analyses indicate that EBF1 and PRDM16 co-repress *Jag1* expression.

EBF1 may directly repress Ccnjl expression to restrict cell proliferation in the developing cochlear epithelium

Loss of EBF1 leads to prolonged and expanded prosensory cell proliferation (Powers et al., 2024). At E16.5, proliferating cells in control cochleae are restricted to Kölliker's organ, whereas EdU^{+} cells are seen in expanded $SOX2^{high+}$ developing SE in *Ebf1*-cKO cochleae (Fig. 3.5A). These cells can be seen throughout the expanded SE but are more concentrated in the medial half. To investigate the mechanism by which EBF1 regulates cell cycle exit, we examined E16.5 *Ebf1*-cKO and control littermates. We detected 71 upregulated and 27 downregulated cell-cycle related genes in *Ebf1*-cKO relative to control cycling cells and identified *Pten*, *Sox2*, and *Ccnjl* as possible targets of EBF1 (Fig. 3.5B; Table 3.S2). PTEN is a well-established tumor suppressor and is downregulated in *Ebf1*-cKO cycling cells (Li et al., 1997; Steck et al., 1997).

Sox2, previously noted for its role in inner ear sensory development, is also linked to stemness and tumor progression and is upregulated in these cells (reviewed in Boiani and Schöler, 2005; Boyer et al., 2005). *Ccnjl* encodes a cyclin-like protein associated with several cancers (Gu et al., 2024; Han et al., 2025; Li et al., 2021; Li et al., 2025; Qin et al., 2024; Viet et al., 2021; Wang et al., 2025) and is upregulated in *Ebf1*-cKO cycling cells (Fig. 3.5C). Of these candidates, *Ccnjl* emerged as the strongest for a direct EBF1 target involved in cell cycle exit. Neither *Pten* nor *Sox2* possess EBF1-binding motifs in open chromatin regions within or around their gene loci that are linked to their RNA expression, ruling them out as direct EBF1 targets. *Ccnjl*, by contrast, possesses an open chromatin region with an EBF1 motif that is more accessible in *Ebf1*-cKO than control cycling cells and strongly correlated with *Ccnjl* RNA expression (Fig. 3.5D). This same region also possesses a SOX2 motif, suggesting that SOX2 directly promotes *Ccnjl* expression. While EBF1's effects on cell cycle exit may be mostly indirect, these results raise the possibility that EBF1 limits proliferation in the cochlear epithelium by repressing *Ccnjl* expression both directly and indirectly, by downregulating *Sox2*.

3.4 Discussion

Proposed mechanism for EBF1's role in restricting cochlear sensory development

We highlighted the importance of EBF1 in restricting sensory development within the cochlea in our previous study (Powers et al., 2024). In this study, we use multiome sequencing to investigate the mechanism by which EBF1 regulates two aspects of prosensory domain establishment: (1) the positioning of the medial boundary of the prosensory domain and (2) the proliferative capacity of the sensory progenitor pool. We generated snRNA-seq and snATAC-seq libraries from the same nuclei isolated from cochlear ducts collected at two key developmental timepoints. This allowed us to screen differentially expressed genes from cell-type-matched populations in the *Ebf1*-cKO and control datasets for differentially accessible

chromatin regions containing binding motifs associated with EBF1 or its direct targets. Analysis of E14.5 Kölliker's organ cells revealed that EBF1 likely prevents these cells from taking on a prosensory fate by directly regulating *Prdm16* and *Jag1* expression and indirectly regulating *Sox2* expression (Fig. 3.6A). A comparable regulatory relationship with *Prdm16* has been described for brown adipose differentiation, during which EBF2 directly promotes *Prdm16* expression (Rajakumari et al., 2013). PRDM16 is also known to act as a coregulator (Seale et al., 2007), and the transcription factor is thought to interact with EBF2 to regulate gene expression during brown adipogenesis (reviewed in Mao et al., 2024). We similarly see evidence that EBF1 and PRDM16 co-repress *Jag1* expression in the developing cochlea. Our multiomic analyses additionally provide evidence that PRMD16 directly represses *Sox2* expression. *Sox2*, however, is not uniformly downregulated in the PRDM16^{+} Kölliker's organ and maintains weak expression in Kölliker's organ cells closest to the E14.5 prosensory domain and E16.5 developing SE before becoming restricted to differentiated SCs (Fig. 3.2A and 3.3A; Dabdoub et al., 2008). This pattern suggests other signals counteract PRDM16 activity and prevent complete repression of *Sox2* expression in this region. Our model of EBF1's direct and indirect interactions with these transcriptional targets is supported by the finding that *Jag1* and *Sox2* are upregulated in *Prdm16* null cochleae (Ebeid et al., 2022). Multiome analysis of a later developmental stage, E16.5, revealed that EBF1 likely promotes cell cycle exit by directly repressing *Ccnjl* expression and indirectly repressing it through downregulation of *Sox2* (Fig. 3.6B). In zebrafish, SOX transcription factors show significant co-occurrence with EBF1 motifs in regeneration-responsive elements in SCs (Jimenez et al., 2022), suggesting potential regulatory interplay. On the basis of our results, we propose that EBF1 regulates sensory development in the cochlea through direct transcriptional control of key regulators of prosensory identity and proliferation. Delayed cell cycle exit combined with an increase in the size of the prosensory domain allows for the over twofold increase in HCs and SCs seen *Ebf1*-cKOs (Kagoshima et al., 2024; Powers et al., 2024).

In another developmental context, B cell lineage specification, EBF1 is known to recruit chromatin remodeling complexes that promote chromatin accessibility (reviewed in Ramírez et al., 2010; Wang et al., 2020; Zolotarev et al., 2022). In the cochlea, however, *Ebf1* excision leads to an overall increase in chromatin accessibility in Kölliker's organ cells at E14.5 (Fig. 3.4A). To gain mechanistic insight into this change, we searched for motif enrichment within the differentially accessible chromatin regions and found that the SOX2 motif was the most significantly enriched of the motifs belonging to transcription factors expressed in the snRNA-seq data. SOX2 is known to act as an activator during hippocampal neurogenesis and cochlear development (Ahmed et al., 2012; Amador-Arjona et al., 2015; Kempfle et al., 2016), and the upregulation of *Sox2* in *Ebf1*-cKO Kölliker's organ cells likely drives the overall increase in their chromatin accessibility. Interestingly, while the changes in gene expression in *Ebf1*-cKO relative to control Kölliker's organ are similar at E14.5 and E16.5 (219 upregulated and 105 downregulated genes in E16.5 Kölliker's organ; Fig. 3.S7B), open chromatin accessibility at E16.5 is less skewed towards an overall increase and not linked to a specific transcription factor or pathway (183 more accessible and 113 less accessible ATAC peaks in E16.5 Kölliker's organ; Fig. 3.S7A), suggesting that this SOX2 driven change is specific to E14.5.

EBF1 interacts with the Notch pathway during cochlear patterning

EBF1 is known to repress gene expression in a dose-dependent manner (Lukin et al., 2011), and Notch signaling has been shown to reduce EBF activity (Smith et al., 2005). Thus, EBF1 expression may need to reach a certain threshold relative to Notch signaling levels to downregulate *Jag1*. At E12.5, EBF1 and JAG1 expression domains overlap, with EBF1 restricted to the medial edge (Kagoshima et al., 2024; Powers et al., 2024) and JAG1 broadly expressed throughout the cochlear floor (Ohyama et al., 2010). At E14.5, JAG1 expression shifts from Kölliker's organ to the prosensory domain (Basch et al., 2016b; Murata et al., 2006), while EBF1 is strongly expressed in the Kölliker's organ and weakly in the prosensory domain

(Fig. 3.4D; Kagoshima et al., 2024; Powers et al., 2024). JAG1 becomes increasingly restricted to differentiated SCs starting around E16.5 (Fig. 3.S7C, D; Murata et al., 2009). At the same stage, EBF1 is only weakly expressed in the developing SE but strongly expressed in the Kölliker's organ, especially in the region of the organ closest to the developing SE (Fig. 3.S7D), and later persists at low levels in adults SCs (Powers et al., 2024). The interplay between EBF1 and JAG1 expression may allow EBF1 to reach the appropriate threshold, relative to Notch activity levels (Murata et al., 2006), needed to downregulate *Jag1* in the Kölliker's organ around E14.5. Relatively low EBF1 levels in the developing SE at E16.5, together with high Notch activity associated with sensory patterning through lateral inhibition (Murata et al., 2006), likely permit JAG1 expression to persist in this portion of the cochlear floor, whereas high EBF1 expression at the lateral edge of the Kölliker's organ may be necessary to maintain the medial boundary of the developing SE.

Just as BMP signaling is essential for establishing the lateral boundary of the prosensory domain (Ohyama et al., 2010), Notch signaling has been proposed to be critical for establishing the medial boundary (Basch et al., 2016b; Maunsell et al., 2023). As JAG1 expression shifts from the Kölliker's organ to the differentiating prosensory domain, its expression becomes localized to a narrow band at the medial boundary of the prosensory domain (Fig. 3.4D). Notch signaling at this boundary is essential for establishing a single row of iHCs (Basch et al., 2016b). The differentiated nascent iHCs send Notch signals to neighboring cells in the Kölliker's organ, preventing them from becoming iHCs or inner phalangeal cells. A modest reduction in Notch signaling has been reported to result in supernumerary iHCs and inner phalangeal cells. Double mutants for *Lfng* and *Mfng*, the genes encoding glycosyltransferases that strengthen Notch receptor affinity for DLL1 over JAG1, possess duplicates of iHCs and inner phalangeal cells (Basch et al., 2016b). A similar phenotype is seen in mice with mutations in *Lrrn1*, which encodes a single-pass membrane protein that facilitates Notch signaling along the medial boundary of the prosensory domain (Maunsell et al., 2023). By contrast, a more pronounced

reduction in Notch signaling impairs lateral inhibition, leading to the formation of supernumerary HCs at the expense of SCs (Kiernan et al., 2005a; Kiernan et al., 2006). Neonatal *Ebf1*-cKOs possess multiple rows of iHCs and these sensory cells are accompanied by supernumerary inner phalangeal cells (Powers et al., 2024). The expanded JAG1 expression domain in E14.5 *Ebf1*-cKOs is consistent with an increase in iHC and inner phalangeal precursors at the medial boundary of the prosensory domain due aberrant Notch signaling.

Understanding ectopic sensory patch formation in Ebf1-cKOs

Loss of EBF1 leads to the formation of ectopic sensory patches (Powers et al., 2024), likely derived from the partial conversion of the Kölliker's organ to SE. Other manipulations, particularly in the Notch pathway, have shown similar phenotypes. For examples, ectopic expression of ATOH1, a transcription factor required for HC differentiation in the inner ear, is sufficient to generate HCs in the Kölliker's organ (Woods et al., 2004; Zheng and Gao, 2000). Similarly, Notch signaling promotes and can directly induce sensory formation in non-SE within the inner ear (Driver et al., 2008; Hartman et al., 2010; Neves et al., 2011; Pan et al., 2010). The upregulation of *Jag1* in *Ebf1*-cKO Kölliker's organ cells, likely leads to increased Notch activity, and ultimately, to the ectopic sensory patches in the Kölliker's organ by neonatal stages (Powers et al., 2024). A similar ectopic patch phenotype is seen in neonatal *Prdm16* null cochlea, which also show an upregulation of *Jag1* relative to controls (Ebeid et al., 2022; Zhang et al., 2025). Interestingly, the *Ebf1*-cKO PRDM16 expression domain is less diminished at E16.5 (Fig. 3.3A and 3.S7) than at E14.5 (Fig. 3.2A and 3.4D). EBF3 and EBF4, which are expressed in the Kölliker's organ at moderate levels during cochlear development (Powers et al., 2024), may limit the extent to which Kölliker's organ cells adopt a prosensory fate in the absence of EBF1. In keeping with this hypothesis, *Ebf3* is upregulated in Kölliker's organ cells of E14.5 *Ebf1*-cKOs compared with controls. The conversion of the Kölliker's organ to SE is likely

patchy, rather than a completely confluent transformation, because of compensatory mechanisms.

EBF1's interactions with regulators of cell cycle

Loss of EBF1 leads to delayed cell cycle exit in the developing cochlea (Fig. 3.5A; Powers et al., 2024). Prolonged prosensory proliferation often leads to the generation of supernumerary HCs and SCs (Chen and Segil, 1999; Jacques et al., 2012; Kiernan et al., 2005a; Löwenheim et al., 1999; Tateya et al., 2011) and contributes to the over twofold increases in sensory cells seen in *Ebf1*-cKOs by neonatal stages (Kagoshima et al., 2024; Powers et al., 2024). EBF1 is known to regulate cell cycle exit during neurogenesis and B cell lineage specification, and emerging evidence points to EBFs, particularly EBF1 and EBF3, involvement in tumor suppression (reviewed in Liao, 2009). During neurogenesis, EBFs couple differentiation and migration to cell cycle exit. Ectopic expression of *Ebf1* in neuroepithelial progenitors leads to their premature exit from the cell cycle (Garcia-Dominguez et al., 2003). In early-stage B cells, EBF1 regulates expression of cell cycle regulator genes, including *E2f2*, *E2f8*, *Cdk2*, *Ccnd2*, *Ccnd3*, and *Cdc6* (György et al., 2012). Though we do not see evidence that EBF1 directly regulates these targets in our E16.5 multiome datasets, EBF1 may directly downregulate *Ccnjl* in cycling cells.

Study limitations

We used multiome sequencing to simultaneously profile gene expression and chromatin accessibility in the same nuclei isolated from the cochleae of *Ebf1*-cKO and control littermates. We used this information to identify cell types, compare differential gene expression and chromatin accessibility in cell-typed-matched populations, and infer transcriptional regulation by EBF1 and its downstream targets. Rather than focusing on EBF1's targets alone, this approach provides a global view of how EBF1 fits into a regulatory network while also minimizing the

confounding noise that comes from analyzing an entire tissue with cell types as diverse as those of the mammalian cochlea. A limitation of our study is that we have not confirmed direct binding of EBF1 to the proposed transcriptional targets. In future studies, Chromatin Immunoprecipitation sequencing (ChIP-seq; Solomon and Varshavsky, 1985), Cleavage Under Targets and Release Using Nuclease (CUT&RUN; Skene and Henikoff, 2017), or Cleavage Under Targets and Tagmentation (CUT&Tag; Kaya-Okur et al., 2019) could be used to accomplish this.

Conclusions

Our findings place EBF1 as an integral regulator within the gene regulator networks controlling cochlear development. By E14.5, EBF1 likely activates *Prdm16* and represses *Jag1* and *Sox2* to prevent Kölliker's organ cells from taking on a prosensory fate and help position the medial boundary of the prosensory domain. By E16.5, EBF1 may promote cell cycle exit in the cochlear epithelium by downregulating *Ccnjl* directly and indirectly, through its downregulation of *Sox2*. Together, the medial shift of the prosensory domain and delayed cell cycle exit drive the pronounced sensory expansion in *Ebf1*-cKOs. EBF1 plays an essential role in restricting sensory establishment within the developing cochlea.

3.5 Materials and Methods

Animal Care and Strains

Mice were housed at the University of Washington Department of Comparative Medicine. All experiments were approved by the Institutional Animal Care and Use Committee of the University of Washington and performed in accordance with the standards outlined by the National Institutes of Health (NIH). Mice were euthanized in accordance with IACUC approved procedures and in line with NIH policies.

Ebf1$^{fl/fl}$ mice were obtained from Jackson labs on a C57BL/6 background (Strain #028104). The *Slc26a9*$^{P2A\text{-}Cre}$ mice were obtained from a colleague on a C57BL/6 background (Urness et al., 2020) and are available from MMRC, Davis, CA (MMRRC:067348-MU). To generate *Slc26a9*-conditional *Ebf1* knockout mice, *Slc26a9*$^{P2A\text{-}Cre}$ males were crossed with *Ebf1*$^{fl/fl}$ females to generate *Slc26a9*$^{P2A\text{-}Cre}$ *Ebf1*$^{fl/+}$ progeny. Male *Slc26a9*$^{P2A\text{-}Cre}$ *Ebf1*$^{fl/+}$ mice identified by genotyping (see below) were then crossed with female *Ebf1*$^{fl/fl}$ mice to generate litters containing *Slc26a9*$^{P2A\text{-}Cre}$ *Ebf1*$^{fl/fl}$ mice. *Slc26a9*$^{P2A\text{-}Cre}$ *Ebf1*$^{fl/fl}$ male mice identified by genotyping were bred with *Ebf1*$^{fl/fl}$ female mice to generate *Slc26a9*$^{P2A\text{-}Cre}$ *Ebf1*$^{fl/fl}$ (*Ebf1*-cKO) and *Ebf1*$^{fl/fl}$ (control) littermates for phenotypic and multiomic analyses. Embryonic stages were verified by Theiler's criteria.

Genotyping

Tail tips or ear punches were collected for genotyping. Mice for multiome sequencing were screened for *Slc26a9*$^{P2A\text{-}Cre}$ using the following qPCR primer pair: GGTGCAAGCTGAACAACAGG and CAGGTGCTGTTGGATGGTCT. All other mice were screened for *Slc26a9*$^{P2A\text{-}Cre}$ using the following PCR primer trio: GGAGGAACACAGTTCACAGT, GTGTCTGGTGTGGCTGATGACC and ATGGGTTCACCAGAGTCTCATC. All mice were genotyped to identify homozygosity for the floxed *Ebf1* allele (*Ebf1*$^{fl/fl}$) using two sets of qPCR primer pairs: (1) TGTGGCAACCGAAATGAG and CCTGTGAGCGACACAAAGC in addition to (2) ACGACTTCTTCAAGTCCGCC and TCTTGTAGTTGCCGTCGTCC. The first primer pair was designed to identify the presence of the wildtype *Ebf1* allele (Vilagos et al., 2012). The second primer pair was used to reveal the presence of the *GFP* associated with the fusion protein encoded in the floxed *Ebf1* allele (Vilagos et al., 2012). Mice were identified as *Ebf1*$^{fl/fl}$ if they tested negative for wildtype *Ebf1* allele and positive for *GFP*.

Immunostaining and EdU Labeling

E14.5 and E16.5 heads were fixed overnight in 4% paraformaldehyde at 4°C. Following fixation, heads were washed in PBS and incubated in a sucrose series consisting of 5%, 10%, 15%, 20%, 25%, and 30% sucrose washes and a final wash in a 1:1 solution of OCT (Tissue-Tek 4583) and 30% sucrose. Heads were then incubated in OCT for 3 h at room temperature prior to being embedded in OCT and frozen for sectioning.

The 12 µm tissue sections were washed with 0.1% Triton X-100 before being blocked for 1 h at RT with a blocking solution consisting of 0.5% Triton X-100 and 10% normal donkey serum. Primary antibodies – mouse anti-EBF (C-8) Alexa Fluor-647 (Santa Cruz sc137065-af647), rabbit anti-JAG1 (Cell Signaling 2620), sheep anti-PRDM16 (R&D Systems af6295), goat anti-SOX2 (R&D Systems af2018), and rabbit anti-SOX2 (Abcam ab97959) – were diluted in blocking solution and applied to the tissue sections overnight at room temperature. Sections were then washed with 0.1% Triton X-100 and labeled with Alexa Fluor-labeled secondary antibodies and Hoechst 33342 (Invitrogen H3570) for 1 h at room temperature.

To detect proliferating cells at E16.5, 5-ethynyl-2'-deoxyuridine (EdU; 50 mg/kg; Invitrogen A10044) reconstituted in sterile PBS was administered to pregnant dams via intraperitoneal injection, 2 h before tissue collection. Click-iT Alexa-Fluor-647 (Invitrogen C10430) was used to detect incorporated EdU in E16.5 cochleae using the manufacturer's protocol.

All tissue sections were imaged on a Zeiss LSM 880 confocal microscope.

Single Nucleus Multiome Library Preparation and Barcoding

After collecting E14.5 or E16.5 embryos from *Ebf1*$^{fl/fl}$ females timed-mated with *Slc26a9*$^{P2A\text{-}Cre}$ *Ebf1*$^{fl/fl}$ males, tail snips were gathered for *Slc26a9*$^{P2A\text{-}Cre}$ qPCR genotyping, and the temporal bones were removed. The cochlear ducts were then dissected in 1% 1 M HEPES

diluted in HBSS and pooled according to genotype in cryogenic tubes. The samples were centrifuged at 300 RCF for 6 min at 4°C, after which the saline solution was removed using an insulin syringe, and the cochlear ducts were snap frozen and stored in liquid nitrogen. Once E14.5 and E16.5 samples with at least six *Slc26a9*$^{P2A\text{-}Cre}$ *Ebf1*$^{fl/fl}$ and six *Ebf1*$^{fl/fl}$ cochlear ducts had been obtained, the samples were thawed on ice, and the nuclei were isolated using a modified version of the protocol for the Chromium Nuclei Isolation Kit (10x Genomics 1000493) that omitted steps involving vortexing or use of a pestle or column. Briefly, samples were incubated in 500 µL lysis buffer for 1 min on ice, then triturated until fully dissociated (~5-6 min). Next the nuclei suspensions were filtered through cell strainer caps (FALCON 352235) into pre-chilled collection tubes and spun down at 500 RCF for 3 min at 4°C. The nuclei pellets were then washed with 500 µL of a 1:1 solution of wash buffer and resuspension buffer, centrifuged at 500 RCF for 10 min at 4°C, and resuspended 500 µL resuspension buffer. Lysis, wash, and resuspension buffers were made using the recipes in the Chromium Nuclei Isolation Kit user guide.

Following nuclei isolation and purification, samples were centrifuged at 300 RCF for 5 min at 4°C and resuspended in HBSS to reach a concentration of 5000 cells/µL. Library construction was done with a 9,000 targeted nuclei recovery using the Chromium Next Cell Multiome ATAC + Gene Expression Reagent Bundle (10x Genomics 10000285) following the manufacturer's protocol. Briefly, nuclei were encapsulated in a gel matrix and uniquely barcoded using the 10x Chromium Controller (Chip J, 10x Genomics 1000230). Libraries were then sequenced using Illumina NovaSeq.

Single Nucleus Multiome Sequencing Data Preparation and Analysis

CellRanger arc count (2.0) was used to align sequencing reads to the mm10 genome and define ATAC peaks. The aligned data was loaded into R and further analyzed using the Signac (v1.14.0; Stuart et al., 2021) and Seurat (v5.2.1; Hao et al., 2024) packages. *Ebf1*-cKO

and control samples from the same timepoint were combined and analyzed together. To ensure consistent peak definitions, overlapping or adjacent genomic intervals between the two conditions were merged into a single peak, and the peak expression matrix was calculated using the new merged peak set in Signac using 'FeatureMatrix' and stored in the ATAC assay.

Next, the gene expression matrix was stored in the RNA assay and processed using the Seurat pipeline. Reads were log-normalized using 'NormalizeData', 2000 variable features were identified using 'FindVariableFeatures', and data integration using CCA was performed to correct for batch effects between the two conditions. The batch-corrected expression of each gene was scaled and used to calculate principal components (PCs) using RunPCA(). The top 20 PCs were used to identify neighbors, find clusters, and generate a UMAP. Canonical markers were used to label clusters epithelium (*Epcam*), immune cells (*C1qa*), spiral ganglion (*Nefm*), Schwann cells (*Fabp7*), mesenchyme (*Pou3f4*), and endothelium (*Pecam1*) at E14.5 and E16.5 (Fig. 3.S1 and 3.S4) in addition to melanocytes (*Pmel*) at E16.5 (Fig. 3.S4). As we were primarily interested in the SE, epithelial cells were separated, and the clustering procedure was repeated on this subset of cells. Canonical markers were used to label the epithelial clusters. E14.5 and E16.5 epithelial clusters were annotated as Kölliker's organ (*Tecta*, *Fgf10*, and *Prdm16*), prosensory domain or developing SE (*Tecta*, *Hey2*, and *Sox2*), early HCs or HCs (*Tecta*, *Sox2*, *Atoh1*, *Pou4f3*, and *Gfi1*), outer sulcus (*Bmp4* and *Fst*), cycling cells (*Top2a*), stria vascularis (*Oc90*), and Reissner's membrane (*Oc90* and *Otx2*) (Fig. 3.S2 and 3.S5). E16.5 epithelial clusters were also labeled as iHCs (*Fgf8*), oHCs, and early lateral SCs (*Hes5*, *Heyl*, and *Ngfr*) (Fig. 3.S5).

Differential expression tests were performed between conditions using a Wilcoxon ranked-sum test implemented in Seurat's 'FindMarkers' command with default parameters. This was applied to find differences in gene expression using the RNA assay and peak accessibility using the ATAC assay.

Cell-cell communication analysis was performed using CellChat (v2.1.2; Jin et al., 2021). Analysis was performed separately for the *Ebf1*-cKO and control conditions, and non-protein signaling interactions were excluded. The average gene expression by cell type was calculated using the trimean and used to infer cell-cell communication probabilities.

Peak-Gene and TF-gene Linkage

After removing peaks associated with contigs, peaks were analyzed for transcription factor binding sites using Signac's 'AddMotifs' function. The Jaspar 2020 database was used for transcription factor motifs. Signac's 'RunChromvar' function was used to estimate transcription factor accessibility within individual cells. To link peak accessibility to gene expression, we used 'LinkPeaks' and searched for peaks within 500 kb of the transcription start site of each gene. rGREAT (v2.4.0; Gu and Hübschmann, 2023) was used to perform gene ontology analysis of the differentially accessible peaks.

3.6 Acknowledgements

We thank Dr. Matsya Ruppari Thulasiram from Dr. Alain Dabdoub's lab for her help with optimizing the protocols used to snap freeze embryonic cochlear ducts in liquid nitrogen and to isolate their nuclei. We also thank Dr. Thomas Reh for comments on this manuscript and Reh lab members for insightful discussions regarding this study.

3.7 Figures

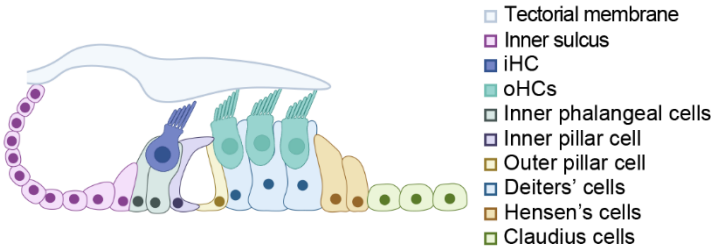

Figure 3.1. Diagram highlighting the arrangement of HC and SC subtypes within the mature organ of Corti.

(created with BioRender.com)

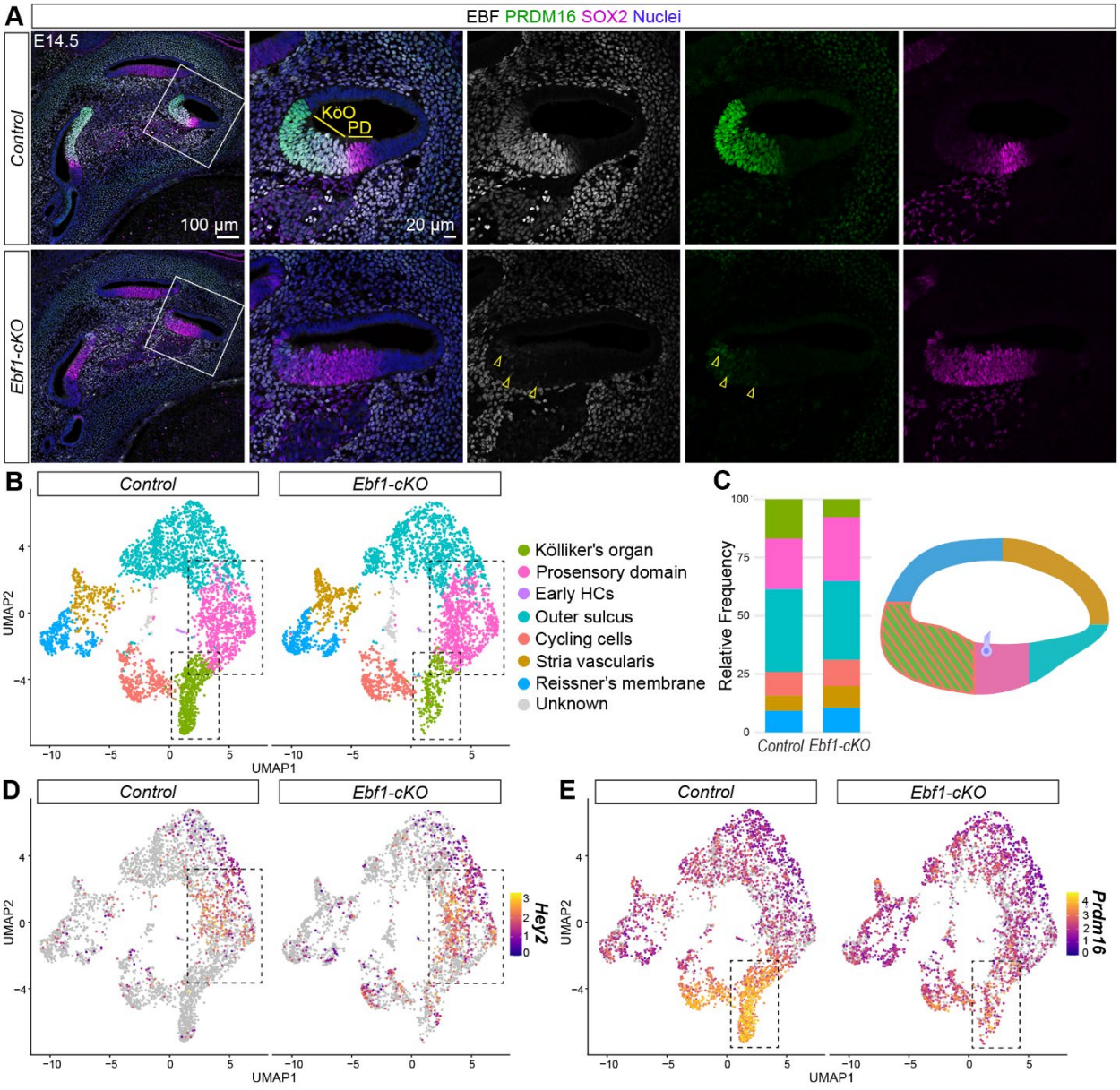

Figure 3.2. Immunostaining and snRNA-seq at E14.5 reveal the co-option of Kölliker's organ cells into the Ebf1-cKO prosensory domain.

(A) Confocal images of E14.5 mid-modiolar sections from control and *Ebf1*-cKO littermates capture an EBF1-dependent expansion of the SOX2^{high+} prosensory domain (PD) and a reduction of the PRDM16^{+} Kölliker's organ (KöO). White boxes indicate regions included in zoomed images. Yellow arrowheads mark example nuclei positive for both EBF and PRMD16 in the *Ebf1*-cKO sample. **(B)** E14.5 snRNA-seq uniform manifold approximation and projection

(UMAP) plots of single nuclei from the cochlear epithelium, separated by genotype. Canonical markers were used to assign cell types to nuclei clusters. **(C)** Relative frequencies of cell types identified in the control (16.9% Kölliker's organ, 21.4% prosensory domain, 0.3% early HCs, 35.4% outer sulcus, 10.3% cycling cells, 6.5% stria vascularis, and 9.2% Reissner's membrane) and the *Ebf1*-cKO datasets (7.6% Kölliker's organ, 27.3% prosensory domain, 0.2% early HCs, 33.7% outer sulcus, 11.2% cycling cells, 9.4% stria vascularis, and 10.5% Reissner's membrane). Cell types in the frequency plot are color-coded to match their assigned colors in the UMAPs and the cross-sectional diagram of an E14.5 control cochlea (created with BioRender.com). E14.5 snRNA-seq feature plots split by genotype highlight *Hey2* expression in the prosensory domain **(D)** and strong *Prdm16* expression Kölliker's organ **(E)**. Dashed boxes indicate regions within the feature plots that contain nuclei assigned to the prosensory domain and Kölliker's organ.

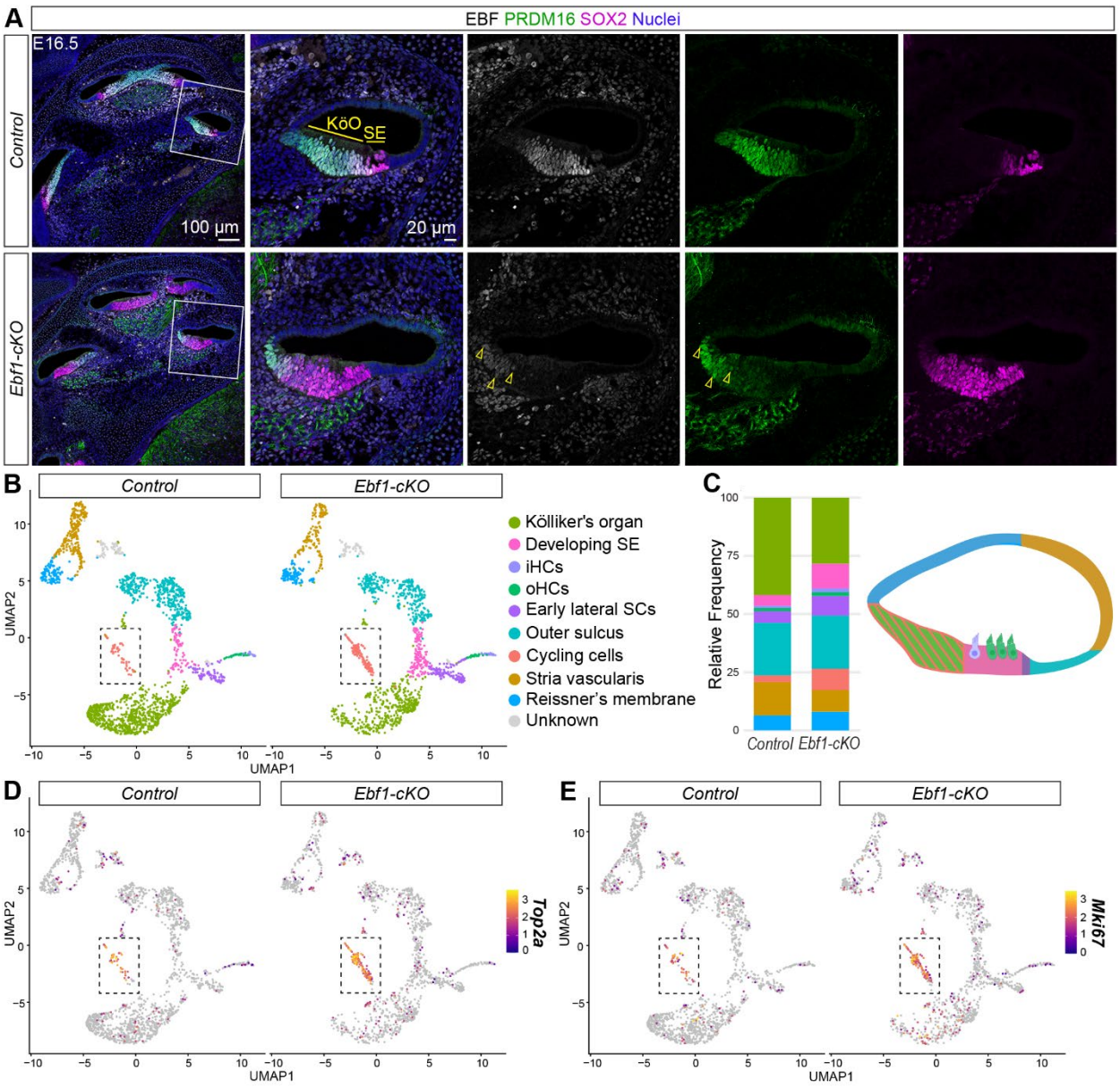

Figure 3.3. Immunostaining and snRNA-seq at E16.5 capture delayed cell cycle exit in Ebf1-cKOs.

(A) Confocal images of E16.5 mid-modiolar sections from control and *Ebf1*-cKO littermates capture an EBF1-dependent expansion of the SOX2^{high+} SE and a reduction of the PRDM16^{+} Kölliker's organ (KöO). White boxes indicate regions included in zoomed images. Yellow arrowheads mark example nuclei positive for both EBF and PRMD16 in the *Ebf1*-cKO sample. **(B)** E16.5 snRNA-seq UMAPs of single nuclei from the cochlear epithelium, separated by

genotype. Canonical markers were used to assign cell types to nuclei clusters. **(C)** Relative frequencies of cell types identified in the control (41.9% Kölliker's organ, 4.6% developing SE, 1.0% iHCs, 1.3% oHCs, 5.0% early lateral SCs, 22.5% outer sulcus, 3.0% cycling cells, 14.3% stria vascularis, and 6.4% Reissner's membrane) and the *Ebf1*-cKO datasets (28.3% Kölliker's organ, 10.6% developing SE, 1.7% iHCs, 1.5% oHCs, 8.5% early lateral SCs, 22.8% outer sulcus, 9.3% cycling cells, 9.2% stria vascularis, and 8.1% Reissner's membrane). Cell types in the frequency plot are color-coded to match their assigned colors in the UMAPs and the cross-sectional diagram of an E16.5 control cochlea (created with BioRender.com). E16.5 snRNA-seq feature plots split by genotype highlight *Top2a* **(D)** and *Mik67* **(E)** expression in nuclei from cycling cells. Dashed boxes indicate regions within the feature plots that contain nuclei assigned to the cycling cells.

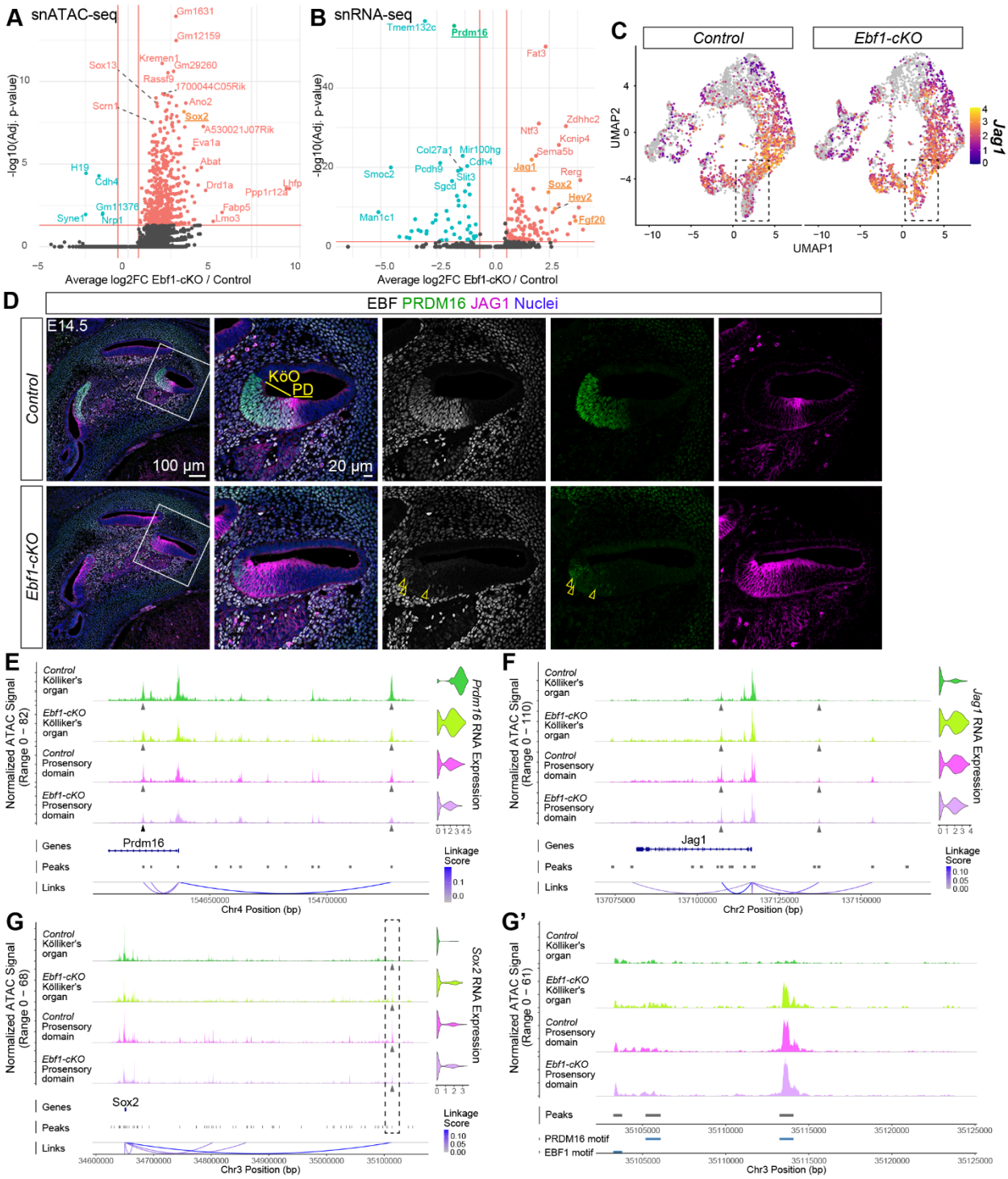

Figure 3.4. E14.5 multiomic analysis identifies potential EBF1 transcriptional targets involved in preventing the recruitment of Kölliker's organ cells into the prosensory domain.

snATAC-seq volcano plot indicates differentially accessible peaks **(A)** and snRNA-seq volcano plot shows differentially expressed genes **(B)** in Kölliker's organ cells of E14.5 *Ebf1*-cKOs relative to control littermates. **(C)** E14.5 snRNA-seq feature plots split by genotype highlight *Jag1* upregulation in the Kölliker's organ. Dashed boxes indicate regions within the feature plots that contain nuclei assigned to the Kölliker's organ. **(D)** Confocal images of E14.5 mid-modiolar sections from control and *Ebf1*-cKO littermates capture an EBF1-dependent medial expansion of the JAG1 expression domain beyond the boundary between the Kölliker's organ (KöO) and prosensory domain (PD). White boxes indicate regions included in zoomed images. **(E)** Multiomic analysis of *Prdm16* gene expression and chromatin accessibility in E14.5 control and *Ebf1*-cKO cells from the Kölliker's organ and prosensory domain. *Top left*: Coverage plots generated from snATAC-seq data. Grey arrowheads indicate ATAC peaks that are strongly correlated with *Prdm16* RNA expression and contain the EBF1-binding motif. *Top right*: *Prmd16* expression violin plots generated from snRNA-seq data. *Bottom*: Peak-to-gene analysis indicates strength of correlation between ATAC peak accessibility and *Prdm16* RNA expression. Similar analyses are shown for ATAC peaks containing both EBF1 and PRDM16 binding motifs that are correlated with *Jag1* expression **(F)** and an ATAC peak containing the PRDM16 binding motif that is correlated with *Sox2* expression **(G)**. **(G')** Zoomed-in view of the ATAC peak ~500 kb upstream of the *Sox2* locus (dashed box in G) that contains the PRDM16 binding motif but not the EBF1-binding motif (bottom track).

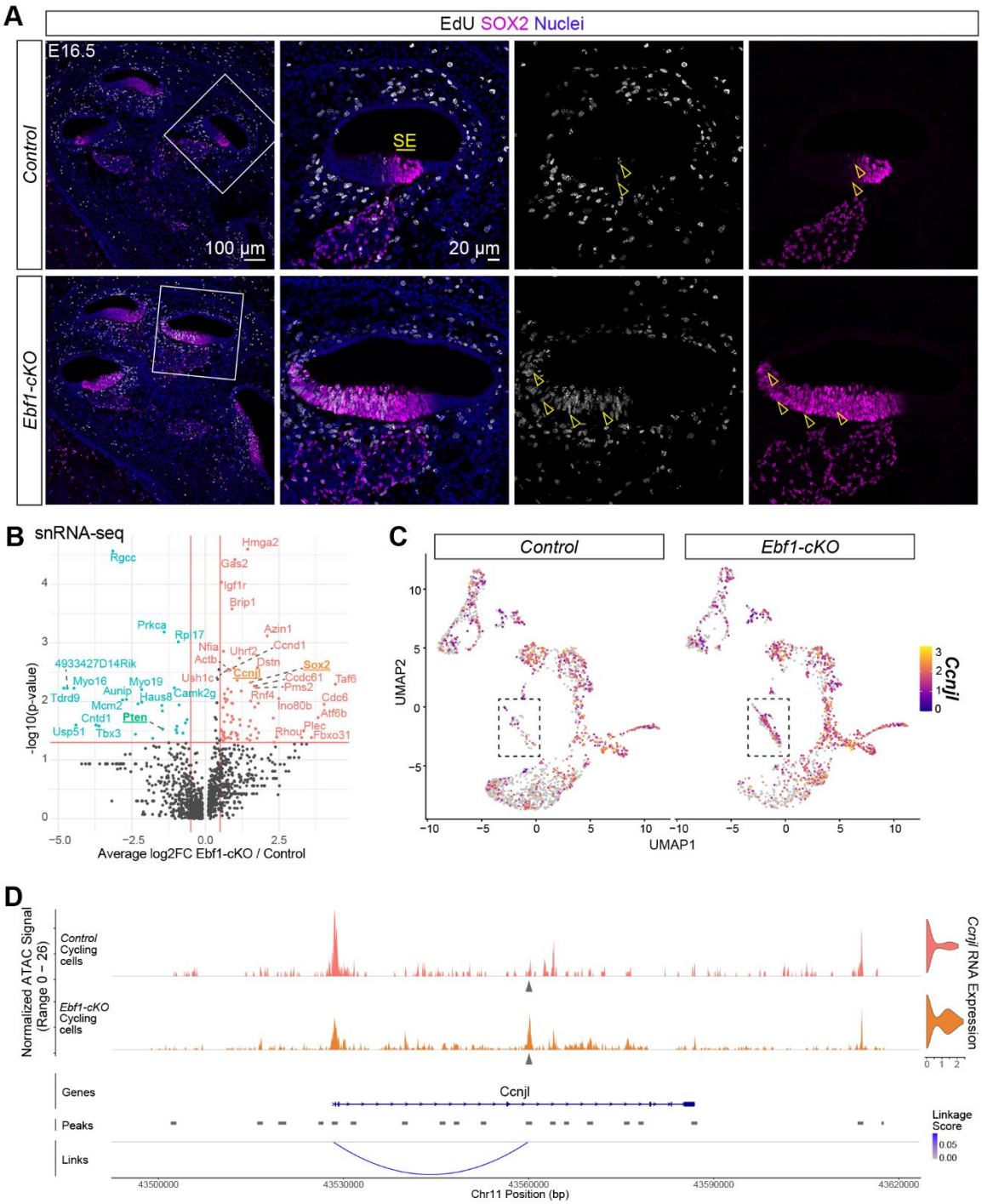

Figure 3.5. E16.5 multiomic analysis identifies an EBF1 transcriptional target potentially important in promoting prolonged prosensory cell proliferation.

(A) Confocal images of E16.5 mid-modiolar sections from control and *Ebf1*-cKO littermates treated with EdU 2 h prior to tissue collection. White boxes indicate regions included in zoomed

images. **(B)** E16.5 snRNA-seq volcano plot shows differentially expressed cycling genes in the cycling cells of *Ebf1*-cKOs relative to control littermates. **(C)** Control and *Ebf1*-cKO snRNA-seq feature plots split by genotype highlight *Ccnjl* upregulation in *Ebf1*-cKO cycling cells. Dashed boxes indicate regions within the feature plots that contain nuclei assigned to the cycling cells. **(D)** Multiomic analysis of E16.5 control and *Ebf1*-cKO cycling cells. *Top left*: *Ccnjl* coverage plot generated from snATAC-seq data. *Top right*: *Ccnjl* expression violin plots generated from snRNA-seq data. *Bottom*: Peak-to-gene analysis shows strength of correlation between ATAC peak accessibility and RNA expression. Grey arrowheads indicate the ATAC peak that is strongly correlated with *Prdm16* RNA expression and contains both EBF1 and SOX2 binding motifs.

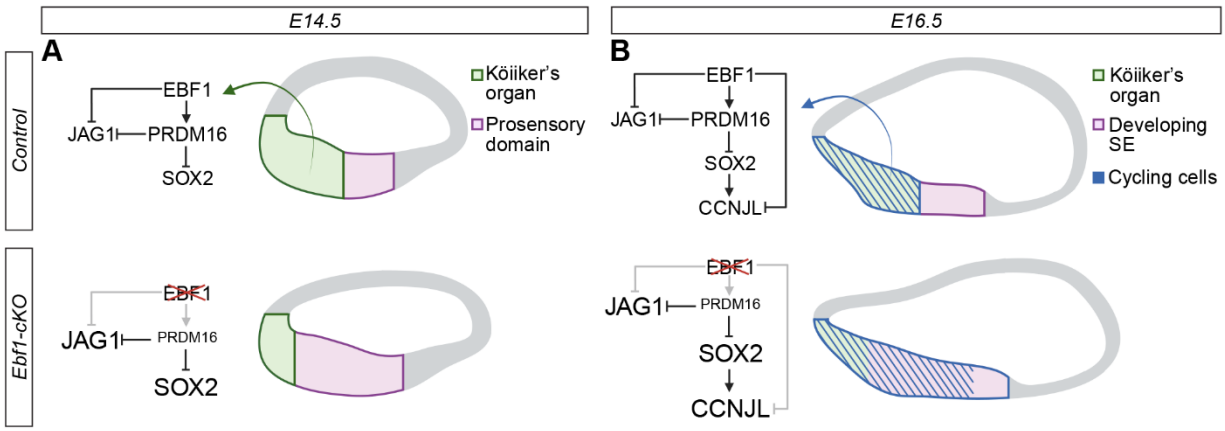

Figure 3.6. EBF1 restricts prosensory domain establishment by both positioning the medial boundary of the prosensory domain and restricting prosensory cell proliferation.

(A, B) Cross-sectional diagrams of control and *Ebf1*-cKO cochleae (created with BioRender.com). **(A)** At E14.5, EBF1 appears to directly promotes *Prdm16* expression and co-represses *Jag1* expression with PRDM16, and in turn, PRDM16 directly represses *Sox2* expression. Consequently, loss of EBF1 leads to *Prdm16* downregulation in addition to *Jag1* and *Sox2* upregulation in the Kölliker's organ, driving these cells towards a more prosensory fate. **(B)** At E16.5, in addition to promoting *Prdm16* expression and repressing *Jag1* and *Sox2* expression, EBF1 seems to be needed to repress *Ccnjl* expression in cycling cells. Loss of EBF1 removes direct repression of *Ccnjl*, while concurrent *Sox2* upregulation promotes further *Ccnjl* expression.

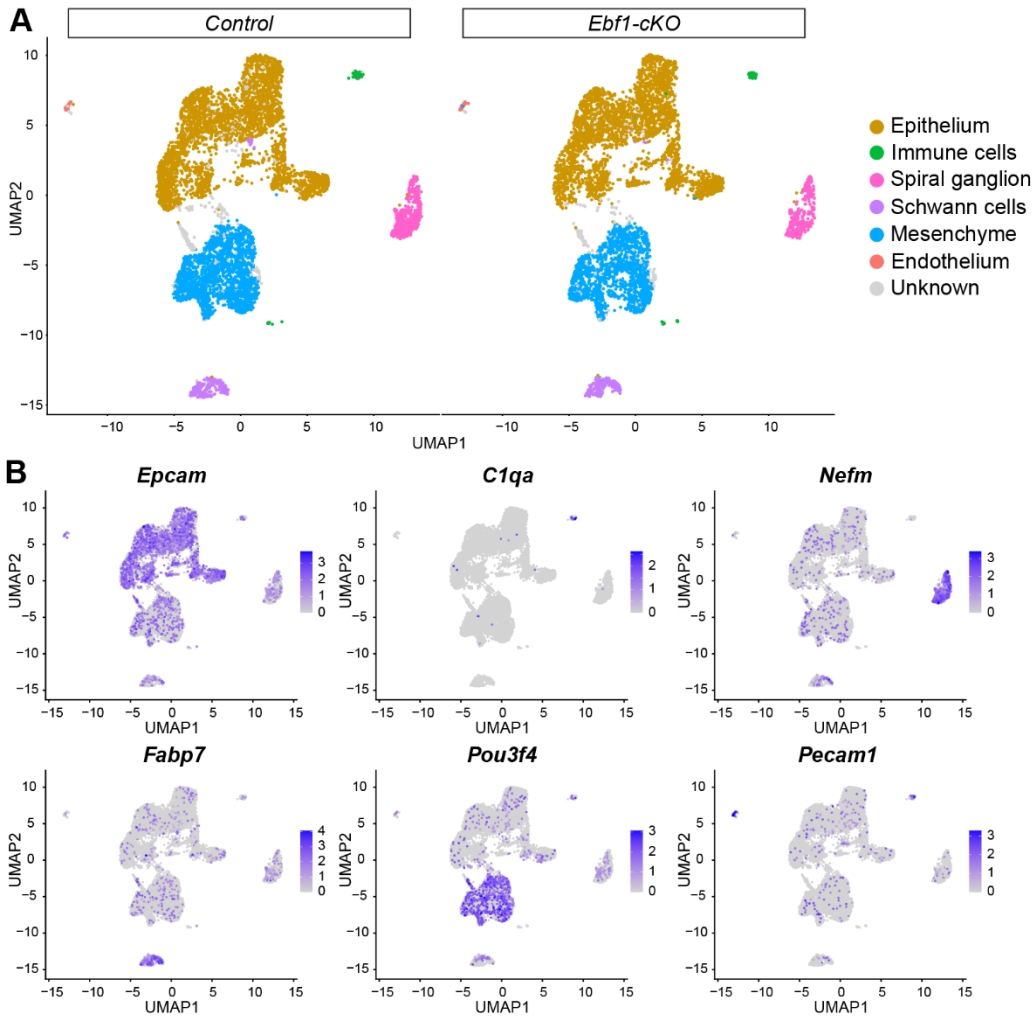

Figure 3.S1. Epithelial and non-epithelial cell types present in E14.5 samples.

(A) E14.5 snRNA-seq UMAPs of single nuclei from entire cochlear ducts, separated by genotype. **(B)** Composite snRNA-seq feature plots for canonical marker genes used assign cell types to nuclei clusters.

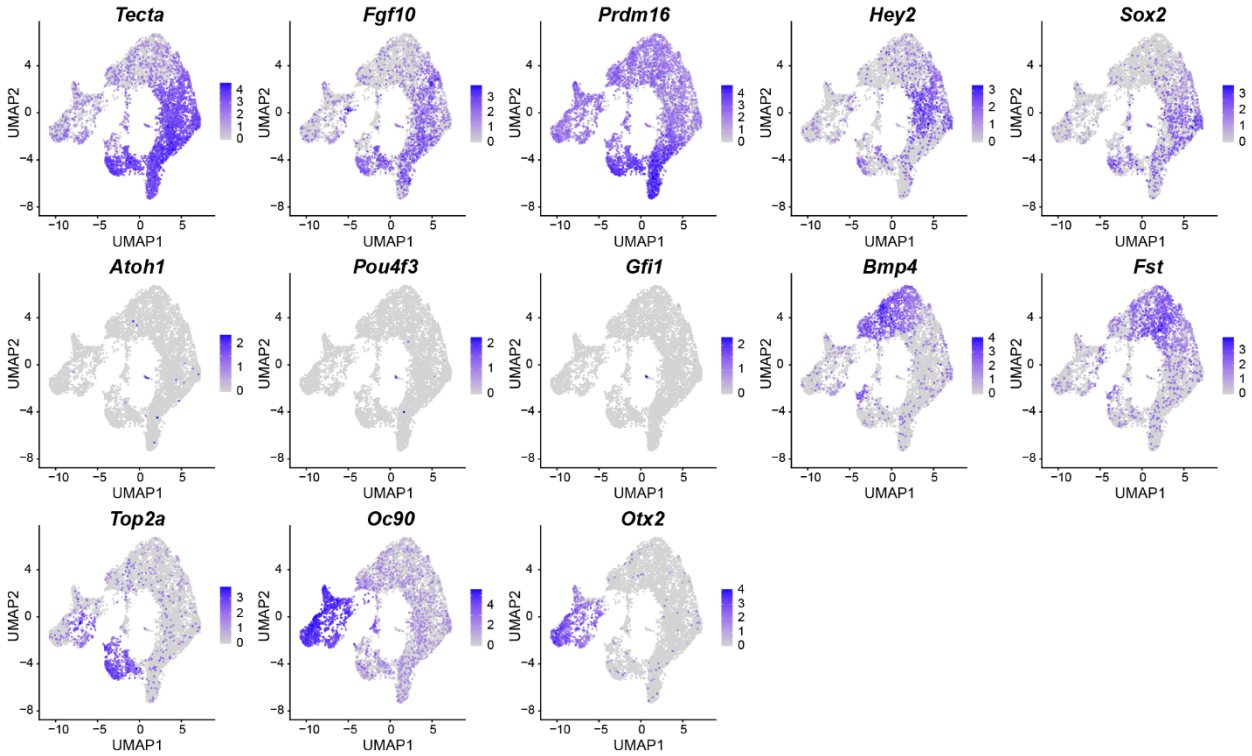

Figure 3.S2. Marker genes used to identify E14.5 epithelial cell types.

Composite snRNA-seq feature plots for canonical marker genes used assign cell types to nuclei clusters in E14.5 control and *Ebf1*-cKO snRNA-seq UMAPs of the cochlear epithelium.

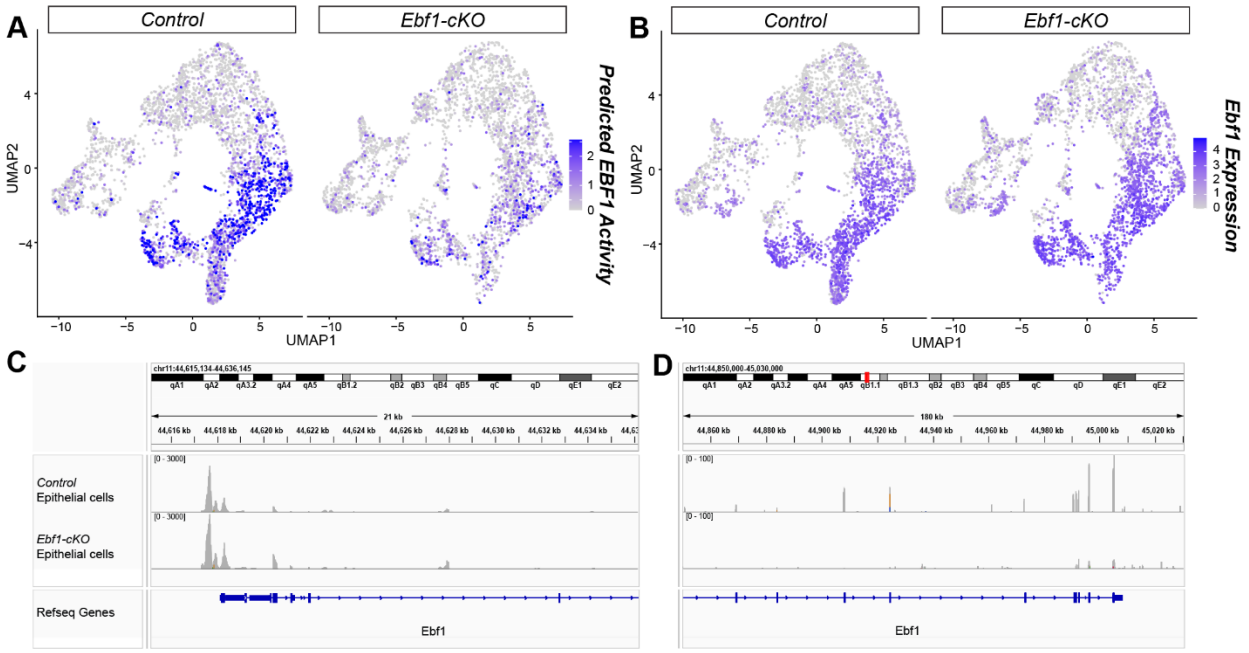

Figure 3.S3. Ebf1-cKOs show decreased predicted EBF1 activity and fewer reads from Ebf1 exons 6-16.

(A) E14.5 snATAC-seq feature plots split by genotype show reduced predicted binding of EBF1 in nuclei from the Kölliker's organ, prosensory domain, and cycling cells of *Ebf1*-cKOs compared with controls. **(B)** E14.5 snRNA-seq feature plots split by genotype indicate *Ebf1* detection in *Ebf1*-cKOs. *Ebf1* exons 1-5 and the first 14 codons of exon 6 remain intact in *Ebf1*-cKOs. Coverage plots generated from snRNA-seq data show that controls and *Ebf1*-cKOs possess similar RNA read coverage near the *Ebf1* transcription start site **(C)**, but *Ebf1*-cKOs have significantly reduced RNA read coverage near the 5' end where exons have been excised **(D)**.

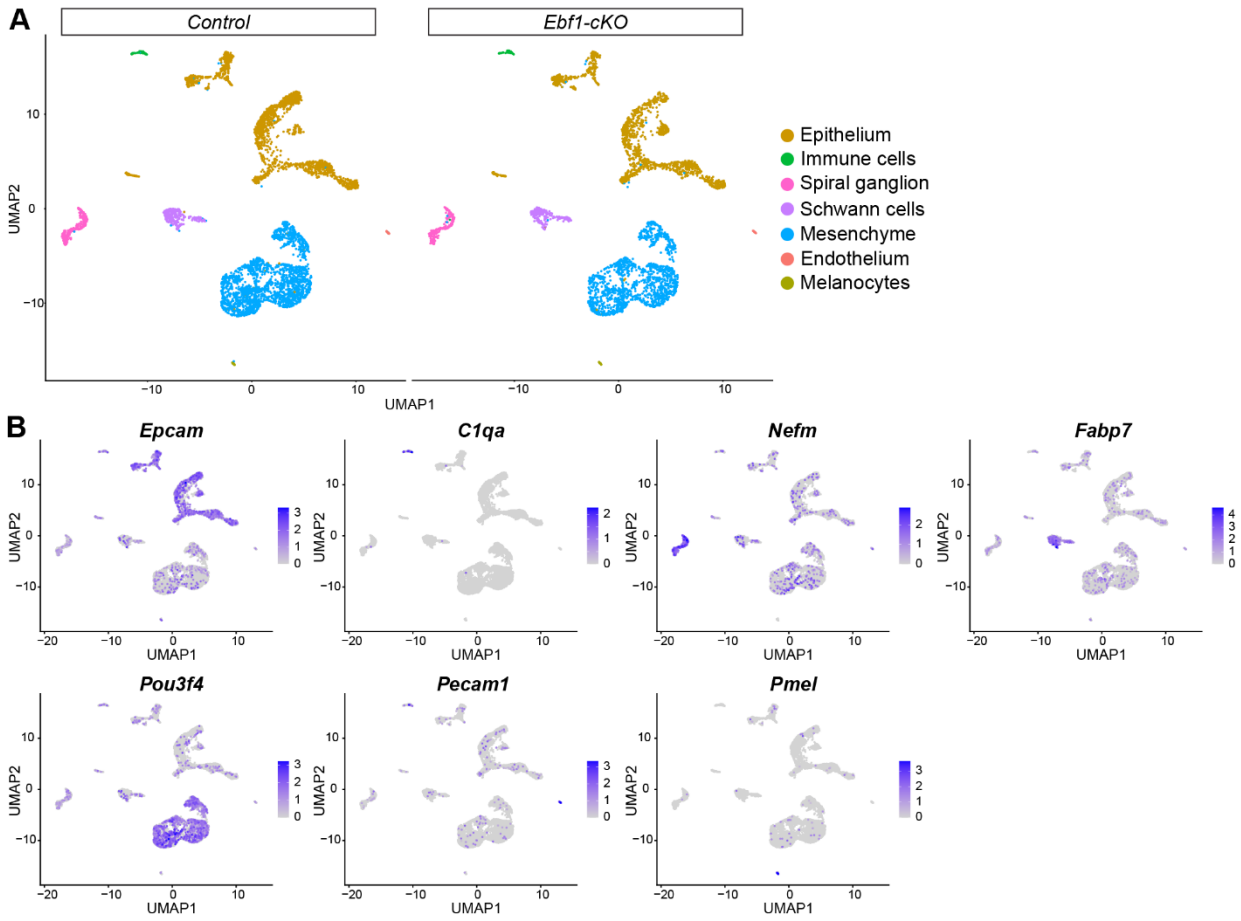

Figure 3.S4. Epithelial and non-epithelial cell types present in E16.5 samples.

(A) E16.5 snRNA-seq UMAPs of single nuclei from entire cochlear ducts, separated by genotype. **(B)** Composite snRNA-seq feature plots for canonical marker genes used assign cell types to nuclei clusters.

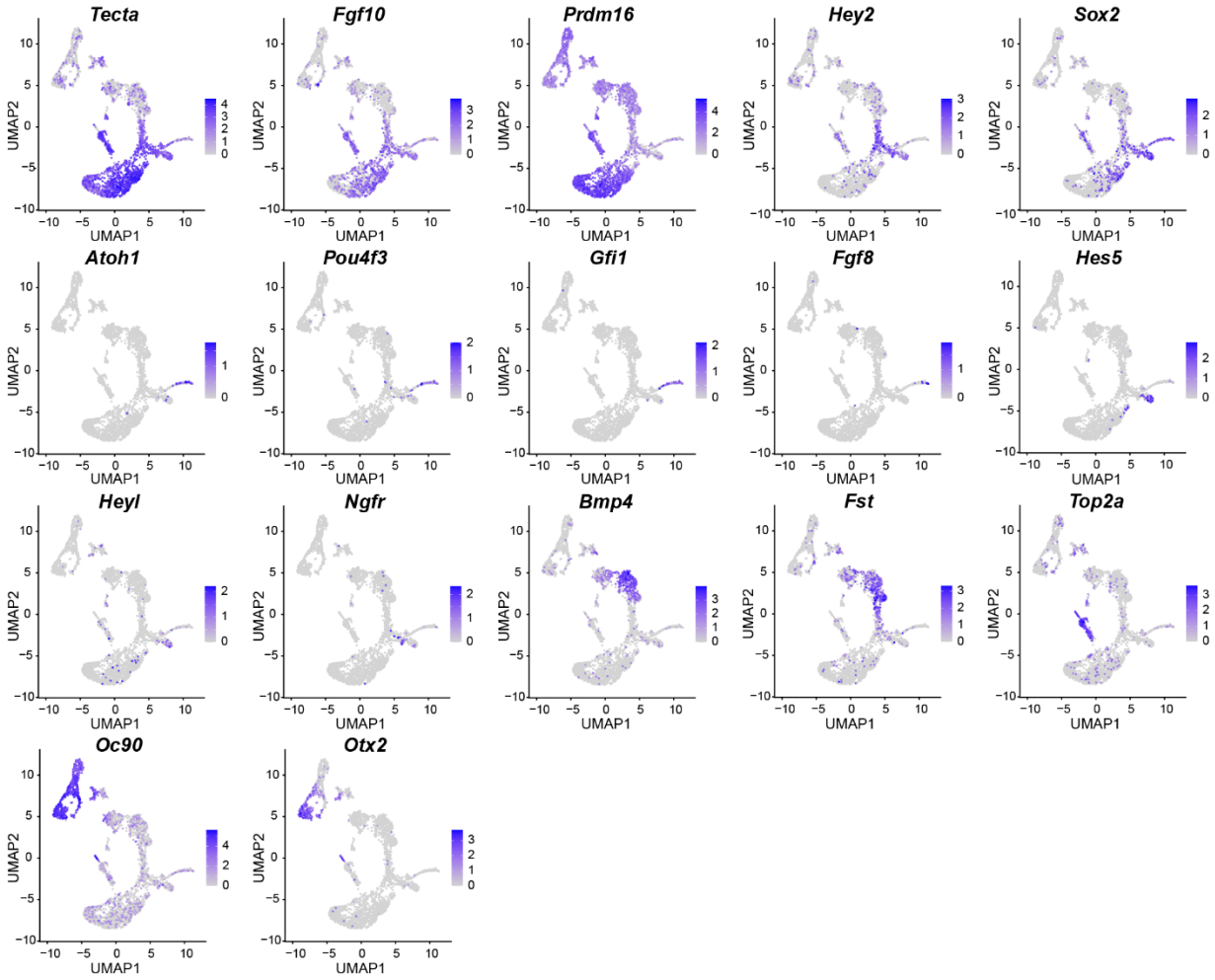

Figure 3.S5. Marker genes used to identify E16.5 epithelial cell types.

Composite snRNA-seq feature plots for canonical marker genes used assign cell types to nuclei clusters in E16.5 control and *Ebf1*-cKO snRNA-seq UMAPs of the cochlear epithelium.

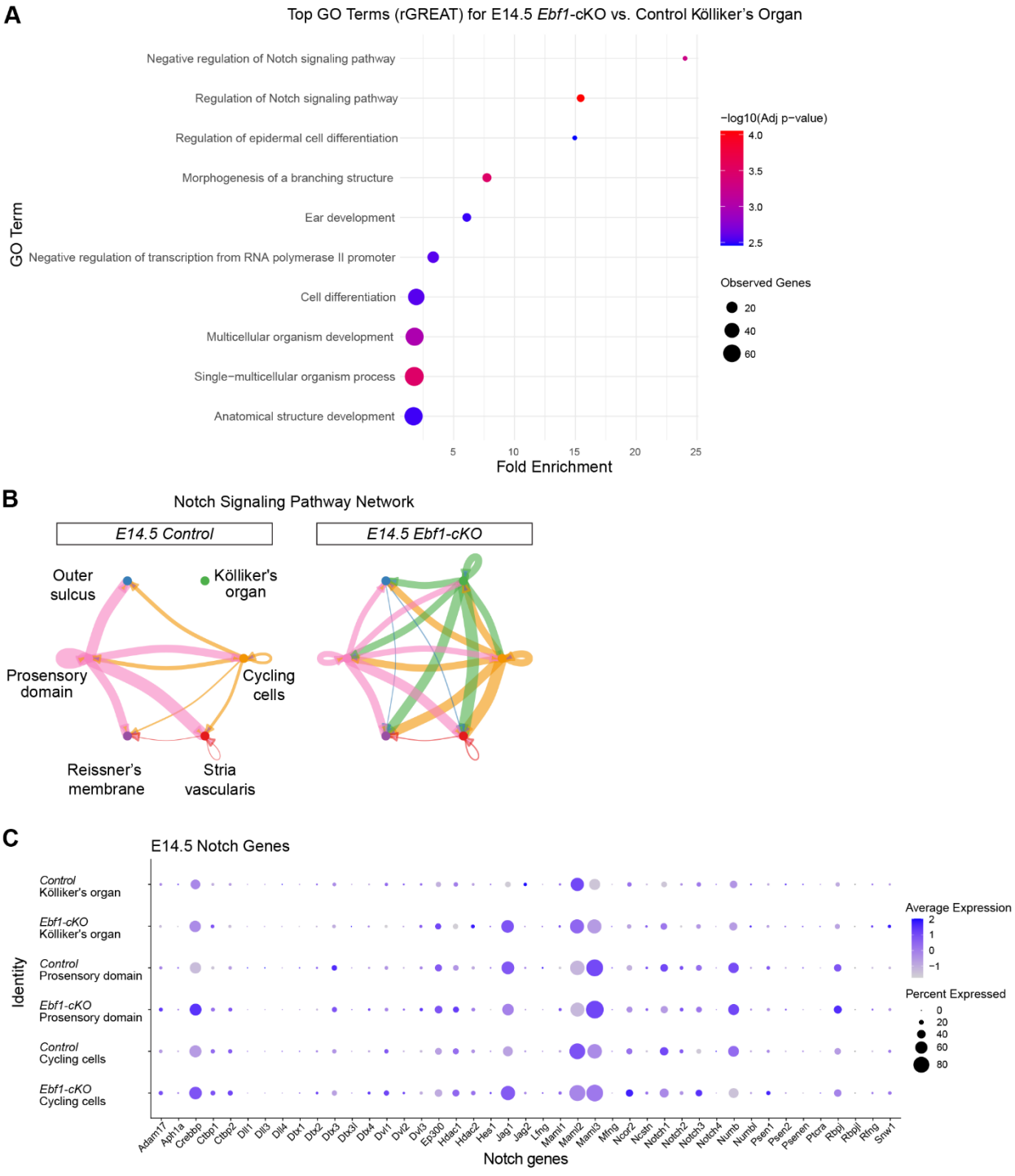

Figure 3.S6. Ebf1-cKO Kölliker's organ cells mimic the Notch signaling levels of prosensory cells.

(A) Top 10 gene ontology (GO) terms identified in E14.5 *Ebf1*-cKO relative to control Kölliker's organ cells using genomic regions enrichment of annotations tool (GREAT). **(B)** CellChat circle

plots split by genotype indicating the strength of Notch signaling between and within E14.5 cell populations present based on receptor-ligand expression. The thickness of the line indicates the relative strength of the interaction. **(C)** E14.5 dot plots broken down by genotype and cell type highlight the Notch gene expression in Kölliker's organ, prosensory domain, and cycling cells.

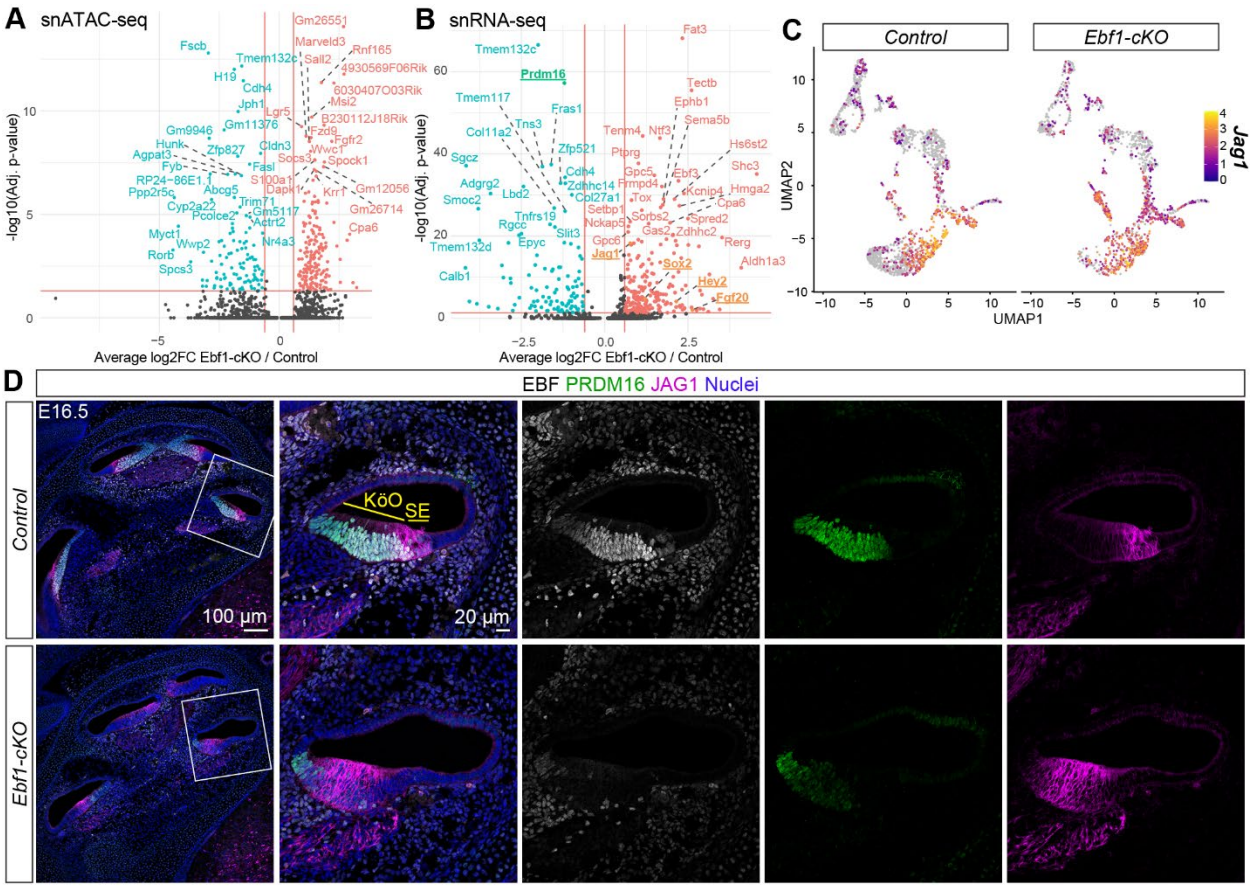

Figure 3.S7. Changes in chromatin accessibility are less skewed and Jag1 upregulation persists in Ebf1-cKOs at E16.5.

snATAC-seq volcano plot indicates differentially accessible peaks **(A)** and snRNA-seq volcano plot shows differentially expressed genes **(B)** in Kölliker's organ cells of E16.5 *Ebf1*-cKOs relative to control littermates. **(C)** E16.5 snRNA-seq feature plots split by genotype highlight *Jag1* expression. **(D)** Confocal images of E16.5 mid-modiolar sections from control and *Ebf1*-cKO littermates capture an EBF1-dependent medial expansion of the JAG1 expression. White boxes indicate regions included in zoomed images.

3.8 Tables

Top 50 Upregulated Genes						Top 50 Downregulated Genes					
Gene	*p_val*	*avg_log2FC*	*pct.Ebf1_cKO*	*pct.Ctrl*	*p_val_adj*	*Gene*	*p_val*	*avg_log2FC*	*pct.Ebf1_cKO*	*pct.Ctrl*	*p_val_adj*
Mylk	1.49E-09	3.992783897	0.079	0.005	4.82E-05	*Smoc2*	3.18E-25	-4.551119667	0.063	0.41	1.03E-20
Rerg	5.13E-22	3.87245808	0.217	0.022	1.66E-17	*Syne1*	9.05E-08	-4.170161008	0.012	0.128	0.00292309
Cybrd1	3.73E-15	3.806332935	0.126	0.007	1.21E-10	*Tmem132d*	1.26E-07	-3.848837696	0.016	0.133	0.00407399
Fgf20	8.85E-12	3.65650848	0.11	0.01	2.86E-07	*Adgrg2*	2.06E-07	-3.714705746	0.016	0.129	0.00665844
Shc3	8.30E-13	3.610771794	0.118	0.01	2.68E-08	*Sgcz*	3.54E-09	-3.628603269	0.028	0.175	0.00011427
Etv4	3.80E-11	3.4129385	0.11	0.012	1.23E-06	*Gsn*	3.49E-12	-3.471784499	0.035	0.229	1.13E-07
Tcf7	2.31E-08	3.310725732	0.075	0.007	0.00074514	*Cdk15*	1.97E-09	-3.326637342	0.024	0.173	6.35E-05
Zdhhc2	1.26E-35	3.234944935	0.382	0.05	4.05E-31	*Rgcc*	3.82E-09	-3.22182711	0.028	0.175	0.00012328
Kcnip4	6.78E-31	2.922454581	0.469	0.126	2.19E-26	*Tmem132c*	4.32E-62	-3.034656764	0.181	0.803	1.40E-57
Mybpc1	6.51E-16	2.912277136	0.201	0.034	2.10E-11	*Otoa*	1.44E-08	-2.969569342	0.035	0.18	0.00046544
Dync1i1	1.60E-09	2.825571899	0.114	0.018	5.15E-05	*Kcnh7*	3.43E-09	-2.956852268	0.055	0.213	0.0001108
Ptprt	9.51E-07	2.755687215	0.083	0.015	0.03070115	*Ldb2*	2.64E-11	-2.691871258	0.035	0.222	8.54E-07
Hey2	8.13E-15	2.749232854	0.173	0.025	2.62E-10	*Snap91*	6.07E-12	-2.556604269	0.063	0.269	1.96E-07
Cpa6	6.19E-14	2.643685099	0.189	0.035	2.00E-09	*Pla2r1*	2.58E-13	-2.533653982	0.102	0.333	8.34E-09
Emx2os	5.20E-09	2.626260973	0.102	0.015	0.00016777	*Cdkn1c*	9.56E-07	-2.358626643	0.047	0.17	0.03085577
Gm4675	3.97E-07	2.487019848	0.079	0.012	0.01281175	*Pcdh9*	2.42E-26	-2.357681523	0.276	0.612	7.82E-22
Sox2	5.46E-19	2.45690822	0.264	0.05	1.76E-14	*Dlgap1*	6.45E-07	-2.286924631	0.059	0.187	0.02082705
Phf21b	1.66E-08	2.39937556	0.11	0.02	0.00053678	*Pid1*	3.96E-09	-2.10808902	0.075	0.245	0.00012778
Fat3	1.10E-55	2.331533508	0.823	0.323	3.55E-51	*Pak3*	5.59E-07	-2.074796104	0.063	0.195	0.01804235
Sall1	1.15E-14	2.306328281	0.224	0.049	3.70E-10	*Tns3*	2.85E-14	-2.073396322	0.189	0.427	9.20E-10
Mettl24	9.69E-09	2.235471035	0.13	0.029	0.00031283	*Galntl6*	3.75E-12	-2.001678989	0.134	0.365	1.21E-07
Tbc1d1	1.12E-11	2.158291955	0.205	0.054	3.62E-07	*Col11a2*	5.09E-10	-1.833170068	0.13	0.324	1.64E-05
Slitrk6	3.94E-07	2.130908331	0.087	0.015	0.01270455	*Sgcd*	8.60E-22	-1.829597945	0.323	0.622	2.78E-17
Plce1	5.43E-10	2.125127705	0.165	0.04	1.75E-05	*Prdm16*	6.58E-61	-1.734730626	0.697	0.961	2.12E-56
9630014M24Rik	1.39E-11	2.109955216	0.181	0.04	4.48E-07	*A230057D06Rik*	2.23E-08	-1.732599921	0.122	0.292	0.00072125
Ntf3	2.72E-36	2.028827819	0.681	0.261	8.78E-32	*Itga8*	4.66E-18	-1.613303437	0.24	0.541	1.50E-13
Rassf9	1.56E-14	2.01861382	0.228	0.05	5.02E-10	*Slit3*	2.24E-24	-1.56126767	0.543	0.78	7.25E-20
Ust	4.27E-08	1.995044416	0.157	0.047	0.00137775	*Tmem117*	6.81E-17	-1.541147665	0.287	0.56	2.20E-12
Kdm5d	5.94E-09	1.939679945	0.13	0.027	0.00019178	*Dpyd*	1.29E-15	-1.537516466	0.299	0.543	4.16E-11
Lgr5	4.07E-15	1.938497994	0.339	0.111	1.32E-10	*Tcf4*	2.63E-11	-1.492600033	0.417	0.59	8.51E-07
Stox1	1.55E-09	1.919134808	0.185	0.054	4.99E-05	*Il1rapl1*	1.86E-07	-1.475592871	0.181	0.343	0.00599174
Sema5b	3.84E-28	1.905997312	0.555	0.175	1.24E-23	*Col27a1*	1.01E-24	-1.42679973	0.484	0.753	3.25E-20
Fgf9	2.54E-09	1.863620253	0.185	0.054	8.20E-05	*Mir100hg*	3.86E-28	-1.357030799	0.559	0.788	1.25E-23
Phlda1	1.07E-08	1.86251145	0.165	0.047	0.00034693	*Fras1*	1.80E-15	-1.263131488	0.406	0.625	5.82E-11
Lhfpl2	1.18E-10	1.840599113	0.189	0.049	3.81E-06	*Zfp521*	3.29E-19	-1.254831793	0.445	0.694	1.06E-14
Socs2	4.52E-11	1.821463956	0.228	0.069	1.46E-06	*Cdh4*	1.44E-25	-1.155322115	0.724	0.887	4.65E-21
Hs6st2	7.71E-20	1.78571513	0.449	0.16	2.49E-15	*Ypel2*	4.97E-07	-1.151655392	0.232	0.388	0.01603829
Etv5	6.36E-10	1.779418542	0.205	0.062	2.05E-05	*Cntn5*	1.26E-09	-1.141621721	0.268	0.462	4.07E-05
Spry2	1.25E-06	1.75922609	0.126	0.037	0.04043911	*C530008M17Rik*	4.47E-07	-1.097320735	0.283	0.435	0.01444146
Trib2	7.05E-10	1.757668742	0.185	0.05	2.28E-05	*Col9a2*	5.00E-07	-1.093130356	0.35	0.477	0.01615804
Tspan15	8.22E-07	1.74005952	0.134	0.04	0.02653628	*Zdhhc14*	9.88E-13	-1.09185552	0.476	0.672	3.19E-08
Mex3b	1.51E-06	1.738183487	0.11	0.029	0.04863217	*Fmn1*	6.34E-21	-1.084750608	0.622	0.81	2.05E-16
Jag1	3.44E-27	1.710009847	0.622	0.245	1.11E-22	*Rbms3*	1.65E-10	-1.060415314	0.402	0.582	5.32E-06
Ephb1	5.15E-10	1.657884158	0.291	0.119	1.66E-05	*Spock1*	2.02E-18	-1.041988956	0.681	0.825	6.51E-14
Sall2	1.09E-10	1.644019219	0.248	0.086	3.52E-06	*Col11a1*	9.52E-09	-1.002914364	0.425	0.573	0.0003073
Etv1	3.33E-08	1.625309016	0.154	0.042	0.0010765	*Kirrel3*	6.86E-08	-0.862978977	0.421	0.582	0.00221468
Tshz2	3.86E-10	1.622660875	0.327	0.143	1.24E-05	*Exoc4*	2.44E-07	-0.848817598	0.488	0.595	0.00787205
Plekha8	4.46E-07	1.582597781	0.126	0.034	0.01439433	*Sox5*	7.09E-11	-0.776471658	0.614	0.741	2.29E-06
Palld	3.79E-12	1.567303072	0.295	0.099	1.22E-07	*Mir99ahg*	5.97E-08	-0.760116586	0.689	0.761	0.00192871
Shank2	3.61E-07	1.47648862	0.22	0.094	0.01165117	*Kcnq1ot1*	2.16E-08	-0.576409484	0.795	0.881	0.00069695

Table 3.S1. Differentially expressed genes in Kölliker's organ cells of E14.5 Ebf1-cKOs relative to control littermates.

Significance values (p_val) were calculated using a Wilcoxon ranked-sum test, and the p-value adjustment (p_val_adj) was performed using Bonferroni correction. Genes with an adjusted p-value of less than 0.05 are provided. The percentage of cells expressing each gene in the *Ebf1*-cKO (pct.Ebf1_cKO) and control (pct.Ctrl) Kölliker's organ are provided, as well as the average log2 fold-change difference in gene expression between the *Ebf1*-cKO and control population (avg_log2FC).

Top 20 Upregulated Genes					Top 20 Downregulated Genes				
Gene	*p_val*	*avg_log2FC*	*pct.Ebf1_cKO*	*pct.Ctrl*	*Gene*	*p_val*	*avg_log2FC*	*pct.Ebf1_cKO*	*pct.Ctrl*
Taf6	0.005067618	4.418524303	0.135	0	*Atm*	0.034249149	-0.970026161	0.286	0.415
Cdc6	0.011186426	4.031144434	0.113	0	*Pten*	0.03030939	-1.001770063	0.331	0.453
Atf6b	0.018863524	3.827807559	0.098	0	*Camk2g*	0.005871157	-1.059375006	0.278	0.453
Fbxo31	0.041176292	3.602592076	0.075	0	*Prkca*	0.000653553	-1.405571498	0.383	0.566
Plec	0.031741752	3.3329118	0.083	0	*Paf1*	0.029591805	-1.454356968	0.098	0.208
Rhou	0.041176292	3.271913087	0.075	0	*Rae1*	0.014466258	-1.467089219	0.158	0.302
Ino80b	0.008932136	2.491287874	0.158	0.019	*Pla2r1*	0.011683998	-1.481164648	0.105	0.245
Inip	0.040620701	2.420785087	0.113	0.019	*Tubg1*	0.042400879	-1.789879351	0.038	0.113
Mad2l1	0.049794773	2.334205712	0.105	0.019	*Haus8*	0.01028251	-2.164048514	0.068	0.189
Cenpm	0.019166013	2.306285692	0.135	0.019	*Myo19*	0.006245523	-2.16804068	0.075	0.208
Azin1	0.000758823	2.098585518	0.263	0.038	*Chmp1a*	0.010959121	-2.295147346	0.015	0.094
Mark4	0.034132424	1.805670877	0.12	0.019	*Pdgfrb*	0.036196951	-2.377091725	0.015	0.075
Azi2	0.010677911	1.793737859	0.241	0.075	*Aunip*	0.009192943	-2.683442491	0.023	0.113
Dstn	0.002642897	1.76894877	0.286	0.075	*Mcm2*	0.009412966	-2.819874147	0.023	0.113
Poldip2	0.042180548	1.753574004	0.143	0.038	*Rgcc*	2.71E-05	-3.150120611	0.045	0.245
Pms2	0.005825494	1.742626142	0.203	0.038	*Tbx3*	0.026208994	-3.615927476	0.023	0.094
Shb	0.029248235	1.703837974	0.203	0.075	*Cntd1*	0.025228568	-3.715906643	0	0.038
Cyp26b1	0.0124845	1.676130264	0.466	0.321	*Usp51*	0.025228568	-4.403095574	0	0.038
Ccdc61	0.005482057	1.660048874	0.263	0.075	*Myo16*	0.005928576	-4.470156846	0	0.057
Inha	0.037586225	1.537500775	0.15	0.038	*Tdrd9*	0.005928576	-4.696933671	0	0.057

Table 3.S2. Differentially expressed cycling genes in the cycling cells of E16.5 Ebf1-cKOs relative to control littermates.

Significance values (p_val) were calculated using a Wilcoxon ranked-sum test. Due to the limited number of cycling cells, p-value adjustment was not performed. Genes with a p-value of less than 0.05 are provided. The percentage of cells expressing each gene in the *Ebf1*-cKO (pct.Ebf1_cKO) and control (pct.Ctrl) cycling cells are provided, as well as the average log2 fold-change difference in gene expression between the *Ebf1*-cKO and control population (avg_log2FC).

CHAPTER 4: Summary and Outlook

Unlike non-mammalian vertebrates, which can generate hair cells (HCs) throughout their lives (Baird et al., 1996; Balak et al., 1990; Corwin, 1981; Corwin, 1983; Corwin, 1985; Corwin and Cotanche, 1988; Harris et al., 2003; Presson et al., 1996; Raphael, 1992; Raphael et al., 1994; Ryals and Rubel, 1988; Shang et al., 2010; Taylor and Forge, 2005; Warchol and Corwin, 1996), mammals undergo a sharp regenerative decline after birth. Although the adult rodent vestibular system demonstrates some regenerative potential (Burns et al., 2012; Forge et al., 1993; Forge et al., 1998; Golub et al., 2012; Kawamoto et al., 2009; Slowik and Bermingham-McDonogh, 2013a), spontaneous HC regeneration in the mouse cochlea is restricted to the first postnatal week (Cox et al., 2014), and adult mammals are unable to replace these once they are lost. Consequently, factors such as aging, noise exposure, ototoxic agents, and congenital conditions often lead to HC loss and irreversible hearing impairment (Chen and Fechter, 2003; Jiang et al., 2006; Korver et al., 2017; Lenoir et al., 1999; Nakagawa et al., 1998; Roberston, 1980; Wu et al., 2020). Insights from cochlear development underpin regenerative approaches to restore auditory function by replacing damaged HCs; however, significant gaps remain in our understanding of the signals that govern cochlear and sensory patterning. The work presented herein shows the role of EBF1 (Early B cell Factor 1) in sensory establishment within the cochlea, and in turn, highlights a novel candidate for future regenerative strategies.

4.1 Conclusions

In Chapter 2, we documented the role of EBF1 in cochlear development. Our lab first became interested in EBFs following a bulk ATAC-seq study performed by Dr. Brent Wilkerson, who detected EBF consensus binding motif enrichment in the open chromatin of prosensory cells collected from embryonic cochleae (Wilkerson et al., 2019). Complementary single cell RNA-seq, in situ hybridization, and immunostaining experiments were conducted on E12-18 cochleae. Together, these analyses revealed that *Ebf1* was expressed in the Kölliker's organ,

prosensory cells, HCs, and SCs while *Ebf2-4* showed little to no expression in the developing cochlear epithelium. I subsequently generated *Ebf1* conditional knockout (cKO) mice to investigate the importance of EBF1 in the developing cochlea. *Ebf1* excision throughout the otocyst that gives rise to inner ear epithelium led to dramatic sensory expansion in the cochlea consisting of supernumerary HCs within the developing organ of Corti and ectopic sensory patches in the Kölliker's organ. HC quantification in *Ebf1*-cKO and control littermates uncovered that *Ebf1*-cKO cochleae possessed approximately triple the number of inner HCs and double the number of outer HCs. I performed additional proliferation assays and immunostaining experiments that showed prolonged prosensory cell proliferation coupled with delayed sensory cell differentiation contributed to *Ebf1*-cKO sensory expansion. Our lab also found that the timing and extent of *Ebf1* excision influenced the level of sensory expansion. When *Ebf1* was excised closer to the onset of cochlear development and in a subset of cochlear epithelial cells (i.e., prosensory cells and Kölliker's organ cells), the resulting sensory expansion was less pronounced. My analysis of patterned postnatal cochleae revealed that *Ebf1*-cKO supernumerary HCs possessed mechanoelectrical transduction channels. These cells also continued to direct proper support cell (SC) patterning and to secrete cues that allow their innervation. In adult *Ebf1*-cKOs, supernumerary HCs and SCs persisted, and auditory brainstem response testing showed the *Ebf1*-cKO mice were deaf. Thus, our findings in Chapter 2 indicate that EBF1 regulates proliferation and patterning in the cochlea, and ultimately, is necessary for hearing.

In Chapter 3, we investigated the mechanism by which EBF1 restricts cochlear sensory development. Immunostaining experiments revealed that the EBF1-dependent aberrant cochlear patterning described in Chapter 2 resulted from co-option of Kölliker's organ by the prosensory domain. To identify the molecular basis of this process, I developed a protocol for isolating nuclei from cochleae snap-frozen in liquid nitrogen and generated both E14.5 and E16.5 single nucleus (sn) RNA-seq and ATAC-seq datasets from the same nuclei. By examining

EBF1 DNA binding motif accessibility within differentially expressed genes in cell-type-matched populations from *Ebf1*-cKO and control littermate datasets I was able to elucidate EBF1's role as a transcriptional activator and repressor for target genes in distinct cell populations. To pinpoint which of EBF1's targets likely mediated its role in preventing Kölliker's organ cells from being recruited to the prosensory domain, E14.5 snRNA-seq datasets were screened for differentially expressed genes in *Ebf1*-cKO relative to control Kölliker's organ cells. This analysis uncovered a gene regulatory network involving *Prdm16*, *Jag1*, and *Sox2*, which respectively encode a transcription factor expressed in the Kölliker's organ (Ebeid et al., 2022; Zhang et al., 2025), a Notch ligand important in prosensory specification (Kiernan et al., 2006), and a transcription factor important in sensory development (Dabdoub et al., 2008; Kiernan et al., 2005b). The snATAC-seq datasets were then used to identify transcription factor binding motifs in open chromatin regions within and around these loci. Multiomic (combining snRNA-seq and snATAC-seq) analyses revealed that EBF1 likely promotes *Prdm16* expression and, together with PRDM16, co-represses *Jag1* expression. PRDM16 also appeared to repress *Sox2* expression. To uncover which of EBF1's transcriptional targets could explain the increased proliferative capacity seen in *Ebf1*-cKOs, differential expression of genes encoding cell cycle exit regulators was assessed in the cycling cells from the E16.5 *Ebf1*-cKO and control snRNA-seq datasets. *Ccnjl*, a cyclin-like protein associated with several cancers (Gu et al., 2024; Han et al., 2025; Li et al., 2021; Li et al., 2025; Qin et al., 2024; Viet et al., 2021; Wang et al., 2025), was upregulated in *Ebf1*-cKO cycling cells. Open chromatin regions within the *Ccnjl* locus contained both EBF1 and SOX2 motifs. Together, these findings suggest that EBF1 directly represses while SOX2 directly promotes *Ccnjl* expression. In summary, these findings support my hypothesis that EBF1 regulates cochlear patterning during early embryonic development and prosensory cell proliferation during later stages. Loss of EBF1 disrupts a regulatory network involving PRDM16, JAG1, SOX2, and CCNJL, allowing for dramatic sensory expansion.

4.2 Future Directions

My loss-of-function experiments in Chapter 2 and Chapter 3 offer valuable insight into EBF1's critical role in restricting sensory development. Loss of EBF1 leads to aberrant sensory establishment resulting from: (1) Kölliker's organ cells acquiring a prosensory fate and (2) delayed cell cycle exit of prosensory cells. Although these studies provide evidence that EBF1 regulates both cell fate and proliferation during cochlear development, many unanswered questions remain. For instance, further research is needed to assess the transcription factor as a target for regenerative therapeutics. To this end, the following additional experiments would serve to investigate EBF1's regulation of transcriptional targets and to assess its functional significance in adult cochlear tissue.

4.2.1 Functional Validation of Transcriptional Targets

In Chapter 3, I identified *Prdm16*, *Jag1*, and *Ccnjl* as likely being direct targets of EBF1 during cochlear development. The multiomic analyses in this chapter indicate that EBF1 restricts prosensory development in the Kölliker's organ by promoting *Prdm16* expression and co-repressing *Jag1* expression with PRDM16, and thus, overexpression of either *Ebf1* or *Prdm16* around E14.5 would likely repress sensory development. Consistent with previous *Jag1* overexpression (Neves et al., 2011) and Notch overactivation studies (Hartman et al., 2010; Pan et al., 2010), my proposed model predicts that *Jag1* overexpression in the developing mouse cochlea would likely lead to sensory expansion consisting of ectopic sensory patches. Finally, because EBF1 appears to promote *Ccnjl* expression directly, *Ccnjl* overexpression around E16.5 may lead to the re-entry of prosensory cells into the cell cycle.

Electroporation can be used to induce long-term transgene expression in the cochlea (Hayashi et al., 2008a; Jones et al., 2006; Woods et al., 2004), and this technique could be used to functionally assess EBF1 as well as its transcriptional targets during development. To

accomplish this, right and left sister cochlear ducts would be collected from wildtype (C57BL/6) litters for explant culture. Sister explant pairs could then be transfected with plasmids designed to drive robust expression under the CMV/chicken β-actin (CAG) promoter of either the gene of interest with GFP (experimental) or GFP alone (control). Loss-of-function experiments from Chapter 3 showed aberrant cochlear patterning at E14.5 and delayed cell cycle exit at E16.5 due to *Ebf1* excision. Based on these findings, and given that only a few transfected cells can be detected during the first 12-18 h after electroporation (Driver and Kelley, 2010), cochlear ducts for *Ebf1*, *Prdm16*, and *Jag1* overexpression should be collected and transfected at E13.5, whereas those for *Ccnjl* overexpression should be collected and transfected at E15.5. After waiting at least 24 h to allow for plasmid expression, one explant from each experimental and control pair could be treated with a pulse of EdU to label proliferating cells and cultured for another few days to allow for sensory differentiation. Subsequent EdU detection and immunostaining with anti-MYO7a antibodies would reveal changes in proliferation and sensory specification. More specifically, to detect changes in proliferation, the percentage of GFP^+ $MYO7a^+$ transfected HCs that are EdU^+ could be calculated for control and experimental explants. If overexpression of the gene of interest promotes proliferation, experimental explants would have more EdU^+ transfected HCs. If overexpression impairs sensory specification, the experimental explants would have fewer transfected cells that differentiate into HCs than control explants. The remaining explant from each experimental and control pair that was not labeled with EdU could be processed for RT-qPCR to confirm overexpression in FAC-sorted GFP^+ transfected cells. These experiments would offer further insight into how perturbing expression of *Ebf1* and the transcription factor's targets influences cell fate and proliferation in the developing cochlea at two key timepoints.

4.2.2 Assessment of EBF1 Binding

The multiomic analyses in Chapter 3 uncovered cell-type-specific changes in gene expression and chromatin accessibility, and this information was used to infer EBF1 binding and regulation of transcriptional targets. While this approach offered a glimpse of EBF1's interactions within a regulatory network and mitigated the confounding noise that comes from bulk tissue analysis, it did not permit assessment of EBF1's direct binding. Epigenomic profiling methods like Chromatin Immunoprecipitation sequencing (ChIP-seq; Solomon and Varshavsky, 1985), Cleavage Under Targets and Release Using Nuclease (CUT&RUN; Skene and Henikoff, 2017), or Cleavage Under Targets and Tagmentation (CUT&Tag; Kaya-Okur et al., 2019) could be used to accomplish this. Although both CUT&RUN and CUT&Tag exhibit lower signal to noise and require fewer cells/nuclei than ChIP-seq (Kaya-Okur et al., 2019; Teytelman et al., 2013), CUT&Tag is the more efficient method, as it avoids DNA end repair and adapter ligation steps that increase time and overall cost. Additionally, unlike CUT&RUN, DNA fragments generated during CUT&Tag are retained within individual nuclei, making the technique more compatible with single cell/nuclei sequencing platforms (Kaya-Okur et al., 2019). For this reason, transcription factor profiling of EBF1 should be performed with CUT&Tag.

CUT&Tag requires a primary antibody that binds with specificity to the protein of interest. A secondary antibody is then added to enhance tethering of the pA-Tn5 transposome. Upon activation with Mg^{2+}, the transposome integrates adapters on either side of the transcription factor binding site. Genomic fragments with adapters at both ends are then purified and enriched via PCR prior to library construction, sequencing, and analysis (Kaya-Okur et al., 2019). Ideally, a primary antibody specific to EBF1 would be used; however, our lab found that the commercially available antibodies that recognize mouse EBF1 worked poorly and demonstrated high background in our immunostaining experiments. For this reason, my studies of EBF1 involved a pan-EBF antibody that labels all members of the transcription factor family,

including EBF1, which was highly expressed in the cochlear epithelium, and EBF3/4, which showed weak expression (Chapter 2 and 3). Because these EBFs are expressed in both the cochlear epithelium and surrounding mesenchyme, additional steps would be required to identify EBF1-specific binding in the cochlear epithelium. This could be achieved by performing CUT&Tag in parallel with snRNA-seq on wildtype cochleae (Xie et al., 2023; Zhu et al., 2021) or, alternatively, by comparing CUT&Tag reads (DNA fragments) from *Ebf1*-cKO and control littermates. Joint analysis involving CUT&Tag and snRNA-seq datasets generated from the same nuclei would allow for the mapping of EBF-binding motifs within distinct cell populations. By using the snRNA-seq data to subset for epithelial cells that express *Ebf1* and not *Ebf3*/*4*, one could identify CUT&Tag reads that reflect EBF1 binding specifically in cochlear epithelial cell populations. Alternatively, comparing CUT&Tag read levels between *Ebf1*-cKO cochleae, which lack *Ebf1* expression in the cochlear epithelium but maintain it in the mesenchyme, and control cochleae would allow the identification of reads in the control dataset that correspond with EBF1 binding in the cochlear epithelium. By performing these experiments on E14.5 and E16.5 cochleae, one could confirm EBF1's direct regulation of *Prdm16*, *Jag1*, and *Ccnjl*.

4.2.3 Role of EBF1 in Adults

I noted in Chapter 2, that EBFs were expressed in the adult mouse cochlea, weakly in pillar cells and strongly in inner phalangeal cells and Deiter's cells. Combined with developmental analyses of EBF1 (Chapters 2 and 3), this observation raises important questions about whether EBF1 continues to regulate cell fate and proliferation in adult cochleae. Is EBF1 needed to promote a SC fate and repress proliferation in the mature tissue? Could *Ebf1* excision during adult stages offer a means to promote the generation of new HCs and SCs? To begin addressing this question, *Ebf1* excision could be induced in adult SCs by treating the $Sox2^{CreER}$ $Ebf1^{fl/fl}$ mice, mentioned in Chapter 2, with tamoxifen. Initial analyses could include HC and SC quantification in addition to proliferation assays, with results evaluated against Cre-

negative littermate controls (*Ebf1*$^{fl/fl}$) and *Sox2*^{CreER} *Ebf1*$^{fl/fl}$ mice not treated with tamoxifen. These experiments would reveal whether manipulation of EBF1 in the adult cochlea could drive the generation of extra HCs and SCs. If so, a logical next step would be to examine whether new HCs and SCs can be generated following HC loss due to injury or damage. Together, these experiments would clarify whether modulation of EBF1 could be leveraged as a strategy to promote sensory regeneration in the adult mammalian cochlea.

BIBLIOGRAPHY

Ahmed, M., Elaine, Sun, J., Xu, J., Wang, F. and Xu, P.-X. (2012). Eya1-Six1 interaction is sufficient to induce hair cell fate in the cochlea by activating Atoh1 expression in cooperation with Sox2. *Dev. Cell* **22**, 377-390. doi:10.1016/j.devcel.2011.12.006

Amador-Arjona, A., Cimadamore, F., Huang, C.-T., Wright, R., Lewis, S., Gage, F. H. and Terskikh, A. V. (2015). SOX2 primes the epigenetic landscape in neural precursors enabling proper gene activation during hippocampal neurogenesis. *Proc. Natl. Acad. Sci. USA* **112**, E1936-E1945. doi:10.1073/pnas.1421480112

Andersson, E. R., Sandberg, R. and Lendahl, U. (2011). Notch signaling: simplicity in design, versatility in function. *Development* **138**, 3593-3612. doi:10.1242/dev.063610

Arnold, K., Sarkar, A., Yram, M. A., Polo, J. M., Bronson, R., Sengupta, S., Seandel, M., Geijsen, N. and Hochedlinger, K. (2011). Sox2(+) adult stem and progenitor cells are important for tissue regeneration and survival of mice. *Cell Stem Cell* **9**, 317-329. doi:10.1016/j.stem.2011.09.001

Atkinson, P. J., Dong, Y., Gu, S., Liu, W., Najarro, E. H., Udagawa, T. and Cheng, A. G. (2018). Sox2 haploinsufficiency primes regeneration and Wnt responsiveness in the mouse cochlea. *J. Clin. Invest.* **128**, 1641-1656. doi:10.1172/JCI97248

Baek, S., Choi, H. and Kim, J. (2014). Ebf3-miR218 regulation is involved in the development of dopaminergic neurons. *Brain Res.* **1587**, 23-32. doi:10.1016/j.brainres.2014.08.059

Baird, R. A., Streyger, P. S. and Schuff, N. R. (1996). Mitotic and nonmitotic hair cell regeneration in the bullfrog vestibular otolith organs. *Ann. NY Acad. Sci.*, 59-70. doi:10.1111/j.1749-6632.1996.tb15693.x

Balak, K., Corwin, J. and Jones, J. (1990). Regenerated hair cells can originate from supporting cell progeny: evidence from phototoxicity and laser ablation experiments in the lateral line system. *J. Neurosci.* **10**, 2502-2512. doi:10.1523/JNEUROSCI.10-08-02502.1990

Basch, M. L., Brown, R. M., 2nd, Jen, H. I. and Groves, A. K. (2016a). Where hearing starts: the development of the mammalian cochlea. *J. Anat.* **228**, 233-254. doi:10.1111/joa.12314

Basch, M. L., Brown, R. M., 2nd, Jen, H. I., Semerci, F., Depreux, F., Edlund, R. K., Zhang, H., Norton, C. R., Gridley, T., Cole, S. E., et al. (2016b). Fine-tuning of Notch signaling sets the boundary of the organ of Corti and establishes sensory cell fates. *eLife* **5**, e19921. doi:10.7554/eLife.19921

Benito-Gonzalez, A. and Doetzlhofer, A. (2014). Hey1 and Hey2 control the spatial and temporal pattern of mammalian auditory hair cell differentiation downstream of Hedgehog signaling. *J. Neurosci.* **34**, 12865-12876. doi:10.1523/JNEUROSCI.1494-14.2014

Bermingham, N. A., Hassan, B. A., Price, S. D., Vollrath, M. A., Ben-Arie, N., Eatock, R. A., Bellen, H. J., Lysakowski, A. and Zoghbi, H. Y. (1999). *Math1*: An essential gene for the generation of inner ear hair cells. *Science* **284**, 1837-1841. doi:doi:10.1126/science.284.5421.1837

Bohnenpoll, T., Trowe, M.-O., Wojahn, I., Taketo, M. M., Petry, M. and Kispert, A. (2014). Canonical Wnt signaling regulates the proliferative expansion and differentiation of fibrocytes in the murine inner ear. *Dev. Biol.* **391**, 54-65. doi:10.1016/j.ydbio.2014.03.023

Boiani, M. and Schöler, H. R. (2005). Regulatory networks in embryo-derived pluripotent stem cells. *Nat. Rev. Mol. Cell Biol.* **6**, 872-884. doi:10.1038/nrm1744

Bok, J., Zenczak, C., Hwang, C. H. and Wu, D. K. (2013). Auditory ganglion source of Sonic hedgehog regulates timing of cell cycle exit and differentiation of mammalian cochlear hair cells. *Proc. Natl. Acad. Sci. USA* **110**, 13869-13874. doi:10.1073/pnas.1222341110

Boyer, L. A., Lee, T. I., Cole, M. F., Johnstone, S. E., Levine, S. S., Zucker, J. P., Guenther, M. G., Kumar, R. M., Murray, H. L., Jenner, R. G., et al. (2005). Core transcriptional regulatory circuitry in human embryonic stem cells. *Cell* **122**, 947-956. doi:10.1016/j.cell.2005.08.020

Brou, C., Logeat, F., Gupta, N., Bessia, C., LeBail, O., Doedens, J. R., Cumano, A., Roux, P., Black, R. A. and Israël, A. (2000). A novel proteolytic cleavage involved in Notch signaling: the role of the disintegrin-metalloprotease TACE. *Mol. Cell* **5**, 207-216. doi:10.1016/s1097-2765(00)80417-7

Brown, R. and Groves, A. K. (2020). Hear, hear for Notch: Control of cell fates in the inner ear by Notch signaling. *Biomolecules* **10**, 370. doi:10.3390/biom10030370

Brückner, K., Perez, L., Clausen, H. and Cohen, S. (2000). Glycosyltransferase activity of Fringe modulates Notch-Delta interactions. *Nature* **406**, 411-415. doi:10.1038/35019075

Burns, J. C., Cox, B. C., Thiede, B. R., Zuo, J. and Corwin, J. T. (2012). In vivo proliferative regeneration of balance hair cells in newborn mice. *J. Neurosci.* **32**, 6570-6577. doi:10.1523/JNEUROSCI.6274-11.2012

Butler, A., Hoffman, P., Smibert, P., Papalexi, E. and Satija, R. (2018). Integrating single-cell transcriptomic data across different conditions, technologies, and species. *Nat. Biotechnol.* **36**, 411-420. doi:10.1038/nbt.4096

Campbell, D. P., Chrysostomou, E. and Doetzlhofer, A. (2016). Canonical Notch signaling plays an instructive role in auditory supporting cell development. *Sci. Rep.* **6**, 19484. doi:10.1038/srep19484

Cao, J., Spielmann, M., Qiu, X., Huang, X., Ibrahim, D. M., Hill, A. J., Zhang, F., Mundlos, S., Christiansen, L., Steemers, F. J., et al. (2019). The single-cell transcriptional landscape of mammalian organogenesis. *Nature* **566**, 496-502. doi:10.1038/s41586-019-0969-x

Catela, C., Correa, E., Wen, K., Aburas, J., Croci, L., Consalez, G. G. and Kratsios, P. (2019). An ancient role for collier/Olf/Ebf (COE)-type transcription factors in axial motor neuron development. *Neural Dev.* **14**, 2. doi:10.1186/s13064-018-0125-6

CDC (2010). Identifying infants with hearing loss - United States, 1999-2007. *MMWR Morb. Mortal. Wkly Rep.* **59**, 220-223.

Chapman, G., Sparrow, D. B., Kremmer, E. and Dunwoodie, S. L. (2011). Notch inhibition by the ligand Delta-Like 3 defines the mechanism of abnormal vertebral segmentation in spondylocostal dysostosis. *Hum. Mol. Genet.* **20**, 905-916. doi:10.1093/hmg/ddq529

Chen, G.-D. and Fechter, L. D. (2003). The relationship between noise-induced hearing loss and hair cell loss in rats. *Hear. Res.* **177**, 81-90. doi:10.1016/s0378-5955(02)00802-x

Chen, P., Johnson, J. E., Zoghbi, H. Y. and Segil, N. (2002). The role of Math1 in inner ear development: Uncoupling the establishment of the sensory primordium from hair cell fate determination. *Development* **10**, 2495-2505. doi:10.1242/dev.129.10.2495

Chen, P. and Segil, N. (1999). p27(Kip1) links cell proliferation to morphogenesis in the developing organ of Corti. *Development* **126**, 1581-1590. doi:10.1242/dev.126.8.1581

Cheng, L. E. and Reed, R. R. (2007). Zfp423/OAZ participates in a developmental switch during olfactory neurogenesis. *Neuron* **54**, 547-557. doi:10.1016/j.neuron.2007.04.029

Chrysostomou, E., Zhou, L., Darcy, Y. L., Graves, K. A., Doetzlhofer, A. and Cox, B. C. (2020). The Notch ligand Jagged1 is required for the formation, maintenance, and survival of Hensen's cells in the mouse cochlea. *J. Neurosci.* **40**, 9401-9413. doi:10.1523/JNEUROSCI.1192-20.2020

Colvin, J. S., Bohne, B. A., Harding, G. W., McEwen, D. G. and Ornitz, D. M. (1996). Skeletal overgrowth and deafness in mice lacking fibroblast growth factor receptor 3. *Nat. Genet.* **12**, 390-397. doi:10.1038/ng0496-390

Corwin, J. T. (1981). Postembryonic production and aging in inner ear hair cells in sharks. *J. Comp. Neurol.* **201**, 541-553. doi:10.1002/cne.902010406

---- (1983). Postembryonic growth of the macula neglecta auditory detector in the ray, Raja clavata: continual increases in hair cell number, neural convergence, and physiological sensitivity. *J. Comp. Neurol.* **217**, 345-356. doi:10.1002/cne.902170309

---- (1985). Perpetual production of hair cells and maturational changes in hair cell ultrastructure accompany postembryonic growth in an amphibian ear. *Proc. Natl. Acad. Sci. USA* **82**, 3911-3915. doi:10.1073/pnas.82.11.3911

Corwin, J. T. and Cotanche, D. A. (1988). Regeneration of sensory hair cells after acoustic trauma. *Science* **240**, 1772-1774. doi:10.1126/science.3381100

Cotanche, D. A. and Corwin, J. T. (1991). Stereociliary bundles reorient during hair cell development and regeneration in the chick cochlea. *Hear. Res.* **52**, 379-402. doi:10.1016/0378-5955(91)90027-7

Cox, B. C., Chai, R., Lenoir, A., Liu, Z., Zhang, L., Nguyen, D. H., Chalasani, K., Steigelman, K. A., Fang, J., Rubel, E. W., et al. (2014). Spontaneous hair cell regeneration in the neonatal mouse cochlea in vivo. *Development* **141**, 816-829. doi:10.1242/dev.103036

Cunningham, L. L. and Tucci, D. L. (2017). Hearing loss in adults. *New Engl. J. Med.* **377**, 2465-2473. doi:10.1056/NEJMra1616601

D'Souza, B., Meloty-Kapella, L. and Weinmaster, G. (2010). Chapter three - Canonical and non-canonical Notch ligands. In *Current Topics in Developmental Biology* (ed. R. Kopan), pp. 73-129: Academic Press. doi:10.1016/S0070-2153(10)92003-6

Dabdoub, A., Donohue, M. J., Brennan, A., Wolf, V., Montcouquiol, M., Sassoon, D. A., Hseih, J.-C., Rubin, J. S., Salinas, P. C. and Kelley, M. W. (2003). Wnt signaling mediates reorientation of outer hair cell stereociliary bundles in the mammalian cochlea. *Development* **130**, 2375-2384. doi:10.1242/dev.00448

Dabdoub, A., Puligilla, C., Jones, J. M., Fritzsch, B., Cheah, K. S. E., Pevny, L. H. and Kelley, M. W. (2008). Sox2 signaling in prosensory domain specification and subsequent hair cell differentiation in the developing cochlea. *Proc. Natl. Acad. Sci. USA* **105**, 18396-18401. doi:10.1073/pnas.0808175105

Davis, J. A. and Reed, R. R. (1996). Role of Olf-1 and Pax-6 transcription factors in neurodevelopment. *J. Neurosci.* **16**, 5082-5094. doi:10.1523/JNEUROSCI.16-16-05082.1996

Decker, T., Pasca Di Magliano, M., McManus, S., Sun, Q., Bonifer, C., Tagoh, H. and Busslinger, M. (2009). Stepwise activation of enhancer and promoter regions of the B cell commitment gene Pax5 in early lymphopoiesis. *Immunity* **30**, 508-520. doi:10.1016/j.immuni.2009.01.012

Denman-Johnson, K. and Forge, A. (1999). Establishment of hair bundle polarity and orientation in the developing vestibular system of the mouse. *J. Neurocytol.* **28**, 821-835. doi:10.1023/a:1007061819934

Doetzlhofer, A., Basch, M. L., Ohyama, T., Gessler, M., Groves, A. K. and Segil, N. (2009). Hey2 regulation by FGF provides a Notch-independent mechanism for maintaining pillar cell fate in the organ of Corti. *Dev. Cell* **16**, 58-69. doi:10.1016/j.devcel.2008.11.008

Driver, E. C. and Kelley, M. W. (2010). Transfection of mouse cochlear explants by electroporation. *Curr. Protoc. Neurosci.* **51**. doi:10.1002/0471142301.ns0434s51

Driver, E. C. and Kelley, M. W. (2020). Development of the cochlea. *Development* **147**, dev162263. doi:10.1242/dev.162263

Driver, E. C., Pryor, S. P., Hill, P., Turner, J., Rüther, U., Biesecker, L. G., Griffith, A. J. and Kelley, M. W. (2008). Hedgehog signaling regulates sensory cell formation and auditory function in mice and humans. *J. Neurosci.* **28**, 7350-7358. doi:10.1523/JNEUROSCI.0312-08.2008

Dubois, L. and Vincent, A. (2001). The COE – Collier/Olf1/EBF – transcription factors: Structural conservation and diversity of developmental functions. *Mech. Dev.* **108**, 3-12. doi:10.1016/s0925-4773(01)00486-5

Ebeid, M., Barnas, K., Zhang, H., Yaghmour, A., Noreikaite, G. and Bjork, B. C. (2022). PRDM16 expression and function in mammalian cochlear development. *Dev. Dyn.* **251**, 1666-1683. doi:10.1002/dvdy.480

Ebeid, M. and Huh, S.-H. (2017). FGF signaling: diverse roles during cochlear development. *BMB Rep.* **50**, 487-495. doi:10.5483/bmbrep.2017.50.10.164

---- (2020). Mesenchymal ETV transcription factors regulate cochlear length. *Hear. Res.* **396**, 108039. doi:10.1016/j.heares.2020.108039

Fariñas, I., Jones, K. R., Tessarollo, L., Vigers, A. J., Huang, E., Kirstein, M., De Caprona, D. C., Coppola, V., Backus, C., Reichardt, L. F., et al. (2001). Spatial shaping of cochlear innervation by temporally regulated neurotrophin expression. *J. Neurosci.* **21**, 6170-6180. doi:10.1523/JNEUROSCI.21-16-06170.2001

Fields, S., Ternyak, K., Gao, H., Ostraat, R., Akerlund, J. and Hagman, J. (2008). The 'zinc knuckle' motif of Early B cell Factor is required for transcriptional activation of B cell-specific genes. *Mol. Immunol.* **45**, 3786-3796. doi:10.1016/j.molimm.2008.05.018

Forge, A., Li, L., Corwin, J. T. and Nevill, G. (1993). Ultrastructural evidence for hair cell regeneration in the mammalian inner ear. *Science* **259**, 1616-1619. doi:10.1126/science.8456284

Forge, A., Li, L. and Nevill, G. (1998). Hair cell recovery in the vestibular sensory epithelia of mature guinea pigs. *J. Comp. Neurol.* **397**, 69-88. doi:10.1002/(sici)1096-9861(19980720)397:1<69::aid-cne6>3.0.co;2-g

Fritzsch, B., Silos-Santiago, I., Bianchi, L. M. and Fariñas, I. (1997). The role of neurotrophic factors in regulating the development of inner ear innervation. *Trends Neurosci.* **20**, 159-164. doi:10.1016/S0166-2236(96)01007-7

Garcia-Dominguez, M., Poquet, C., Garel, S. and Charnay, P. (2003). Ebf gene function is required for coupling neuronal differentiation and cell cycle exit. *Development* **130**, 6013-6025. doi:10.1242/dev.00840

Garel, S., Garcia-Dominguez, M. and Charnay, P. (2000). Control of the migratory pathway of facial branchiomotor neurones. *Development* **127**, 5297-5307. doi:10.1242/dev.127.24.5297

Garel, S., Marín, F., Grosschedl, R. and Charnay, P. (1999). Ebf1 controls early cell differentiation in the embryonic striatum. *Development* **126**, 5285-5294. doi:10.1242/dev.126.23.5285

Garel, S., Marín, F., Mattéi, M. G., Vesque, C., Vincent, A. and Charnay, P. (1997). Family of Ebf/Olf-1-related genes potentially involved in neuronal differentiation and regional specification in the central nervous system. *Dev. Dyn.* **210**, 191-205. doi:10.1002/(sici)1097-0177(199711)210:3<191::Aid-aja1>3.0.Co;2-b

Geng, R., Noda, T., Mulvaney, J. F., Lin, V. Y. W., Edge, A. S. B. and Dabdoub, A. (2016). Comprehensive expression of Wnt signaling pathway genes during development and maturation of the mouse cochlea. *PLOS ONE* **11**, e0148339. doi:10.1371/journal.pone.0148339

Gnedeva, K. and Hudspeth, A. J. (2015). SoxC transcription factors are essential for the development of the inner ear. *Proc. Natl. Acad. Sci. USA* **112**, 14066-14071. doi:10.1073/pnas.1517371112

Golub, J. S., Tong, L., Ngyuen, T. B., Hume, C. R., Palmiter, R. D., Rubel, E. W. and Stone, J. S. (2012). Hair cell replacement in adult mouse utricles after targeted ablation of hair cells with diphtheria toxin. *J. Neurosci.* **32**, 15093-15105. doi:10.1523/JNEUROSCI.1709-12.2012

Greenbaum, S. and Zhuang, Y. (2002). Identification of E2A target genes in B lymphocyte development by using a gene tagging-based chromatin immunoprecipitation system. *Proc. Natl. Acad. Sci. USA* **99**, 15030-15035. doi:10.1073/pnas.232299999

Groves, A. K. and Fekete, D. M. (2012). Shaping sound in space: the regulation of inner ear patterning. *Development* **139**, 245-257. doi:10.1242/dev.067074

Gu, C., Jin, L., Lv, X., Wang, C., Wen, C. and Su, X. (2024). Development and validation of a prognostic model for colon cancer based on mitotic gene signatures and immune microenvironment analysis. *Discov. Oncol.* **15**, 535. doi:10.1007/s12672-024-01421-2

Gu, Z. and Hübschmann, D. (2023). *rGREAT*: an R/bioconductor package for functional enrichment on genomic regions. *Bioinformatics* **39**. doi:10.1093/bioinformatics/btac745

Györy, I., Boller, S., Nechanitzky, R., Mandel, E., Pott, S., Liu, E. and Grosschedl, R. (2012). Transcription factor Ebf1 regulates differentiation stage-specific signaling, proliferation, and survival of B cells. *Genes Dev.* **26**, 668-682. doi:10.1101/gad.187328.112

Hagman, J., Belanger, C., Travis, A., Turck, C. W. and Grosschedl, R. (1993). Cloning and functional characterization of early B-cell factor, a regulator of lymphocyte-specific gene expression. *Genes Dev.* **7**, 760-773. doi:10.1101/gad.7.5.760

Hagman, J., Gutch, M. J., Lin, H. and Grosschedl, R. (1995). EBF contains a novel zinc coordination motif and multiple dimerization and transcriptional activation domains. *EMBO J.* **14**, 2907-2916. doi:10.1002/j.1460-2075.1995.tb07290.x

Haile, L. M., Kamenov, K., Briant, P. S., Orji, A. U., Steinmetz, J. D., Abdoli, A., Abdollahi, M., Abu-Gharbieh, E., Afshin, A., Ahmed, H., et al. (2021). Hearing loss prevalence and years lived with disability, 1990-2019: findings from the Global Burden of Disease Study 2019. *The Lancet* **397**, 996-1009. doi:10.1016/S0140-6736(21)00516-X

Han, Y., Zeng, A., Liang, X., Jiang, Y., Wang, F. and Song, L. (2025). Multi-omics analyses develop and validate the optimal prognostic model on overall survival prediction for resectable hepatocellular carcinoma. *J. Gastrointest. Oncol.* **16**, 628-649. doi:10.21037/jgo-24-710

Hao, Y., Stuart, T., Kowalski, M. H., Choudhary, S., Hoffman, P., Hartman, A., Srivastava, A., Molla, G., Madad, S., Fernandez-Granda, C., et al. (2024). Dictionary learning for integrative, multimodal and scalable single-cell analysis. *Nat. Biotechnol.* **42**, 293-304. doi:10.1038/s41587-023-01767-y

Harris, J. A., Cheng, A. G., Cunningham, L. L., MacDonald, G., Raible, D. W. and Rubel, E. W. (2003). Neomycin-induced hair cell death and rapid regeneration in the lateral line of zebrafish (Danio rerio). *J. Assoc. Res. Otolaryngol.* **4**, 219-234. doi:10.1007/s10162-002-3022-x

Hartman, B. H., Basak, O., Nelson, B. R., Taylor, V., Bermingham-McDonogh, O. and Reh, T. A. (2009). Hes5 expression in the postnatal and adult mouse inner ear and the drug-damaged cochlea. *J. Assoc. Res. Otolaryngol.* **10**, 321-340. doi:10.1007/s10162-009-0162-2

Hartman, B. H., Hayashi, T., Nelson, B. R., Bermingham-McDonogh, O. and Reh, T. A. (2007). Dll3 is expressed in developing hair cells in the mammalian cochlea. *Dev. Dyn.* **236**, 2875-2883. doi:10.1002/dvdy.21307

Hartman, B. H., Reh, T. A. and Bermingham-McDonogh, O. (2010). Notch signaling specifies prosensory domains via lateral induction in the developing mammalian inner ear. *Proc. Natl. Acad. Sci. USA* **107**, 15792-15797. doi:10.1073/pnas.1002827107

Hayashi, T., Cunningham, D. and Bermingham-McDonogh, O. (2007). Loss of Fgfr3 leads to excess hair cell development in the mouse organ of Corti. *Dev. Dyn.* **236**, 525-533. doi:10.1002/dvdy.21026

Hayashi, T., Kokubo, H., Hartman, B. H., Ray, C. A., Reh, T. A. and Bermingham-McDonogh, O. (2008a). Hesr1 and Hesr2 may act as early effectors of Notch signaling in the developing cochlea. *Dev. Biol.* **316**, 87-99. doi:10.1016/j.ydbio.2008.01.006

Hayashi, T., Ray, C. A. and Bermingham-McDonogh, O. (2008b). Fgf20 is required for sensory epithelial specification in the developing cochlea. *J. Neurosci.* **28**, 5991-5999. doi:10.1523/JNEUROSCI.1690-08.2008

Hayashi, T., Ray, C. A., Younkins, C. and Bermingham-McDonogh, O. (2010). Expression patterns of FGF receptors in the developing mammalian cochlea. *Dev. Dyn.* **239**, 1019-1026. doi:10.1002/dvdy.22236

Hertzano, R., Puligilla, C., Chan, S.-L., Timothy, C., Depireux, D. A., Ahmed, Z., Wolf, J., Eisenman, D. J., Friedman, T. B., Riazuddin, S., et al. (2010). CD44 is a marker for the outer pillar cells in the early postnatal mouse inner ear. *J. Assoc. Res. Otolaryngol.* **11**, 407-418. doi:10.1007/s10162-010-0211-x

Hicks, C., Johnston, S. H., diSibio, G., Collazo, A., Vogt, T. F. and Weinmaster, G. (2000). Fringe differentially modulates Jagged1 and Delta1 signalling through Notch1 and Notch2. *Nat. Cell Biol.* **2**, 515-520. doi:10.1038/35019553

Hollnagel, A., Oehlmann, V., Heymer, J., Rüther, U. and Nordheim, A. (1999). Id genes are direct targets of bone morphogenetic protein induction in embryonic stem cells. *J. Biol. Chem.* **274**, 19838-19845. doi:10.1074/jbc.274.28.19838

Huh, S. H., Jones, J., Warchol, M. E. and Ornitz, D. M. (2012). Differentiation of the lateral compartment of the cochlea requires a temporally restricted FGF20 signal. *PLoS Biol.* **10**, e1001231. doi:10.1371/journal.pbio.1001231

Huh, S. H., Warchol, M. E. and Ornitz, D. M. (2015). Cochlear progenitor number is controlled through mesenchymal FGF receptor signaling. *Elife* **4**. doi:10.7554/eLife.05921

Iwai, R., Tabata, H., Inoue, M., Nomura, K. I., Okamoto, T., Ichihashi, M., Nagata, K. I. and Mizutani, K. I. (2018). A Prdm8 target gene Ebf3 regulates multipolar-to-bipolar transition in migrating neocortical cells. *Biochem. Biophys. Res. Commun.* **495**, 388-394. doi:10.1016/j.bbrc.2017.11.021

Jacques, B. E., Montcouquiol, M. E., Layman, E. M., Lewandoski, M. and Kelley, M. W. (2007). Fgf8 induces pillar cell fate and regulates cellular patterning in the mammalian cochlea. *Development* **134**, 3021-3029. doi:10.1242/dev.02874

Jacques, B. E., Puligilla, C., Weichert, R. M., Ferrer-Vaquer, A., Hadjantonakis, A.-K., Kelley, M. W. and Dabdoub, A. (2012). A dual function for canonical Wnt/β-catenin signaling in the developing mammalian cochlea. *Development* **139**, 4395-4404. doi:10.1242/dev.080358

Jansson, L., Kim, G. S. and Cheng, A. G. (2015). Making sense of Wnt signaling-linking hair cell regeneration to development. *Front. Cell Neurosci.* **9**, 66. doi:10.3389/fncel.2015.00066

Jiang, H., Sha, S. H., Forge, A. and Schacht, J. (2006). Caspase-independent pathways of hair cell death induced by kanamycin in vivo. *Cell Death Differ.* **13**, 20-30. doi:10.1038/sj.cdd.4401706

Jimenez, E., Slevin, C. C., Song, W., Chen, Z., Frederickson, S. C., Gildea, D., Wu, W., Elkahloun, A. G., Ovcharenko, I. and Burgess, S. M. (2022). A regulatory network of Sox and Six transcription factors initiate a cell fate transformation during hearing regeneration in adult zebrafish. *Cell Genom.* **2**, 100170. doi:10.1016/j.xgen.2022.100170

Jimenez, M. A., Akerblad, P., Sigvardsson, M. and Rosen, E. D. (2007). Critical role for Ebf1 and Ebf2 in the adipogenic transcriptional cascade. *Mol. Cell Biol.* **27**, 743-757. doi:10.1128/mcb.01557-06

Jin, S., Guerrero-Juarez, C. F., Zhang, L., Chang, I., Ramos, R., Kuan, C.-H., Myung, P., Plikus, M. V. and Nie, Q. (2021). Inference and analysis of cell-cell communication using CellChat. *Nat. Commun.* **12**, 1088. doi:10.1038/s41467-021-21246-9

Johnson, K. R., Gagnon, L. H., Tian, C., Longo-Guess, C. M., Low, B. E., Wiles, M. V. and Kiernan, A. E. (2018). Deletion of a long-range Dlx5 enhancer disrupts inner ear development in mice. *Genetics* **208**, 1165-1179. doi:10.1534/genetics.117.300447

Jones, J. M., Montcouquiol, M., Dabdoub, A., Woods, C. and Kelley, M. W. (2006). Inhibitors of differentiation and DNA binding (Ids) regulate Math1 and hair cell formation during the development of the organ of Corti. *J. Neurosci.* **26**, 550-558. doi:10.1523/JNEUROSCI.3859-05.2006

Kagoshima, H., Ohnishi, H., Yamamoto, R., Yasumoto, A., Tona, Y., Nakagawa, T., Omori, K. and Yamamoto, N. (2024). EBF1 limits the numbers of cochlear hair and supporting cells and forms the scala tympani and spiral limbus during inner ear development. *J. Neurosci.* **44**, e1060232023. doi:10.1523/JNEUROSCI.1060-23.2023

Kawamoto, K., Izumikawa, M., Beyer, L. A., Atkin, G. M. and Raphael, Y. (2009). Spontaneous hair cell regeneration in the mouse utricle following gentamicin ototoxicity. *Hear. Res.* **247**, 17-26. doi:10.1016/j.heares.2008.08.010

Kaya-Okur, H. S., Wu, S. J., Codomo, C. A., Pledger, E. S., Bryson, T. D., Henikoff, J. G., Ahmad, K. and Henikoff, S. (2019). CUT&Tag for efficient epigenomic profiling of small samples and single cells. *Nat. Commun.* **10**, 1930. doi:10.1038/s41467-019-09982-5

Kee, B. L. and Murre, C. (1998). Induction of early B cell factor (EBF) and multiple B lineage genes by the basic helix-loop-helix transcription factor E12. *J. Exp. Med.* **188**, 699-713. doi:10.1084/jem.188.4.699

Kempfle, J. S., Turban, J. L. and Edge, A. S. B. (2016). Sox2 in the differentiation of cochlear progenitor cells. *Sci. Rep.* **6**, 23293. doi:10.1038/srep23293

Kiernan, A. E. (2013). Notch signaling during cell fate determination in the inner ear. *Semin. Cell Dev. Biol.* **24**, 470-479. doi:10.1016/j.semcdb.2013.04.002

Kiernan, A. E., Cordes, R., Kopan, R., Gossler, A. and Gridley, T. (2005a). The Notch ligands DLL1 and JAG2 act synergistically to regulate hair cell development in the mammalian inner ear. *Development* **132**, 4353-4362. doi:10.1242/dev.02002

Kiernan, A. E., Pelling, A. L., Leung, K. K. H., Tang, A. S. P., Bell, D. M., Tease, C., Lovell-Badge, R., Steel, K. P. and Cheah, K. S. E. (2005b). Sox2 is required for sensory organ development in the mammalian inner ear. *Nature* **434**, 1031-1035. doi:10.1038/nature03487

Kiernan, A. E., Xu, J. and Gridley, T. (2006). The Notch ligand JAG1 is required for sensory progenitor development in the mammalian inner ear. *PLoS Genet.* **2**, e4. doi:10.1371/journal.pgen.0020004

Knipper, M., Zimmermann, U., Rohbock, K., Köpschall, I. and Zenner, H. P. (1996). Expression of neurotrophin receptor trkB in rat cochlear hair cells at time of rearrangement of innervation. *Cell Tissue Res.* **283**, 339-353. doi:10.1007/s004410050545

Kopan, R. and Ilagan, M. X. G. (2009). The Canonical Notch Signaling Pathway: Unfolding the Activation Mechanism. *Cell* **137**, 216-233. doi:10.1016/j.cell.2009.03.045

Korver, A. M., Smith, R. J., Van Camp, G., Schleiss, M. R., Bitner-Glindzicz, M. A., Lustig, L. R., Usami, S. I. and Boudewyns, A. N. (2017). Congenital hearing loss. *Nat. Rev. Dis. Primers* **3**, 16094. doi:10.1038/nrdp.2016.94

Kubo, S., Kataria, R., Yao, Y., Gabrielski, J. Q., Zheng, L., Markowitz, T. E., Chan, W., Song, J., Boddapati, A. K., Saeki, K., et al. (2022). Early B cell factor 4 modulates FAS-

mediated apoptosis and promotes cytotoxic function in human immune cells. *Proc. Natl. Acad. Sci. USA* **119**, e2208522119. doi:10.1073/pnas.2208522119

Ladi, E., Nichols, J. T., Ge, W., Miyamoto, A., Yao, C., Yang, L.-T., Boulter, J., Sun, Y. E., Kintner, C. and Weinmaster, G. (2005). The divergent DSL ligand Dll3 does not activate Notch signaling but cell autonomously attenuates signaling induced by other DSL ligands. *J. Cell Biol.* **170**, 983-992. doi:10.1083/jcb.200503113

Lanford, P. J., Lan, Y., Jiang, R., Lindsell, C., Weinmaster, G., Gridley, T. and Kelley, M. W. (1999). Notch signalling pathway mediates hair cell development in mammalian cochlea. *Nat. Genet.* **21**, 289-292. doi:10.1038/6804

LeBon, L., Lee, T. V., Sprinzak, D., Jafar-Nejad, H. and Elowitz, M. B. (2014). Fringe proteins modulate Notch-ligand cis and trans interactions to specify signaling states. *eLife* **3**, e02950. doi:10.7554/eLife.02950

Lenoir, M., Daudet, N., Humbert, G., Renard, N., Gallego, M., Pujol, R., Eybalin, M. and Vago, P. (1999). Morphological and molecular changes in the inner hair cell region of the rat cochlea after amikacin treatment. *J. Neurocytol.* **28**, 925-937. doi:10.1023/a:1007034508547

Li, J., Yen, C., Liaw, D., Podsypanina, K., Bose, S., Wang, S. I., Puc, J., Miliaresis, C., Rodgers, L., McCombie, R., et al. (1997). PTEN, a putative protein tyrosine phosphatase gene mutated in human brain, breast, and prostate cancer. *Science* **275**, 1943-1947. doi:10.1126/science.275.5308.1943

Li, J., Zhou, L., Liu, Y., Yang, L., Jiang, D., Li, K., Xie, S., Wang, X. and Wang, S. (2021). Comprehensive analysis of cyclin family gene expression in colon cancer. *Front. Oncol.* **11**, 674394. doi:10.3389/fonc.2021.674394

Li, R., Cauchy, P., Ramamoorthy, S., Boller, S., Chavez, L. and Grosschedl, R. (2018). Dynamic EBF1 occupancy directs sequential epigenetic and transcriptional events in B-cell programming. *Genes Dev.* **32**, 96-111. doi:10.1101/gad.309583.117

Li, S., Mark, S., Radde-Gallwitz, K., Schlisner, R., Chin, M. T. and Chen, P. (2008). Hey2 functions in parallel with Hes1 and Hes5 for mammalian auditory sensory organ development. *BMC Dev. Biol.* **8**, 20. doi:10.1186/1471-213x-8-20

Li, S., Wang, X., Xiao, J. and Yi, J. (2025). SLC7A11, a disulfidptosis-related gene, correlates with multi-omics prognostic analysis in hepatocellular carcinoma. *Eur. J. Med. Res.* **30**, 161. doi:10.1186/s40001-025-02411-y

Liao, D. (2009). Emerging roles of the EBF family of transcription factors in tumor suppression. *Mol. Cancer Res.* **7**, 1893-1901. doi:10.1158/1541-7786.Mcr-09-0229

Liberg, D., Sigvardsson, M. and Akerblad, P. (2002). The EBF/Olf/Collier family of transcription factors: regulators of differentiation in cells originating from all three embryonal germ layers. *Mol. Cell Biol.* **22**, 8389-8397. doi:10.1128/MCB.22.24.8389-8397.2002

Liberman, M. C., Dodds, L. W. and Pierce, S. (1990). Afferent and efferent innervation of the cat cochlea: quantitative analysis with light and electron microscopy. *J. Comp. Neurol.* **301**, 443-460. doi:10.1002/cne.903010309

Lin, H. and Grosschedl, R. (1995). Failure of B-cell differentiation in mice lacking the transcription factor EBF. *Nature* **376**, 263-267. doi:10.1038/376263a0

Lobo, M. K., Yeh, C. and Yang, X. W. (2008). Pivotal role of early B-cell factor 1 in development of striatonigral medium spiny neurons in the matrix compartment. *J. Neurosci. Res.* **86**, 2134-2146. doi:10.1002/jnr.21666

Logeat, F., Bessia, C., Brou, C., LeBail, O., Jarriault, S., Seidah, N. G. and Israël, A. (1998). The Notch1 receptor is cleaved constitutively by a furin-like convertase. *Proc. Natl. Acad. Sci. USA* **95**, 8108-8112. doi:10.1073/pnas.95.14.8108

Löwenheim, H., Furness, D. N., Kil, J., Zinn, C., Gültig, K., Fero, M. L., Frost, D., Gummer, A. W., Roberts, J. M., Rubel, E. W., et al. (1999). Gene disruption of p27(Kip1) allows cell proliferation in the postnatal and adult organ of corti. *Proc. Natl. Acad. Sci. USA* **96**, 4084-4088. doi:10.1073/pnas.96.7.4084

Lukin, K., Fields, S., Guerrettaz, L., Straign, D., Rodriguez, V., Zandi, S., Månsson, R., Cambier, J. C., Sigvardsson, M. and Hagman, J. (2011). A dose-dependent role for EBF1 in repressing non-B-cell-specific genes. *Eur. J. Immunol.* **41**, 1787-1793. doi:10.1002/eji.201041137

Mansour, S. L., Li, C. and Urness, L. D. (2013). Genetic rescue of Muenke syndrome model hearing loss reveals prolonged FGF-dependent plasticity in cochlear supporting cell fates. *Genes Dev.* **27**, 2320-2331. doi:10.1101/gad.228957.113

Mansour, S. L. and Urness, L. D. (2025). Early and transient requirements for FGFR2b/1b ligands in cochlear sensory and neural cell subtype differentiation. *Dev. Biol.* doi:10.1016/j.ydbio.2025.08.017

Mao, L., Lu, J., Hou, Y. and Nie, T. (2024). Directly targeting PRDM16 in thermogenic adipose tissue to treat obesity and its related metabolic diseases. *Front. Endocrinol. (Lausanne)* **15**, 1458848. doi:10.3389/fendo.2024.1458848

Maunsell, H. R., Ellis, K., Kelley, M. W. and Driver, E. C. (2023). Lrrn1 regulates medial boundary formation in the developing mouse organ of Corti. *J. Neurosci.* **43**, 5305-5318. doi:10.1523/JNEUROSCI.2141-22.2023

McInnes, L. and Healy, J. (2018). UMAP: Uniform Manifold Approximation and Projection for Dimension Reduction. *ArXiv* **abs/1802.03426**. doi:10.48550/arXiv.1802.03426

Morrison, A., Hodgetts, C., Gossler, A., Hrabé de Angelis, M. and Lewis, J. (1999). Expression of Delta1 and Serrate1 (Jagged1) in the mouse inner ear. *Mech. Dev.* **84**, 169-172. doi:10.1016/s0925-4773(99)00066-0

Morsli, H., Choo, D., Ryan, A., Johnson, R. and Wu, D. K. (1998). Development of the mouse inner ear and origin of its sensory organs. *J. Neurosci.* **18**, 3327-3335. doi:10.1523/JNEUROSCI.18-09-03327.1998

Morton, C. C. and Nance, W. E. (2006). Newborn hearing screening--a silent revolution. *N. Engl. J. Med.* **354**, 2151-2164. doi:10.1056/NEJMra050700

Mueller, K. L., Jacques, B. E. and Kelley, M. W. (2002). Fibroblast growth factor signaling regulates pillar cell development in the organ of Corti. *J. Neurosci.* **22**, 9368-9377. doi:10.1523/JNEUROSCI.22-21-09368.2002

Mumm, J. S., Schroeter, E. H., Saxena, M. T., Griesemer, A., Tian, X., Pan, D. J., Ray, W. J. and Kopan, R. (2000). A ligand-induced extracellular cleavage regulates gamma-secretase-like proteolytic activation of Notch1. *Mol. Cell* **5**, 197-206. doi:10.1016/s1097-2765(00)80416-5

Munnamalai, V. and Fekete, D. M. (2016). Notch-Wnt-Bmp crosstalk regulates radial patterning in the mouse cochlea in a spatiotemporal manner. *Development* **143**, 4003-4015. doi:10.1242/dev.139469

Munnamalai, V. and Fekete, D. M. (2020). The acquisition of positional information across the radial axis of the cochlea. *Dev. Dyn.* **249**, 281-297. doi:10.1002/dvdy.118

Murata, J., Ohtsuka, T., Tokunaga, A., Nishiike, S., Inohara, H., Okano, H. and Kageyama, R. (2009). Notch-Hes1 pathway contributes to the cochlear prosensory formation potentially through the transcriptional down-regulation of p27Kip1. *J. Neurosci. Res.* **87**, 3521-3534. doi:10.1002/jnr.22169

Murata, J., Tokunaga, A., Okano, H. and Kubo, T. (2006). Mapping of notch activation during cochlear development in mice: implications for determination of prosensory domain and cell fate diversification. *J. Comp. Neurol.* **497**, 502-518. doi:10.1002/cne.20997

Musse, A. A., Meloty-Kapella, L. and Weinmaster, G. (2012). Notch ligand endocytosis: Mechanistic basis of signaling activity. *Semin. Cell Dev. Biol.* **23**, 429-436. doi:10.1016/j.semcdb.2012.01.011

Najarro, E. H., Huang, J., Jacobo, A., Quiruz, L. A., Grillet, N. and Cheng, A. G. (2020). Dual regulation of planar polarization by secreted Wnts and Vangl2 in the developing mouse cochlea. *Development* **147**. doi:10.1242/dev.191981

Nakagawa, T., Yamane, H., Takayama, M., Sunami, K. and Nakai, Y. (1998). Apoptosis of guinea pig cochlear hair cells following chronic aminoglycoside treatment. *Eur. Arch. Otorhinolaryngol.* **255**, 127-131. doi:10.1007/s004050050027

Nakahiro, T., Kurooka, H., Mori, K., Sano, K. and Yokota, Y. (2010). Identification of BMP-responsive elements in the mouse Id2 gene. *Biochem. Biophys. Res. Commun.* **399**, 416-421. doi:10.1016/j.bbrc.2010.07.090

Nelson, T., Velazquez, H., Troiano, N. and Fretz, J. A. (2019). Early B Cell Factor 1 (EBF1) regulates glomerular development by controlling mesangial maturation and consequently COX-2 expression. *J. Am. Soc. Nephrol.* **30**, 1559-1572. doi:10.1681/asn.2018070699

Nelson, T. A., Tommasini, S. and Fretz, J. A. (2024). Deletion of the transcription factor EBF1 in perivascular stroma disrupts skeletal homeostasis and precipitates premature aging of the marrow microenvironment. *Bone* **187**, 117198. doi:10.1016/j.bone.2024.117198

Neves, J., Parada, C., Chamizo, M. and Giráldez, F. (2011). Jagged 1 regulates the restriction of Sox2 expression in the developing chicken inner ear: A mechanism for sensory organ specification. *Development* **138**, 735-744. doi:10.1242/dev.060657

NIDCD (2023). Calculations based on 2015–2020 NHANES data using the Global Burden of Disease definition of disabling hearing loss (≥35 dB in the better ear).

Nieminen-Pihala, V., Tarkkonen, K., Laine, J., Rummukainen, P., Saastamoinen, L., Nagano, K., Baron, R. and Kiviranta, R. (2021). Early B-cell Factor1 (Ebf1) promotes early osteoblast differentiation but suppresses osteoblast function. *Bone* **146**, 115884. doi:10.1016/j.bone.2021.115884

Ohyama, T., Basch, M. L., Mishina, Y., Lyons, K. M., Segil, N. and Groves, A. K. (2010). BMP signaling is necessary for patterning the sensory and nonsensory regions of the developing mammalian cochlea. *J. Neurosci.* **30**, 15044-15051. doi:10.1523/JNEUROSCI.3547-10.2010

Pan, W., Jin, Y., Stanger, B. and Kiernan, A. E. (2010). Notch signaling is required for the generation of hair cells and supporting cells in the mammalian inner ear. *Proc. Natl. Acad. Sci. USA* **107**, 15798-15803. doi:10.1073/pnas.1003089107

Patil, M., Sharma, B. K., Elattar, S., Chang, J., Kapil, S., Yuan, J. and Satyanarayana, A. (2017). Id1 promotes obesity by suppressing brown adipose thermogenesis and white adipose browning. *Diabetes* **66**, 1611-1625. doi:10.2337/db16-1079

Pauley, S., Wright, T. J., Pirvola, U., Ornitz, D., Beisel, K. and Fritzsch, B. (2003). Expression and function of FGF10 in mammalian inner ear development. *Dev. Dyn.* **227**, 203-215. doi:10.1002/dvdy.10297

Pickles, J. O. (2012). *An introduction to the physiology of hearing* (Fourth edition. edn). Bingley, United Kingdom: Emerald Group Publishing, Limited.

Pirvola, U., Spencer-Dene, B., Xing-Qun, L., Kettunen, P., Thesleff, I., Fritzsch, B., Dickson, C. and Ylikoski, J. (2000). FGF/FGFR-2(IIIb) signaling is essential for inner ear morphogenesis. *J. Neurosci.* **20**, 6125-6134. doi:10.1523/JNEUROSCI.20-16-06125.2000

Pirvola, U., Ylikoski, J., Trokovic, R., Hébert, J. M., McConnell, S. K. and Partanen, J. (2002). FGFR1 is required for the development of the auditory sensory epithelium. *Neuron* **35**, 671-680. doi:10.1016/s0896-6273(02)00824-3

Pirvola, U., Zhang, X., Mantela, J., Ornitz, D. M. and Ylikoski, J. (2004). Fgf9 signaling regulates inner ear morphogenesis through epithelial–mesenchymal interactions. *Dev. Biol.* **273**, 350-360. doi:10.1016/j.ydbio.2004.06.010

Pongubala, J. M., Northrup, D. L., Lancki, D. W., Medina, K. L., Treiber, T., Bertolino, E., Thomas, M., Grosschedl, R., Allman, D. and Singh, H. (2008). Transcription factor EBF restricts alternative lineage options and promotes B cell fate commitment independently of Pax5. *Nat. Immunol.* **9**, 203-215. doi:10.1038/ni1555

Powers, K. G., Wilkerson, B. A., Beach, K. E., Seo, S. S., Rodriguez, J. S., Baxter, A. N., Hunter, S. E. and Bermingham-McDonogh, O. (2024). Deletion of the *Ebf1*, a mouse deafness gene, causes a dramatic increase in hair cells and support cells of the organ of Corti. *Development* **151**. doi:10.1242/dev.202816

Presson, J. C., Lanford, P. J. and Popper, A. N. (1996). Hair cell precursors are ultrastructurally indistinguishable from mature support cells in the ear of a postembryonic fish. *Hear. Res.* **100**, 10-20. doi:10.1016/0378-5955(96)00109-8

Puligilla, C., Feng, F., Ishikawa, K., Bertuzzi, S., Dabdoub, A., Griffith, A. J., Fritzsch, B. and Kelley, M. W. (2007). Disruption of fibroblast growth factor receptor 3 signaling results in defects in cellular differentiation, neuronal patterning, and hearing impairment. *Dev. Dyn.* **236**, 1905-1917. doi:10.1002/dvdy.21192

Qian, D., Jones, C., Rzadzinska, A., Mark, S., Zhang, X., Steel, K. P., Dai, X. and Chen, P. (2007). Wnt5a functions in planar cell polarity regulation in mice. *Dev. Biol.* **306**, 121-133. doi:10.1016/j.ydbio.2007.03.011

Qin, T. and Bronner, M. E. (2025). Multifaceted roles of sonic hedgehog signaling in mammalian inner ear development. *Dev. Biol.* **524**, 97-104. doi:10.1016/j.ydbio.2025.05.007

Qin, X., Sun, H., Hu, S., Pan, Y. and Wang, S. (2024). A hypoxia-glycolysis-lactate-related gene signature for prognosis prediction in hepatocellular carcinoma. *BMC Med. Genomics* **17**, 88. doi:10.1186/s12920-024-01867-x

Rai, V., Tu, S., Frank, J. R. and Zuo, J. (2022). Molecular pathways modulating sensory hair cell regeneration in adult mammalian cochleae: progress and perspectives. *Int. J. Mol. Sci.* **23**, 66. doi:10.3390/ijms23010066

Rajakumari, S., Wu, J., Ishibashi, J., Lim, H.-W., Giang, A.-H., Won, K.-J., Randall and Seale, P. (2013). EBF2 Determines and Maintains Brown Adipocyte Identity. *Cell Metab.* **17**, 562-574. doi:10.1016/j.cmet.2013.01.015

Ramírez, J., Lukin, K. and Hagman, J. (2010). From hematopoietic progenitors to B cells: mechanisms of lineage restriction and commitment. *Curr. Opin. Immunol.* **22**, 177-184. doi:10.1016/j.coi.2010.02.003

Raphael, Y. (1992). Evidence for supporting cell mitosis in response to acoustic trauma in the avian inner ear. *J. Neurocytol.* **21**, 663-671. doi:10.1007/bf01191727

Raphael, Y., Adler, H. J., Wang, Y. and Finger, P. A. (1994). Cell cycle of transdifferentiating supporting cells in the basilar papilla. *Hear. Res.* **80**, 53-63. doi:10.1016/0378-5955(94)90008-6

Riccomagno, M. M., Martinu, L., Mulheisen, M., Wu, D. K. and Epstein, D. J. (2002). Specification of the mammalian cochlea is dependent on Sonic hedgehog. *Genes Dev.* **16**, 2365-2378. doi:10.1101/gad.1013302

Roberston, D. (1980). Acoustic trauma in the guinea pig cochlea: Early changes in ultrastructure and neural threshold. *Hear. Res.* **3**, 167-179. doi:10.1016/0378-5955(80)90044-1

Roby, Y. A., Bushey, M. A., Cheng, L. E., Kulaga, H. M., Lee, S. J. and Reed, R. R. (2012). Zfp423/OAZ mutation reveals the importance of Olf/EBF transcription activity in olfactory neuronal maturation. *J. Neurosci.* **32**, 13679-13688a. doi:10.1523/JNEUROSCI.6190-11.2012

Roessler, S., György, I., Imhof, S., Spivakov, M., Williams, R. R., Busslinger, M., Fisher, A. G. and Grosschedl, R. (2007). Distinct promoters mediate the regulation of Ebf1 gene expression by interleukin-7 and Pax5. *Mol. Cell Biol.* **27**, 579-594. doi:10.1128/mcb.01192-06

Ruben, R. J. (1967). Development of the inner ear of the mouse: a radioautographic study of terminal mitoses. *Acta Otolaryngol.* **220**, 1-44.

Ryals, B. M. and Rubel, E. W. (1988). Hair cell regeneration after acoustic trauma in adult Coturix quail. *Science* **240**, 1774-1776. doi:10.1126/science.3381101

Sahly, I., El-Amraoui, A., Abitbol, M., Petit, C. and Dufier, J.-L. (1997). Expression of myosin VIIA during mouse embryogenesis. *Anat. Embryol. (Berl.)* **196**, 159-170. doi:10.1007/s004290050088

Sajan, S. A., Rubenstein, J. L., Warchol, M. E. and Lovett, M. (2011). Identification of direct downstream targets of Dlx5 during early inner ear development. *Hum. Mol. Genet.* **20**, 1262-1273. doi:10.1093/hmg/ddq567

Satija, R., Farrell, J. A., Gennert, D., Schier, A. F. and Regev, A. (2015). Spatial reconstruction of single-cell gene expression data. *Nat. Biotechnol.* **33**, 495-502. doi:10.1038/nbt.3192

Seale, P., Kajimura, S., Yang, W., Chin, S., Rohas, L. M., Uldry, M., Tavernier, G., Langin, D. and Spiegelman, B. M. (2007). Transcriptional control of brown fat determination by PRDM16. *Cell Metab.* **6**, 38-54. doi:10.1016/j.cmet.2007.06.001

Shang, J., Cafaro, J., Nehmer, R. and Stone, J. (2010). Supporting cell division is not required for regeneration of auditory hair cells after ototoxic injury in vitro. *J. Assoc. Res. Otolaryngol.* **11**, 203-222. doi:10.1007/s10162-009-0206-7

Sheffield, A. M. and Smith, R. J. H. (2019). The Epidemiology of Deafness. *Cold Spring Harb. Perspect. Med.* **9**. doi:10.1101/cshperspect.a033258

Shi, F., Cheng, Y.-f., Wang, X. L. and Edge, A. S. B. (2010). β-Catenin Up-regulates Atoh1 Expression in Neural Progenitor Cells by Interaction with an Atoh1 3′ Enhancer*. *J. Biol. Chem.* **285**, 392-400. doi:10.1074/jbc.M109.059055

Shim, K., Minowada, G., Coling, D. E. and Martin, G. R. (2005). Sprouty2, a mouse deafness gene, regulates cell fate decisions in the auditory sensory epithelium by antagonizing FGF signaling. *Dev. Cell* **8**, 553-564. doi:10.1016/j.devcel.2005.02.009

Skene, P. J. and Henikoff, S. (2017). An efficient targeted nuclease strategy for high-resolution mapping of DNA binding sites. *eLife* **6**, e21856. doi:10.7554/eLife.21856

Slowik, A. D. and Bermingham-McDonogh, O. (2013a). Hair cell generation by notch inhibition in the adult mammalian cristae. *J. Assoc. Res. Otolaryngol.* **14**, 813-828. doi:10.1007/s10162-013-0414-z

---- (2013b). Notch signaling in mammalian hair cell regeneration. *Trends Dev. Biol.* **7**, 73-89.

Smith, E. M., Gisler, R. and Sigvardsson, M. (2002). Cloning and characterization of a promoter flanking the early B cell factor (EBF) gene indicates roles for E-proteins and autoregulation in the control of EBF expression. *J. Immunol.* **169**, 261-270. doi:10.4049/jimmunol.169.1.261

Smith, E. M. K., ÅKerblad, P., Kadesch, T., Axelson, H. K. and Sigvardsson, M. (2005). Inhibition of EBF function by active Notch signaling reveals a novel regulatory pathway in early B-cell development. *Blood* **106**, 1995-2001. doi:10.1182/blood-2004-12-4744

Solomon, M. J. and Varshavsky, A. (1985). Formaldehyde-mediated DNA-protein crosslinking: a probe for in vivo chromatin structures. *Proc. Natl. Acad. Sci. USA* **82**, 6470-6474. doi:10.1073/pnas.82.19.6470

Souabni, A., Cobaleda, C., Schebesta, M. and Busslinger, M. (2002). Pax5 promotes B lymphopoiesis and blocks T cell development by repressing Notch1. *Immunity* **17**, 781-793. doi:10.1016/s1074-7613(02)00472-7

Steck, P. A., Pershouse, M. A., Jasser, S. A., Yung, W. K., Lin, H., Ligon, A. H., Langford, L. A., Baumgard, M. L., Hattier, T., Davis, T., et al. (1997). Identification of a candidate tumour suppressor gene, MMAC1, at chromosome 10q23.3 that is mutated in multiple advanced cancers. *Nat. Genet.* **15**, 356-362. doi:10.1038/ng0497-356

Struhl, G. and Adachi, A. (2000). Requirements for Presenilin-Dependent Cleavage of Notch and Other Transmembrane Proteins. *Mol. Cell* **6**, 625-636. doi:10.1016/S1097-2765(00)00061-7

Stuart, T., Srivastava, A., Madad, S., Lareau, C. A. and Satija, R. (2021). Single-cell chromatin state analysis with Signac. *Nat. Methods* **18**, 1333-1341. doi:10.1038/s41592-021-01282-5

Sun, B., Mallampati, S., Gong, Y., Wang, D., Lefebvre, V. and Sun, X. (2013). Sox4 is required for the survival of pro-B cells. *J. Immunol.* **190**, 2080-2089. doi:10.4049/jimmunol.1202736

Takemura, T., Sakagami, M., Takebayashi, K., Umemoto, M., Nakase, T., Takaoka, K., Kubo, T., Kitamura, Y. and Nomura, S. (1996). Localization of bone morphogenetic protein-4 messenger RNA in developing mouse cochlea. *Hear. Res.* **95**, 26-32. doi:10.1016/0378-5955(95)00233-2

Tateya, T., Imayoshi, I., Tateya, I., Hamaguchi, K., Torii, H., Ito, J. and Kageyama, R. (2013). Hedgehog signaling regulates prosensory cell properties during the basal-to-apical wave

of hair cell differentiation in the mammalian cochlea. *Development* **140**, 3848-3857. doi:10.1242/dev.095398

Tateya, T., Imayoshi, I., Tateya, I., Ito, J. and Kageyama, R. (2011). Cooperative functions of Hes/Hey genes in auditory hair cell and supporting cell development. *Dev. Biol.* **352**, 329-340. doi:10.1016/j.ydbio.2011.01.038

Taylor, R. R. and Forge, A. (2005). Hair cell regeneration in sensory epithelia from the inner ear of a urodele amphibian. *J. Comp. Neurol.* **484**, 105-120. doi:10.1002/cne.20450

Teytelman, L., Thurtle, D. M., Rine, J. and Van Oudenaarden, A. (2013). Highly expressed loci are vulnerable to misleading ChIP localization of multiple unrelated proteins. *Proc. Natl. Acad. Sci. USA* **110**, 18602-18607. doi:10.1073/pnas.1316064110

Thal, M. A., Carvalho, T. L., He, T., Kim, H. G., Gao, H., Hagman, J. and Klug, C. A. (2009). Ebf1-mediated down-regulation of Id2 and Id3 is essential for specification of the B cell lineage. *Proc. Natl. Acad. Sci. USA* **106**, 552-557. doi:10.1073/pnas.0802550106

Tolomeo, J. A. and Holley, M. C. (1997). Mechanics of microtubule bundles in pillar cells from the inner ear. *Biophys. J.* **73**, 2241-2247. doi:10.1016/S0006-3495(97)78255-9

Travis, A., Hagman, J., Hwang, L. and Grosschedl, R. (1993). Purification of Early-B-cell Factor and characterization of its DNA-binding specificity. *Mol. Cell Biol.* **13**, 3392-3400. doi:10.1128/mcb.13.6.3392-3400.1993

Treiber, T., Mandel, E. M., Pott, S., Györy, I., Firner, S., Liu, E. T. and Grosschedl, R. (2010). Early B cell Factor 1 regulates B cell gene networks by activation, repression, and transcription- independent poising of chromatin. *Immunity* **32**, 714-725. doi:10.1016/j.immuni.2010.04.013

Tsai, R. Y. and Reed, R. R. (1997). Cloning and functional characterization of Roaz, a zinc finger protein that interacts with O/E-1 to regulate gene expression: implications for olfactory neuronal development. *J. Neurosci.* **17**, 4159-4169. doi:10.1523/JNEUROSCI.17-11-04159.1997

---- (1998). Identification of DNA recognition sequences and protein interaction domains of the multiple-Zn-finger protein Roaz. *Mol. Cell Biol.* **18**, 6447-6456. doi:10.1128/mcb.18.11.6447

Tucker, J. B., Mackie, J. B., Bussoli, T. J. and Steel, K. P. (1999). Cytoskeletal integration in a highly ordered sensory epithelium in the organ of Corti: reponse to loss of cell partners in the Bronx waltzer mouse. *J. Neurocytol.* **28**, 1017-1034. doi:10.1023/a:1007092105185

Urness, L. D., Wang, X., Li, C., Quadros, R. M., Harms, D. W., Gurumurthy, C. B. and Mansour, S. L. (2020). Slc26a9(P2ACre): A new CRE driver to regulate gene expression in the otic placode lineage and other FGFR2b-dependent epithelia. *Development* **147**. doi:10.1242/dev.191015

Urness, L. D., Wang, X., Shibata, S., Ohyama, T. and Mansour, S. L. (2015). Fgf10 is required for specification of non-sensory regions of the cochlear epithelium. *Dev. Biol.* **400**, 59-71. doi:10.1016/j.ydbio.2015.01.015

Ved, N., Curran, A., Ashcroft, F. M. and Sparrow, D. B. (2019). Tamoxifen administration in pregnant mice can be deleterious to both mother and embryo. *Lab Animal* **53**, 630-633. doi:10.1177/0023677219856918

Viet, C. T., Yu, G., Asam, K., Thomas, C. M., Yoon, A. J., Wongworawat, Y. C., Haghighiabyaneh, M., Kilkuts, C. A., McGue, C. M., Couey, M. A., et al. (2021). The REASON score: an epigenetic and clinicopathologic score to predict risk of poor survival in patients with early stage oral squamous cell carcinoma. *Biomark. Res.* **9**, 42. doi:10.1186/s40364-021-00292-x

Vilagos, B., Hoffmann, M., Souabni, A., Sun, Q., Werner, B., Medvedovic, J., Bilic, I., Minnich, M., Axelsson, E., Jaritz, M., et al. (2012). Essential role of EBF1 in the generation and function of distinct mature B cell types. *J. Exp. Med.* **209**, 775-792. doi:10.1084/jem.20112422

Vos, T., Lim, S. S., Abbafati, C., Abbas, K. M., Abbasi, M., Abbasifard, M., Abbasi-Kangevari, M., Abbastabar, H., Abd-Allah, F., Abdelalim, A., et al. (2020). Global burden of 369 diseases and injuries in 204 countries and territories, 1990–2019: A systematic analysis for the Global Burden of Disease Study 2019. *The Lancet* **396**, 1204-1222. doi:10.1016/s0140-6736(20)30925-9

Wan, G., Corfas, G. and Stone, J. S. (2013). Inner ear supporting cells: rethinking the silent majority. *Semin. Cell Dev. Biol.* **24**, 448-459. doi:10.1016/j.semcdb.2013.03.009

Wang, M. M. and Reed, R. R. (1993). Molecular cloning of the olfactory neuronal transcription factor Olf-1 by genetic selection in yeast. *Nature* **364**, 121-126. doi:10.1038/364121a0

Wang, R. N., Green, J., Wang, Z., Deng, Y., Qiao, M., Peabody, M., Zhang, Q., Ye, J., Yan, Z., Denduluri, S., et al. (2014). Bone Morphogenetic Protein (BMP) signaling in development and human diseases. *Genes Dis.* **1**, 87-105. doi:10.1016/j.gendis.2014.07.005

Wang, S. S., Lewcock, J. W., Feinstein, P., Mombaerts, P. and Reed, R. R. (2004). Genetic disruptions of O/E2 and O/E3 genes reveal involvement in olfactory receptor neuron projection. *Development* **131**, 1377-1388. doi:10.1242/dev.01009

Wang, S. S., Tsai, R. Y. and Reed, R. R. (1997). The characterization of the Olf-1/EBF-like HLH transcription factor family: implications in olfactory gene regulation and neuronal development. *J. Neurosci.* **17**, 4149-4158. doi:10.1523/JNEUROSCI.17-11-04149.1997

Wang, X., Llamas, J., Trecek, T., Shi, T., Tao, L., Makmura, W., Crump, J. G., Segil, N. and Gnedeva, K. (2023). SoxC transcription factors shape the epigenetic landscape to establish competence for sensory differentiation in the mammalian organ of Corti. *Proc. Natl. Acad. Sci. USA* **120**, e2301301120. doi:10.1073/pnas.2301301120

Wang, Y., Sun, J., Wang, D., Liu, H., Ma, Q. and Chen, S. (2025). Integrated analysis of slow transit constipation and colorectal cancer reveals the co-Pathogenic targets and their potential clinical value. *Cancer Invest.* **43**, 337-354. doi:10.1080/07357907.2025.2506102

Wang, Y., Zolotarev, N., Yang, C.-Y., Rambold, A., Mittler, G. and Grosschedl, R. (2020). A prion-like domain in transcription factor EBF1 promotes phase separation and enables B cell programming of progenitor chromatin. *Immunity* **53**, 1151-1167.e1156. doi:10.1016/j.immuni.2020.10.009

Warchol, M. E. and Corwin, J. T. (1996). Regenerative proliferation in organ cultures of the avian cochlea: Identification of the initial progenitors and determination of the latency of the proliferative response. *J. Neurosci.* **16**, 5466-5477. doi:10.1523/JNEUROSCI.16-17-05466.1996

Wilkerson, B. A., Chitsazan, A. D., VandenBosch, L. S., Wilken, M. S., Reh, T. A. and Bermingham-McDonogh, O. (2019). Open chromatin dynamics in prosensory cells of the embryonic mouse cochlea. *Sci. Rep.* **9**, 9060. doi:10.1038/s41598-019-45515-2

Wilkerson, B. A., Zebroski, H. L., Finkbeiner, C. R., Chitsazan, A. D., Beach, K. E., Sen, N., Zhang, R. C. and Bermingham-McDonogh, O. (2021). Novel cell types and developmental lineages revealed by single-cell RNA-seq analysis of the mouse crista ampullaris. *eLife* **10**, e60108. doi:10.7554/eLife.60108

Woods, C., Montcouquiol, M. and Kelley, M. W. (2004). Math1 regulates development of the sensory epithelium in the mammalian cochlea. *Nat. Neurosci.* **7**, 1310-1318. doi:10.1038/nn1349

Wu, P. Z., O'Malley, J. T., de Gruttola, V. and Liberman, M. C. (2020). Age-related hearing loss is dominated by damage to inner ear sensory cells, not the cellular battery that powers them. *J. Neurosci.* **40**, 6357-6366. doi:10.1523/JNEUROSCI.0937-20.2020

Xie, Y., Zhu, C., Wang, Z., Tastemel, M., Chang, L., Li, Y. E. and Ren, B. (2023). Droplet-based single-cell joint profiling of histone modifications and transcriptomes. *Nat . Struct. Mol. Biol.* **30**, 1428-1433. doi:10.1038/s41594-023-01060-1

Yang, Q., Liu, S., Yin, M., Yin, Y., Zhou, G. and Zhou, J. (2015). Ebf2 is required for development of dopamine neurons in the midbrain periaqueductal gray matter of mouse. *Dev. Neurobiol.* **75**, 1282-1294. doi:10.1002/dneu.22284

Yin, M., Liu, S., Yin, Y., Li, S., Li, Z., Wu, X., Zhang, B., Ang, S. L., Ding, Y. and Zhou, J. (2009). Ventral mesencephalon-enriched genes that regulate the development of dopaminergic neurons in vivo. *J. Neurosci.* **29**, 5170-5182. doi:10.1523/JNEUROSCI.5569-08.2009

Zhang, H., Papiernik, T., Tian, S., Yaghmour, A., Alzein, A., Lennon, J. B., Maini, R., Tan, X., Niazi, A., Park, J., et al. (2025). Kölliker's organ functions as a developmental hub in mouse cochlea regulating spiral limbus and tectorial membrane development. *J. Neurosci.* **45**, e0721242025. doi:10.1523/JNEUROSCI.0721-24.2025

Zheng, J. L. and Gao, W.-Q. (2000). Overexpression of Math1 induces robust production of extra hair cells in postnatal rat inner ears. *Nat. Neurosci.* **3**, 580-586. doi:10.1038/75753

Zhu, C., Zhang, Y., Li, Y. E., Lucero, J., Behrens, M. M. and Ren, B. (2021). Joint profiling of histone modifications and transcriptome in single cells from mouse brain. *Nat. Methods* **18**, 283-292. doi:10.1038/s41592-021-01060-3

Zine, A., Aubert, A., Qiu, J., Therianos, S., Guillemot, F., Kageyama, R. and De Ribaupierre, F. (2001). *Hes1* and *Hes5* activities are required for the normal development of the hair cells in the mammalian inner ear. *J. Neurosci.* **21**, 4712-4720. doi:10.1523/JNEUROSCI.21-13-04712.2001

Zolotarev, N., Bayer, M. and Grosschedl, R. (2022). EBF1 is continuously required for stabilizing local chromatin accessibility in pro-B cells. *Proc. Natl. Acad. Sci. USA* **119**, e2210595119. doi:10.1073/pnas.2210595119